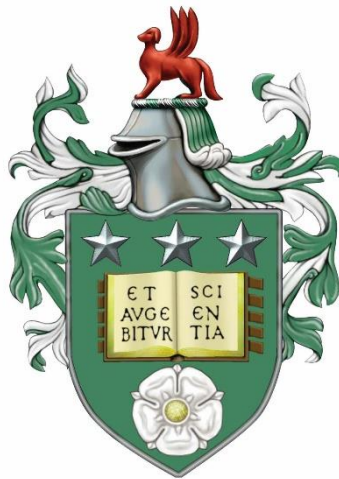


Structure and Stability of Phospholipid Membranes Found in Dermatological Formulations



Ngai Ying Denise Li

Submitted in accordance with the requirements for the
degree of Doctor of Philosophy

School of Food Science & Nutrition

The University of Leeds

October 2018

Declaration

The candidate confirms that the work submitted is her own, except where work which has formed part of jointly authored publications has been included. The contribution of the candidate and the other authors to this work has been explicitly indicated below. The candidate confirms that appropriate credit has been given within the thesis where reference has been made to the work of others.

The details of X-ray scattering outlined in Chapter 2 has appeared in the publication:
Li, N. Y. D., Perutková, Š, Siglic, A. and Rappolt, M. My first electron density map: A beginner's guide to small angle X-ray diffraction. *Electrotechnical Review*. 2017, 84(3), pp.69-75.

Contributions of the authors:

Li, N. Y. D.: Analysed the data and drafted the manuscript.

Perutková, Š: Helped to proofread the manuscript and contributed to the Slovenian abstract.

Siglic, A: Helped to proofread the manuscript and wrote the Slovenian abstract.

Rappolt, M.: Collected the data, provided supervision, edited and proofread the manuscript.

This copy has been supplied on the understanding that it is copyright material and that no quotation from the thesis may be published without proper acknowledgement.

The right of Ngai Ying Denise Li to be identified as Author of this work has been asserted by Ngai Ying Denise Li in accordance with the Copyright, Designs and Patents Act 1988.

“The true scientist should be like the bee, which extracts the matter from the flowers of the garden and the field, but works and fashions it by its own efforts.”

Francis Bacon

Acknowledgements

Firstly, I owe huge gratitude to my academic supervisor, Professor Michael Rappolt, you have been so patient and guided me through the world of lipids and X-rays. I hope that I have been a great, first (official) PhD student for you. You have supported me through so much both academically and personally, I cannot thank you enough – you have been like my father during my stay in Leeds. Secondly, to my industrial supervisor Dr Eloise Welfare, although you may be on the other side of the world, I have never felt out of touch from you – thank you for being a constant presence. You have not only guided me through a vastly interesting PhD, you have also given me tremendous amount of encouragement and I will move on from the PhD a more confident person. Throughout my PhD I have also had vast support from Dr David Moore, Dr Michael Thompson and Dr Amin Sadeghpour. Thank you to David and Michael for all of your advice and flexibility – I hope you agree with me when I say that we've established a great collaboration. To Amin, you supported me the most during the beginning of my PhD, I learnt a lot concerning X-ray scattering thanks to you. Not only that, you were always a calming presence whenever I did something wrong or when things weren't going right. I have also endured this journey with the support from fellow PhD students at the FS&N @ Parkinson PhD cluster, and worked alongside the SAXS beauties Dr Arwen Tyler, Zexi, Rashmi and Marjorie. Next, I move on to my SOFI family, I have to thank in particular, Professor Lian Hutchings not only for encouraging me to apply to SOFI but for constantly supporting me throughout my PhD. From the very beginning of the PhD, I gained strong friendships with my fellow SOFI cohort and these individuals really have become my support network and PhD family, thank you all – may we be SOFI CDT's best ever first guinea pig cohort! From one family to another, I could never have gotten to where I am without my lifetime support - mum and dad, I've done it. Thank you for all the sacrifices you have made for me, I can never thank you enough. Mum, who knew that when my biology teacher said I could be a doctor, that he would be right, just not that kind of doctor! To Adam, you helped me through tough times during the PhD, even if you may not have known. I really enjoyed having you in Leeds too and I hope you agree that it's made us become closer again. Last but not least, my dearest Victor, thank you for always understanding, for being patient and fully supportive of my decisions. You have kept me going during the good times and the bad times.

Conferences and External Events

- Royal Society Discussion: Soft interfacial materials: from fundamentals to formulation (Oct 12-13 2015).
- School of Food Science and Nutrition Postgraduate Conference (Nov 16 2015), poster presentation.
- Scattering School for Soft Condensed Matter (Jun 20-27 2016), oral presentation.
- UK Soft Matter Showcase SOFI CDT Conference (Jun 28-29 2016), poster presentation.
- UK Soft Matter Showcase SOFI CDT Conference (Jul 5-6 2017), poster presentation.
- SOFI CDT Industry Day (Jul 7 2017), oral presentation with GSK.
- Eurofed Lipids Conference (Aug 27-30 2017), poster presentation.
- School of Food Science and Nutrition Postgraduate Conference (Nov 22 2017), poster presentation.
- Formulation Forum Launch Event (Jan 17-18 2018), poster presentation.
- BPS Conference (Feb 17-21 2018), poster presentation.
- Pint of Science Leeds Launch event (April 9 2018), oral presentation.
- University of Leeds Research Nights (April 17 2018), oral presentation.
- Inter-CDT Formulation and Soft Matter Conference (Jun 4-5 2018), oral presentation.
- GSK PHD Science Symposium (Jun 13-14 2018), oral presentation.
- UK Soft Matter Showcase SOFI CDT Conference (Jul 4-5 2018), poster presentation.

Awards:

- School of Food Science and Nutrition Postgraduate Conference (Nov 16 2015). Runner up poster prize.
- Formulation Forum Launch Event (Jan 17-18 2018) Runner up poster prize.
- Inter-CDT Formulation and Soft Matter Conference (Jun 4-5 2018). Joint winner of best oral presentation.
- GSK PHD Science Symposium (Jun 13-14 2018). Best 10 minute oral presentation.

Manuscripts in Preparation

Li, N. Y. D., Thompson, M., Moore, D., Welfare, E. and Rappolt, M. The influence of humectants on the thermotropic behaviour and nanostructure of fully hydrated dipalmitoylphosphatidylcholine bilayers.

Li, N. Y. D., Thompson, M., Moore, D., Welfare, E. and Rappolt, M. The thermotropic behaviour and nanostructure of phosphatidylcholine lipid mixtures differing by two methylene groups.

Abstract

Dry skin condition remains one of the major dermatological problems and to tackle or prevent this condition, consumers turn to the use of moisturising skin creams. Dry skin manifests from reduced barrier performance of the upper layer of the skin, the stratum corneum. This reduced barrier leads to increased water loss from the skin, which is due to the depletion of orthogonally packed lipids in the stratum corneum. To improve the skin barrier and thus reduce dry skin, one method is to deliver lipids with such a dense chain packing to the skin via the skin cream. It is important therefore, to understand in depth, the properties of such lipids to make more informed formulation development decisions in industry as well as providing novel insights to the scientific community.

This thesis investigates the detailed structure of lipids used typically in dermatological formulations and their stability to temperature change and interactions with other components found in formulations. The combination of X-ray scattering and differential scanning calorimetry, DSC, techniques reveal information on the nanostructure and thermal behaviour of PCs and thus are employed as suitable analytical methods.

Three different systems are studied: (i) the influence of humectants on lipids; (ii) comparison of industrial lipid samples with high purity lipid samples; (iii) more complex multi-component formulations. Humectants are found commonly in skin cream formulations as they provide hydration to the skin by attracting water molecules. Thus, there is a need for understanding their effect on the overall lipid structure and in turn, the overall structure of the skin cream. Mixed lipid systems, both pure lipid mixtures and industrial lipid mixtures (containing impurities) are studied to understand how similar lipid mixtures behave compared to pure lipids. Finally, more complex formulations enable the formulator to understand and predict the structure of the final product formulation. This thesis reports new understandings on the influence of humectants on the structure of lipids at low concentrations ($< 1\text{M}$), as well as detailed structural analysis and evidence for phase separation in lipid mixtures, and existence of coexisting lamellar phases from the lipid and oil components of multi-component systems, for the first time.

The insights and knowledge generated from this thesis will contribute positively to the formulation industry and help the industry transform from being an art to science.

Table of Contents

Declaration	i
Acknowledgements	iii
Abstract	vi
Abbreviations	x
Table of Figures	xii
Chapter 1 Introduction	1
1.1 The Structure of Pure Phosphatidylcholine Lipids and their Thermal Properties	1
1.1.1 The Sub-Gel Phase, L_C	5
1.1.2 The Gel Phase, $L_{\beta'}$	5
1.1.3 The Stable Ripple Phase, $P_{\beta'}$	8
1.1.4 The Fluid Phase, L_{α}	10
1.1.5 The Metastable Ripple Phase, $P_{\beta'}$	12
1.1.6 Anomalous Swelling.....	13
1.2 Phosphatidylcholine Lipid Mixtures and their Thermal and Structural Properties	16
1.3 The Interactions of Phosphatidylcholine Lipid Bilayers with Hydrophilic Small Molecules.....	24
1.3.1 The Influence of Kosmotropes	24
1.3.2 The Influence of Chaotropes	29
1.4 The Structure and Properties of Humectants	31
1.5 Research Aims	33
Chapter 2 Materials and Methods	36
2.1 Materials	36
2.2 Sample Preparation	36
2.2.1 Preparation of Pure DPPC and DSPC Liposomes.....	36
2.2.2 Preparation of DPPC Liposomes with Humectant	36
2.2.3 Preparation of Phospholipon 90H Liposomes	37
2.2.4 Preparation of DPPC/DSPC Mixture Liposomes.....	37
2.2.5 Preparation of Novel Multi-Component Formulations	37
2.3 X-ray Scattering	39
2.3.1 X-ray Measurement	40
2.3.2 Data Reduction	41

2.3.3	Determining the <i>d</i> spacing	43
2.3.4	Calculating Electron Density Profiles	44
2.3.5	Calculating the Area per Lipid Chain.....	45
2.4	Differential Scanning Calorimetry.....	46
2.4.1	Differential Scanning Calorimetry Measurements	46
2.4.2	Determining the Transition Temperatures and Enthalpy Values	47
2.4.3	Determining the FWHM and Offset Values.....	48
2.5	Isothermal Titration Calorimetry	49
2.5.1	Isothermal Titration Calorimetry Measurements	49
2.5.2	Background Subtraction	50
2.5.3	Determining the Enthalpy of Interaction.....	50
Chapter 3 Results		51
3.1	The Influence of Humectants on the Thermotropic Behaviour and Nanostructure of DPPC.....	51
3.1.1	Introduction	51
3.1.2	Thermotropic Changes	52
3.1.3	Nanostructural Changes.....	59
3.1.4	Discussion.....	69
3.1.5	Conclusion.....	73
3.2	The Structural and Thermotropic Properties of DPPC/DSPC Mixtures....	75
3.2.1	Introduction	75
3.2.2	Thermotropic Changes	77
3.2.3	Structural Changes.....	81
3.2.4	Discussion.....	89
3.2.5	Conclusion.....	92
3.3	The Nanostructure of Commercial Lecithin-Containing Novel Multi-Component Formulations.....	95
3.3.1	Introduction	95
3.3.2	Nanostructural Changes.....	98
3.3.3	Discussion.....	109
3.3.4	Conclusion.....	111
Chapter 4 General Conclusion.....		113
Chapter 5 Outlook		118
5.1	FT-IR Spectroscopy	118
5.2	Neutron Scattering	121
5.3	Molecular Dynamics Simulations.....	121

5.4	Calculation of the Van der Waals Forces.....	124
5.5	Mass Spectrometry.....	125
5.6	Further X-ray Scattering Measurements	126
5.7	Further DSC Measurements.....	126
	References	128

Abbreviations

A_C	Area per chain
AMEA	Acetaminde monoethanolamine
d_{HH}	Head-to-headgroup thickness
DHPC	1,2-o-dihexadecyl-sn-glycero-3-phosphocholine
DHPE	1,2-dihexadecyl-sn-glycero-3-phosphoethanolamine
DLPC	Dilauroyl phosphatidylcholine
DMPC	1,2-dimyristoyl-sn-glycero-3-phosphocholine
DMPE	1,2-dimyristoyl-sn-glycero-3-phosphoethanolamine
DMU	Dimethylurea
DOPC	1,2-dioleoylphosphatidylcholine
DOPE	1,2-dioleoyl-sn-glycero-3-phosphatidylcholine
DPPC	1,2-dipalmitoyl-sn-glycero-3-phosphocholine
DSC	Differential scanning calorimetry
DSPC	1,2-distearylphosphatidylcholine
DVLO theory	Derjaguin- Landau-Verwey-Overbeek theory
d_w	Interstitial water layer thickness
EDP	Electron density profile
FT-IR	Fourier transform infra-red
FWHM	Full width half maximum
H_{II}	Hexagonal phase

ISIS	Isostearyl isostearate
ITC	Isothermal titration calorimetry
L_C	Sub-gel phase
L_α	Fluid phase
L_β'	Gel phase
MLV	Multilamellar vesicle
PC	Phosphatidylcholine
POPC	1-palmitoyl-2-oleoyl-sn-glycero-3-phosphocholine
POPE	Palmitoleoylphosphatidylethanolamine
P_β'	Ripple phase
SAXS	Small angle X-ray scattering
SOS	1,3-distearoyl-2-oleoyl-sn-glycerol
T_M	Main transition temperature
TMAO	Trimethylamine-N-oxide
TMU	Tetramethylurea
T_{pre}	Pre-transition temperature
ULV	Unilamellar vesicle
WAXS	Wide angle X-ray scattering
η	Caillé parameter
σ	Mean fluctuations of the membrane position

Table of Figures

Figure 1: The structure of DPPC.....	2
Figure 2: An illustration of the DVLO theory showing the van der Waals attractions dominating at longer distances and electrostatic repulsive forces dominating at closer distances. Adapted from (12).	3
Figure 3: A differential calorimetry scan of DPPC illustrating the different phases observed via a temperature scan. The sub-gel phase transforms at 22 °C into the lamellar gel-phase, followed by the pre-transition to the ripple gel-phase at around 35 °C and finally by the formation of the fluid lamellar phase at 41 °C at the main transition. Taken from (13).	4
Figure 4: The stacking structure of the bilayers showing the chains tilted perpendicular to the plane, and the lipid packing arrangement (inset) of the lamellar gel phase of PCs. Taken from (20).	6
Figure 5: The temperature and chain length dependence of the d spacing in the gel phase of PCs. Taken from (17).	7
Figure 6: A plot to show the temperature and chain length dependence of the area per lipid chain for the gel phase of PCs. Taken from (17).....	7
Figure 7: The structure of the stable ripple phase showing the stacking structure of the bilayers of PCs with two possible lipid chain conformations. 1. Shows the ripple phase with the presence of co-existing chains with all- <i>trans</i> and <i>trans-gauche</i> conformations. 2. Shows the ripple phase with the presence of chains in only all- <i>trans</i> conformations (i.e. gel-type chains). Taken from (20).	9
Figure 8: The electron density profile for the ripple phase including a schematic of the packing of the hydrocarbon chains. The purple chains represent the gel-like hydrocarbons chains in the major side of the ripple. The red, orange and green chains represent the more fluid-like hydrocarbon chains in the minor side of the ripple. Taken from (28).	9
Figure 9: The EDP of DLPC at -7 °C and 77 wt.% water. Taken from (30).	10
Figure 10: The structure of the fluid phase of PCs showing the stacking of the bilayers. Taken from (20).	11
Figure 11: The change in the main transition temperature with change in hydrocarbon chain length for PCs, where n is the length of hydrocarbon chain. Taken from (14).	11
Figure 12: The temperature dependence of the lamellar d spacing. The circles are for 1,2-dimyristoyl-sn-glycero-3-phosphocholine and the triangles are for 1,2-dimyristoyl-sn-glycero-3-phosphoethanolamine bilayers. Taken from (20)..	14
Figure 13: The chain length dependence of the anomalous swelling component, Δd_{an} . Taken from (41).	15
Figure 14: The DSC results of DMPC/DPPC lipid mixtures. a) The DSC thermograms for different molar ratios of the lipid mixtures. b) The change in cooperativity with change in lipid composition by plotting the onset (open) vs. offset (filled) temperatures of the main transition. The triangles are results from simulations and the circles are calculated from experimental results. Both figures taken from (44).	17

Figure 15: The phase diagram of DPPC/DSPC mixtures. Taken from (45).	17
Figure 16: The phases of DOPC/DPPC mixtures at different ratios at 24 °C observed via ² H NMR with deuterated DPPC. Adapted from (46).....	19
Figure 17: The phase diagram for DOPC/DPPC mixtures. Taken from (46).	19
Figure 18: The structure of DHPC.	20
Figure 19: DSC thermograms of DPPC/DHPC mixtures in excess water with their mol % indicated. Adapted from (48).	21
Figure 20: The change in <i>d</i> spacing as DHPC is added in increasing amounts to DPPC. Taken from (48).	22
Figure 21: The phase diagram for DPPC/DHPC mixtures. Taken from (48).	22
Figure 22: The structure of DMPE.....	23
Figure 23: The structures of a) betaine and b) sarcosine.....	27
Figure 24: The change in <i>d</i> spacing at 7 °C of DOPE bilayers with increasing concentration of urea (circles), DMU (filled squares) and TMU (open squares). Taken from (69).	28
Figure 25: Langmuir isotherms of DPPC monolayers spread on different concentration of urea solutions. Taken from (74).....	30
Figure 26: The hydrogen bond interactions in the first hydration shell of a) betaine with 7 water molecules and b) sarcosine with 9 water molecules. Taken from (89) and (87), respectively.	33
Figure 27: A photograph showing both sides of an Anton Paar paste cell filled with sample before being placed inside a vacuum desiccator.....	38
Figure 28: An illustration of the structure of phospholipid bilayers in multilamellar vesicles and definition of their structural parameters. Taken from (20).....	40
Figure 29: An illustration of the X-ray beamline set-up for measurements.....	41
Figure 30: Example of subtracting a capillary filled with MilliQ water from the DPPC sample curve. The red line is the DPPC curve after subtraction of the empty capillary curve. The blue line is the capillary filled with water curve after subtraction of the empty capillary curve. The green line is the DPPC curve after subtraction of the capillary filled with water curve after using a multiplication factor.	42
Figure 31: Example of performing a linear regression of the peak positions to calculate the <i>d</i> spacing in the gel phase.	43
Figure 32: The de-smearred WAXS curve of the gel phase of DPPC with peak fitting performed by OriginPro. The red and green curves are the fit results of peak 1 at <i>q</i> ₂₀ and 2 at <i>q</i> ₁₁ , respectively. The blue curve is the cumulative peak fit result.	46
Figure 33: A DSC curve showing the <i>T</i> _M peak where the determined onset of transition temperature and enthalpy from the Pyris 13.3 software.	48

Figure 34: The main transition peak of DPPC collected by DSC where the range selected for peak analysis is shown by the two blue vertical lines either side of the peak. The results from the peak analyser tool in OriginPro are displayed below the curve.	49
Figure 35: The structure of a) betaine b) sarcosine and c) AMEA.	51
Figure 36: The SAXS curves for the gel, ripple and fluid phase and the structures of the lipid bilayers shown in the inset of each phase. *Insets taken from (20). ..	53
Figure 37: The structural changes of DPPC observed between 25 to 50 °C by small angle X-ray scattering. The z axis is Intensity (a.u.) where the dark blue areas are lowest in intensity and the red areas are highest.	54
Figure 38: The change in d spacing of DPPC with increasing temperature.	54
Figure 39: The phase diagrams of DPPC with increasing concentrations a) betaine b) sarcosine and c) AMEA.	55
Figure 40: The enthalpy values for the phase transitions of DPPC with addition of a) betaine b) sarcosine and c) AMEA.	57
Figure 41: The ITC results for a) 0.4 M betaine b) 0.4 M sarcosine and c) 0.4 M AMEA injections to water.	58
Figure 42: The change in FWHM for the main transition of DPPC with change in concentration of humectant.	59
Figure 43: The electron density profile of fully hydrated DPPC in the gel phase. The parameters d , d_{HH} , and d_W are indicated in relation to the EDP. An illustration of two lipid bilayers is presented above the EDP to facilitate interpretation of the EDP.	60
Figure 44: The change in a) d_{HH} b) d_W and c) d spacing of gel phase DPPC at 25 °C with increasing concentration of humectant.	61
Figure 45: An illustration of the effect of betaine on the nanostructure of fully hydrated DPPC in the gel phase.	61
Figure 46: The SAXS curves for the fluid phase of DPPC with a) 0 M betaine b) 0.05 M betaine c) 0.15 M betaine d) 0.4 M betaine e) 1 M betaine and f) 2 M betaine. The global fitting results are presented by the black lines (for details of the fitting method see Section 2.3.4) for each concentration and temperature. The SAXS curves have been stack-plotted for clarity.	63
Figure 47: The change in a) d_{HH} b) d_W c) d spacing and d) η of DPPC with temperature in the fluid phase at different concentrations of betaine.	64
Figure 48: The change in a) d_{HH} b) d_W c) d spacing and d) η of DPPC with increasing concentration of humectant. Temperature is equal to $T_M + 2$ °C. ..	65
Figure 49: The different phases of pure DPPC as seen by WAXS at different temperatures. The black curve is the gel phase, the blue curve corresponds to the ripple phase and the pink curve is the fluid phase.	66
Figure 50: The change in the WAXS pattern of fully hydrated of DPPC with temperature for a) pure DPPC b) with 0.05 M betaine c) with 0.15 M betaine d) 0.40 M betaine e) 1.00 M betaine and f) 2.00 M. The z axis is the Intensity (a.u.) of the counts.	66

Figure 51: The unit cell and Miller Indices of the orthogonal lattice of the gel phase DPPC.....	67
Figure 52: The change in area per lipid chain for a) the gel phase and b) the fluid phase of fully hydrated DPPC with each humectant.	68
Figure 53: The change in peak shape of the WAXS peak for DPPC with AMEA at 25 °C.	68
Figure 54: The change in ratio of the DPPC WAXS gel phase peak $I(q_{20}):I(q_{11})$ ratio with increasing concentration of humectant at 25 °C.	69
Figure 55: a) DSC heating thermograms for DPPC/DSPC mixtures at various compositions b) DSC heating thermogram for DPPC/DSPC mixture at 50:50 wt.% composition. The blue arrows indicate the splitting of the pre-transition temperatures of DPPC and DSPC, respectively, and the red arrows display the splitting of the main transition.	78
Figure 56: The phase diagram for DPPC/DSPC lipid mixture at different compositions. Literature values are taken from (14).	78
Figure 57: The change in peak full width half maximum for both phase transitions with change in DPPC/DSPC composition. a) the peak onset-offset difference for T_{pre} , b) the peak onset-offset difference for T_M , c) the change in FWHM for T_{pre} and d) the change in FWHM for T_M	80
Figure 58: The change in enthalpy with change in DPPC/DSPC composition for both the pre-transition and the main transition. Literature values are taken from (14).	81
Figure 59: a) The SAXS curves of DSPC:DPPC, 85:15 wt.% mixtures respectively, and P90H at 30 °C. The black line is for higher purity lipid samples and the red line is for commercially available lipid sample named P90H. b) The SAXS curves of P90H at different temperatures. The SAXS curves have been stack-plotted for clarity.....	82
Figure 60: The change in d spacing with temperature for P90H.	83
Figure 61: The change in structural parameters of the lipid bilayer with changing DSPC composition at 30 °C. The change in a) head-to-headgroup thickness b) water layer thickness c) d spacing. d) The electron density profiles for each composition.....	84
Figure 62: The SAXS curves of the fluid phase and their global fit results represented by the black lines of a) DPPC pure b) 15 % DSPC c) 25 % DSPC d) 50 % DSPC e) 75 % DSPC f) 85 % DSPC and g) 100% DSPC pure. The SAXS curves of different temperatures are stacked for clarity.	85
Figure 63: The change in structural parameters of the lipid bilayer with changing DSPC composition in the fluid phase. The change in a) head-to-headgroup thickness b) water layer thickness c) d spacing and d) mean fluctuations of the membrane position, σ	87
Figure 64: The change in structural parameters with change in lipid composition for the fluid phase at $T=T_M + 2$ °C. The change in a) head-to-headgroup thickness b) water layer thickness c) d spacing and d) mean fluctuations of the membrane position, σ	88

Figure 65: A plot of the change in average number of bilayers in registry in the fluid phase with increasing concentration of DSPC.....	88
Figure 66: An illustration explaining two co-existing lamellar phases displaying (a) both phases in stacking-registry and (b) lateral phase separation without stacking-registry. SAXS measurements would show two distinct sets of Bragg peaks in the first case, while for the latter case the SAXS pattern would display only one set of diffraction peaks (i.e. 1 lattice is given).....	89
Figure 67: The structure of the upper layer of skin – 1) the stratum corneum, 2) using the bricks and mortar analogy and 3) showing the structure of the lipids surrounding the corneocytes. The right-hand side also shows the difference in lateral organisation of the lipids between orthorhombic, hexagonal and liquid packing. Adapted from (123).....	96
Figure 68: The structure of isostearyl isostearate.	97
Figure 69: The SAXS curves of the different sample compositions at 25 °C with their formulation code shown in the legend. The reader is referred to Table 4 in Section 2.2.5 for details of each formulation code. The red arrows correspond to d spacing = 17.0 nm, the blue arrows, d spacing = 5.92 nm and the black arrows, d spacing = 4.47 nm. The curves have been stacked for clarity.	100
Figure 70: The thermal behaviour of each formulation code a) 000 b) 100 c) 010 d) 001 e) 001 f) 101 g) 110 h)111 between 25 – 70 °C. The SAXS curves of each temperature have been stack-plotted for clarity.....	103
Figure 71: The SAXS curves of the “dried” formulations at 32 °C. The curves have been stacked for clarity.	104
Figure 72: A comparison of the SAXS curves for each formulation after their “wet” and “dried” protocol. The SAXS curves are stacked for clarity.	106
Figure 73: The thermal behaviour of each dried formulation a) 000 b) 100 c) 010 d) 001 e) 001 f) 101 g) 110 h) 111 between 25 – 70 °C as shown in the legends. The SAXS curves of each temperature have been stack-plotted for clarity. .	108
Figure 74: The different sub-phases of the lamellar structures formed for triglycerides. Two-chained layers exhibited by the α_1 -phase and three-chained layers exhibited by the other phases. Figure taken from (12).....	110
Figure 75: The FT-IR spectra of DPPC at 47 °C for a) fully hydrated MLVs and b) partially hydrated MLVs. Taken from (137).	119
Figure 76: FT-IR spectra of DPPC either dehydrated in the presence or absence of trehalose, or in the presence of trehalose and after heating to 60 °C or fully hydrated. Taken from (138).	120
Figure 77: A snapshot of a molecular dynamics simulation of 164 DPPC lipids in excess water at 91 °C.	122
Figure 78: The calculated area per lipid of DPPC at 91 °C over the simulation period of 150 ns.....	122
Figure 79: The electron density profile of DPPC at 91 °C over 150 ns simulation.	123
Figure 80: The formation of a water defect as a result of asparagine penetrating a DOPC bilayer captured by simulations performed by MacCallum <i>et al.</i> (144).	124

Figure 81: The mass spectrum of melittin with POPC liposomes. Taken from (147).
..... 126

Chapter 1 Introduction

1.1 The Structure of Pure Phosphatidylcholine Lipids and their Thermal Properties

Phosphatidylcholines, PCs, are a class of lipids that have been studied rigorously due to their significance in biological systems. Mammalian membranes generally contain 40-80% phospholipids, with PC and phosphatidylethanolamine making up the biggest share. Not only are phospholipids studied due to their biological relevance, but they are also used in a vast range of products and applications including cosmetics, skin and hair care, and targeted drug delivery (1).

Since the discovery of liposomes in 1963 (2) they have attracted much attention for skin care applications, due to the similarities in structure of the liposomes with biological membranes (3). Phospholipids are used widely in dermatological formulations as the main structural component of oil in water emulsions (4, 5). But due to their biocompatibility, their applications are not limited to skin care and are used widely as drug delivery systems as they are able to house both hydrophilic and hydrophobic therapeutics (6). It is well known that the stratum corneum has a high barrier to penetration for the skin which has caused challenges to deliver drugs in to the body via the skin. However, the use of phospholipids as carriers for drug delivery in topical applications has shown promising results and appears to improve penetration and permeation in to the skin. Earlier studies in to the encapsulation of drugs by lipid vesicles have shown to increase penetration in to the skin (7, 8).

The properties of phospholipids have been reported and explained in many comprehensive texts and the reader is referred in particular to (9, 10). The structure of PC consists of a choline head group containing three methyl groups attached to a nitrogen atom which is then attached to the phosphate via an ethyl linkage. Figure 1 displays the structure of 1,2-dipalmitoyl-*sn*-glycero-3-phosphocholine, DPPC. DPPC is a saturated diacyl PC, with 16 carbons in both of the hydrocarbon chains. All PCs have the same choline head group but can differ in the linkage and the hydrocarbon chains. Other types of PCs may have dialkyl, alkyl-acyl or other types of linkages and may

contain different number of carbons between the two hydrocarbon chains as well as the presence of double bonds.

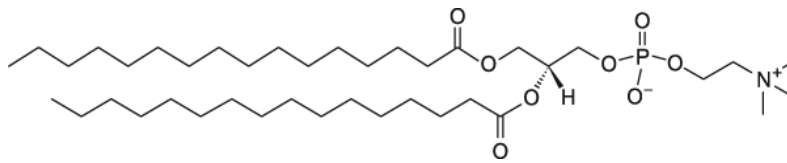


Figure 1: The structure of DPPC.

When in excess water, phospholipids self-assemble into lyotropic liquid crystalline structures due to the hydrophobic effect (10). They form aggregates such that the hydrophobic hydrocarbon chains are shielded from the water molecules by the hydrophilic headgroups. For fully saturated diacyl PCs in particular, they will self-assemble into the lamellar phase, also known as the smectic liquid crystal phase. There are four main forces known to act between the lipid bilayers: (i) attractive van der Waals forces, (ii) electrostatic or Coulombic interactions (if the headgroups are charged), (iii) repulsive hydration forces at small distances ($< 10 \text{ \AA}$) and (iv) repulsive undulation forces are dominant at longer distances. This is in fact, a combination of the Derjaguin- Landau-Verwey-Overbeek theory, DVLO theory (11), and repulsive hydration forces. The DVLO theory describes colloid stability as the sum of electrostatic repulsion, which dominates as two surfaces are in close vicinity with each other, and attractive van der Waals forces which dominate at larger distances, see Figure 2. Repulsive hydration forces occur when the lipid bilayers come into close contact such that the water bound to the headgroups must be expelled.

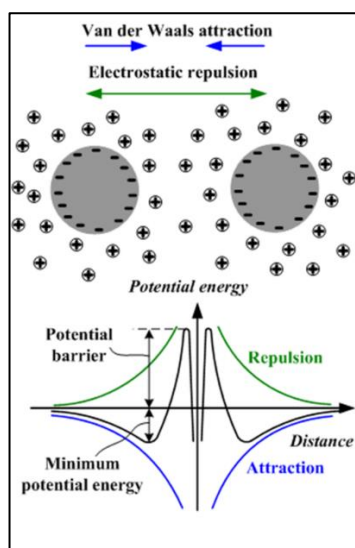


Figure 2: An illustration of the DVLO theory showing the van der Waals attractions dominating at longer distances and electrostatic repulsive forces dominating at closer distances. Adapted from (12).

When water is added to the dry lipid, although the general lamellar structure of the lipid remains the same, a loosening of the lipid packing by disrupting the headgroup-headgroup intermolecular forces occurs, this leads to increased mobility of the lipids. The extent of lipid bilayer hydration depends on the type of lipid headgroup and the physiochemical state (10). Hydration is dependent on the headgroup as interactions occur mainly between the headgroup phosphate, choline, carbonyl and carboxyl groups and water molecules. Hydration at the hydrocarbon chain region is much smaller and restricted due to its hydrophobicity, but the conformation of the chains determines the extent of hydration of the lipid bilayer in total. As the fluidity of the chains increase, so does the bilayer hydration as the lipid molecules occupy a larger area leading to greater headgroup and hydrocarbon chain exposure to the water molecules. The creation of interfacial water leads to a highly ordered hydrogen-bonded liquid water structure which differs from the bulk water structure. The hydrogen bonding between the headgroup and water molecules leads to two different hydration pressures: the aforementioned interbilayer hydration repulsions, and lateral pressure of hydration. The lateral hydration pressure decreases with increasing depth of water penetration into the bilayer whereas it increases with increasing interfacial water thickness and with increasing temperature.

The phase behaviour of PCs differs slightly depending on their hydrocarbon chain length. In this review, only PCs with C16 and above will be discussed. PCs self-

assemble in to the gel phase lamellar structure with the hydrocarbon chains in an all-*trans* conformation, at temperatures below their main transition temperature, T_M . A phase transition to the fluid phase occurs at T_M , where all the chains are now molten and switch from all-*trans* to *trans-gauche* conformation. In addition to these two phases, PCs can form an intermediate ripple phase, between the gel and fluid phase; the temperature of the transition to the ripple phase is called the pre-transition temperature, T_{pre} . The ripple phase can be further distinguished as a stable and a metastable ripple phase. The stable ripple phase is observed when heating from gel to fluid as well as cooling from fluid to gel phases whereas the metastable ripple phase is only observed upon cooling from fluid to gel phase. The phase transitions are clearly illustrated by differential scanning calorimetry, DSC, as shown in Figure 3.

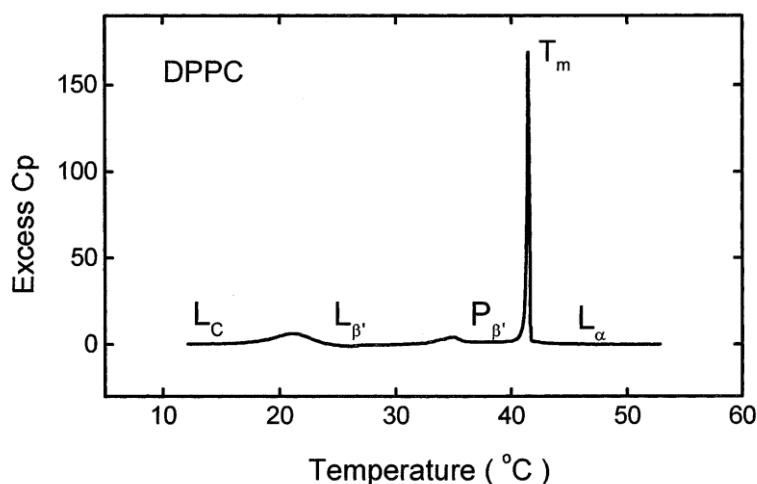


Figure 3: A differential calorimetry scan of DPPC illustrating the different phases observed via a temperature scan. The sub-gel phase transforms at 22 °C into the lamellar gel-phase, followed by the pre-transition to the ripple gel-phase at around 35 °C and finally by the formation of the fluid lamellar phase at 41 °C at the main transition. Taken from (13).

In addition to using DSC, various other techniques can be used to study PCs. These include NMR, infra-red spectroscopy and neutron or X-ray scattering, as well as theoretical computer simulations. Information on the structure in addition to the phase transitions can be learned from small angle- and wide angle X-ray scattering techniques, SAXS and WAXS. The content of this review will highlight these variety of techniques that have been used to study phospholipids. The first part of the review will focus on identifying the individual phases of fully hydrated saturated diacyl PCs.

1.1.1 The Sub-Gel Phase, L_C

Saturated diacyl PCs that have 15-22 carbon chain length, such as DPPC, form the lamellar crystalline sub-gel phase when equilibrated at low temperatures. In the sub-gel phase, also known as the smectic-C phase, the hydrocarbon chains are tilted considerably towards their nearest neighbour (14), and at the sub-transition temperature going from the sub-gel to the gel phase, the tilt is reduced to some extent. The phase transition temperature is somewhat interesting; using DPPC as an example, it is reported that when cooling from the gel phase, the sub-gel phase starts to form at around 7 °C, but when heating from the sub-gel to the gel phase, the transition occurs at a higher temperature of 19 ± 3 °C, see Figure 3. This hysteresis behaviour is probably due to the fact that the formation of the sub-gel phase requires two processes: dehydration of the polar head group and rearrangement of the chains to a more ordered packing mode compared to the gel phase (14), hence requiring a lower temperature to form and then being relatively stable once formed. Despite this, Nagle and Wilkinson (15) have claimed an absolute transition temperature of 14 °C. The time required for the formation of the sub-gel phase increases with chain length, but is around 10 days for DPPC at 14 °C. The sub-gel phase has not been reported for PCs with 23 or 24 carbons in their hydrocarbon chains.

1.1.2 The Gel Phase, L_β

In the lamellar gel phase, also known as the smectic-C phase, the hydrocarbon chains are tilted at around 32° for DPPC, towards their nearest neighbour (16), see Figure 4. Note that the gel phase also exists with no tilt of the hydrocarbon chains (L_β), however this is not observed for DPPC. The tilt angle increases slightly with increasing chain length (17), increasing water content (18) and decreasing temperature (19). Furthermore, the hydrocarbon chains are in an all-*trans* conformation. The insert of Figure 4 shows how the chains pack on a lattice which can be described as an orthorhombic or a distorted hexagonal unit cell. This information is obtained from wide angle X-ray scattering, the scattering pattern shows a sharp (20 Miller index) Bragg peak and a broad (11 Miller index) Bragg peak which are characteristic of an orthorhombic lattice (17). This will be discussed further in Chapter 3.

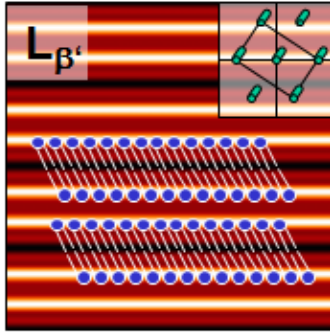


Figure 4: The stacking structure of the bilayers showing the chains tilted perpendicular to the plane, and the lipid packing arrangement (inset) of the lamellar gel phase of PCs. Taken from (20).

Sun *et al.* (17) studied how the structure of the gel phase changes with respect to the hydrocarbon chain length and temperature. It was found that both the d spacing, see Figure 5, and the area per chain, A_C , see Figure 6, increases linearly with temperature. The increase in d spacing is a result of a decrease in the chain tilt and increase in the head-to-headgroup thickness, d_{HH} , whereas the interstitial water layer thickness, d_w , remains more or less constant ($d = d_w + d_{HH}$). However, A_C decreases with increasing chain length as the chains become more densely packed. As a consequence, the unit cell of the lipid chain packing becomes more and more distorted from a hexagonal packed unit cell when the chain length is increased, however this distortion value approaches the same value for any chain length as the lipid approaches T_M .

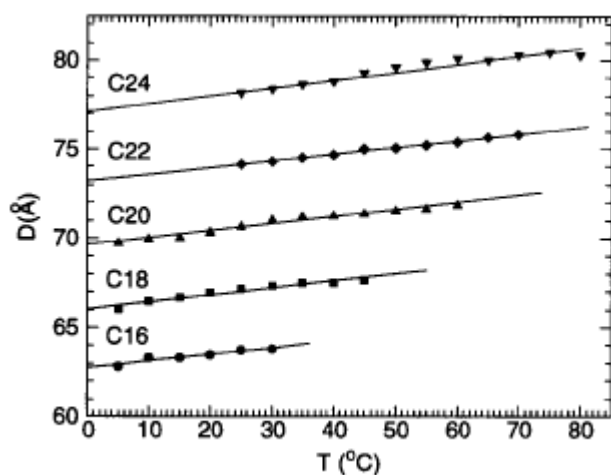


Figure 5: The temperature and chain length dependence of the d spacing in the gel phase of PCs. Taken from (17).

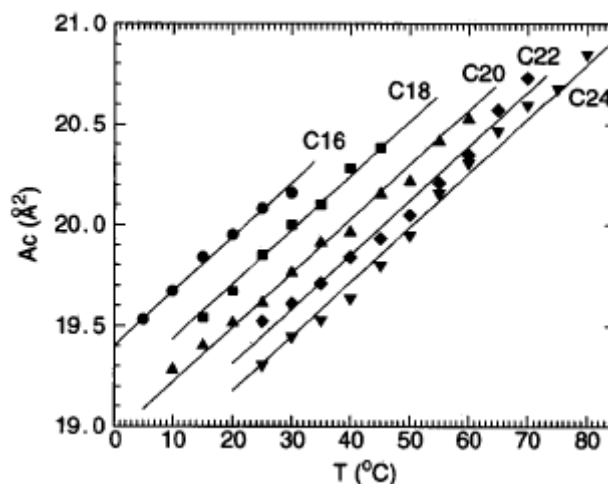


Figure 6: A plot to show the temperature and chain length dependence of the area per lipid chain for the gel phase of PCs. Taken from (17).

The trends described above are consistent for PCs with chain length from 16 to 20. When the chain length is more than 20 carbons long, then a different phase starts to appear (16, 17, 21). Furthermore, the extent of hydration for the gel phase has been studied by Wiener *et al.* (22) who calculated the number of waters of hydration per lipid which yielded a value of 10.6 ± 2.0 for a fully hydrated lipid sample.

1.1.3 The Stable Ripple Phase, P_{β}

In contrast to other lipids, short to medium chained PCs form an additional gel phase: the ripple phase. The transition from gel to ripple phase, T_{pre} , is at 35-36 °C for DPPC. The ripple phase is best described as an asymmetric saw-tooth like height modulation of bilayers that repeat every 120-160 Å with a more or less constant bilayer thickness (23). The hydrocarbon chains are mainly considered to be all-*trans*, like the L_{β}' phase, however some authors argue that there are some *gauche* isomers present as well (24). The chains are also tilted however at a slightly smaller angle around 28° for DPPC (23), see Figure 7.

Despite a well-defined structure supported by well resolved electron density profiles, EDPs, (25), the lipid chain packing and conformation are still a subject of dispute with compelling arguments from both sides. Some authors believe the ripple phase to have alternate fluid and gel domains coexisting in a micro-phase separation, which agrees with the work carried out by Rappolt *et al.* (26), whereas others believe the stable ripple phase to consist only gel state lipid molecules (27). The structural parameters and EDPs calculated by Sun *et al.* (25) strongly suggested that the major side (longer) of the ripple is similar to the gel phase whereas the minor side (shorter) of the ripple is thinner and hence is more similar to a fluid-like phase. This hypothesis is supported by recent work carried out by Akabori and Nagle (28) who used oriented samples to achieve highly ordered lipids. The high resolution data enabled the authors to go one step further by looking at the packing of the lipids and also suggest that not only is the minor side bilayer thinner, but also that the hydrocarbon chains in the two monolayers of the ripple phase are not in registry, see Figure 8. Interestingly, de Vries *et al.* (29) presented molecular simulations of the ripple phase achieved via cooling from the fluid phase. The simulations not only showed structures similar to experimental studies but also showed that the chains in the thinner, minor arms are in fact interdigitated. Other studies to support this notion are required and the results from this study should be taken with care, as the metastable ripple phase may form when cooling from the fluid phase, which was not discussed. On the other hand, Sengupta *et al.* (30) discuss why this micro-phase separation theory is not compatible with diffusion and calorimetric experiments. Sengupta *et al.* also discovered that there is little dependence on temperature for the shape and structural parameters of the ripple phase. Furthermore, they discovered that although most of the saturated diacyl PCs have a similar ripple structure, there is one

exception being dilauryl phosphatidylcholine, DLPC, with 12 carbon long hydrocarbon chains. DLPC ripple phase is more of a triangular shape rather than an asymmetric saw tooth profile, and both the major and minor arms are almost identical and are comparable to the bilayer thickness, see Figure 9.

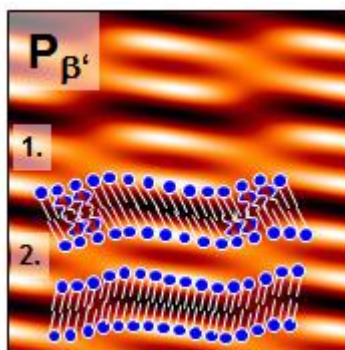


Figure 7: The structure of the stable ripple phase showing the stacking structure of the bilayers of PCs with two possible lipid chain conformations. 1. Shows the ripple phase with the presence of co-existing chains with all-*trans* and *trans-gauche* conformations. 2. Shows the ripple phase with the presence of chains in only all-*trans* conformations (i.e. gel-type chains). Taken from (20).

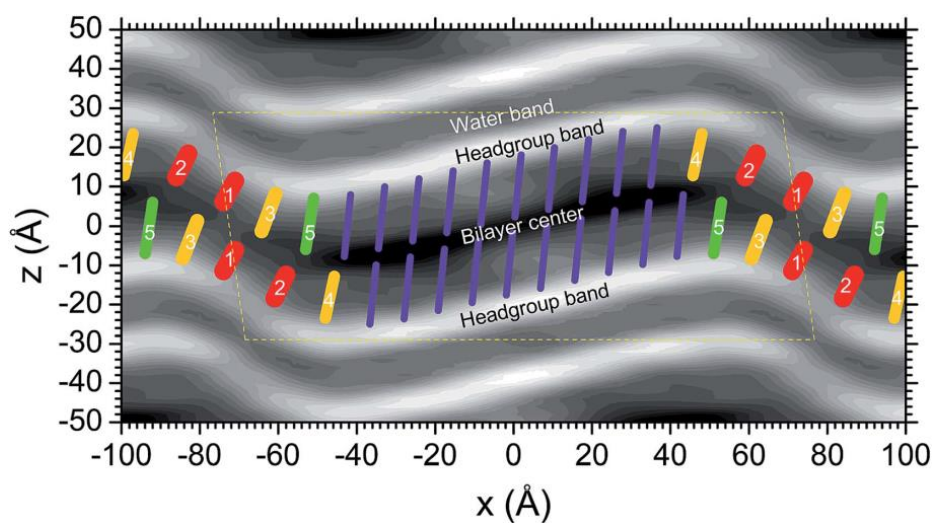


Figure 8: The electron density profile for the ripple phase including a schematic of the packing of the hydrocarbon chains. The purple chains represent the gel-like hydrocarbons chains in the major side of the ripple. The red, orange and green chains represent the more fluid-like hydrocarbon chains in the minor side of the ripple. Taken from (28).

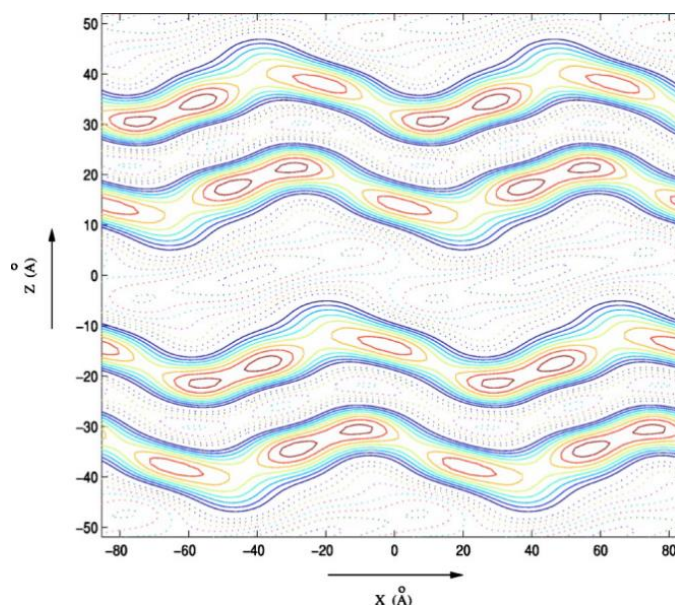


Figure 9: The EDP of DLPC at $-7\text{ }^{\circ}\text{C}$ and 77 wt.% water. Taken from (30).

The origin of the stable ripple phase is yet to be confirmed, even though there have been many models presented over the years, including (i) a coupling of water molecules with the polar lipid head groups (31), (ii) a coupling of membrane curvature with molecular tilt (32), and (iii) the generation of curvature by linear arrays of liquid-state lipid molecules (33).

1.1.4 The Fluid Phase, L_{α}

PCs return to planar lamellar sheets when at a temperature above their T_M , i.e. when the fluid phase forms, also known as the smectic-A phase. The transition to the fluid phase is a first order phase transition (20) where the hydrocarbon chains go from all-*trans* to *trans-gauche* conformation. At T_M the hydrocarbon chains are molten, and are no longer tilted, see Figure 10, (note that T_M is different to the melting point of anhydrous PC which can typically be as high as $230\text{ }^{\circ}\text{C}$ (34)). The permeability of the membrane increases as T_M is approached and hits maximum at T_M . At T_M , there is also an increased rotational mobility for the hydrocarbon chains as well as for the polar head groups. Both the transition temperature and enthalpy values increases with increasing hydrocarbon chain length, which is mainly attributed to the volume expansion and the presence of *trans-gauche* isomerisations (20). The chain length dependence, as shown in Figure 11, shows T_M increasing linearly with increasing chain length. Lewis *et al.* (35) also observed that the difference between T_{pre} and T_M becomes smaller as the chain length

increases as result of T_{pre} increasing more in magnitude than T_M . Furthermore the value of T_M depends on the nature of the hydrocarbon chain and state of hydration of the lipids; (i) decreasing chain length, (ii) increasing chain unsaturation and (iii) increasing the number of water molecules per lipid, thus extent of hydration, are all factors which lead to a lower T_M (34).

Above T_M the d spacing of the fluid phase is larger than that of its corresponding gel phase. For example, the d spacing of DPPC is 67.2 \AA (36) in the fluid phase compared to 63.4 \AA in the gel phase. This is due to the expansion of d_W to such an extent that it masks the decrease in the d_{HH} due to the now *trans-gauche* conformations, which decreases the extension of the hydrocarbon chains in the fluid phase ($d = d_W + d_{HH}$). Concomitantly the area per lipid, A , increases from 47.9 \AA^2 to 62.9 \AA^2 for the DPPC gel phase and fluid phase, respectively.

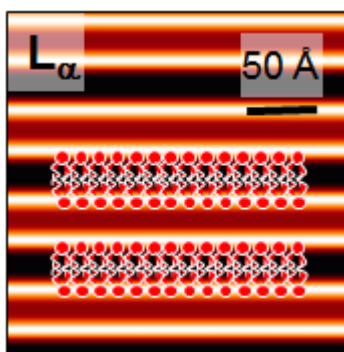


Figure 10: The structure of the fluid phase of PCs showing the stacking of the bilayers. Taken from (20).

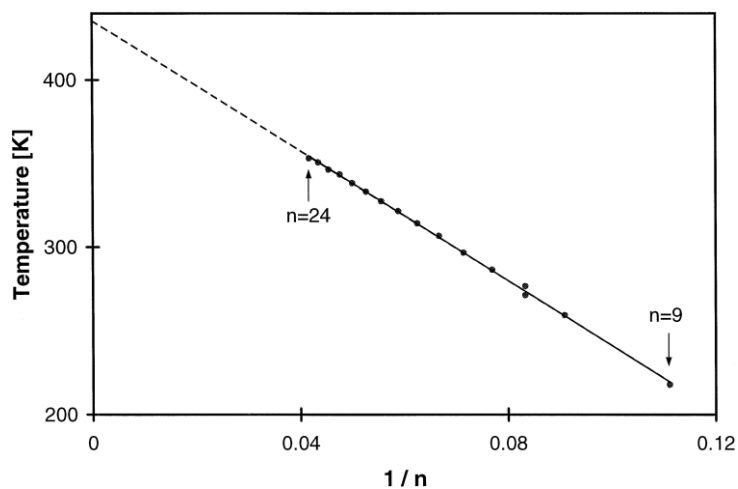


Figure 11: The change in the main transition temperature with change in hydrocarbon chain length for PCs, where n is the length of hydrocarbon chain. Taken from (14).

The increased temperature in the fluid phase leads to increased disorder and lattice defects of the lamellar structure. Hosemann and Bagchi (37) have classified two types of thermal disorder: disorder of the first type and disorder of the second type. The thermal disorder of first type is caused by small fluctuations of the bilayers with equal distances of the bilayer separation, thus maintaining long range order. The thermal disorder of second type, also known as the stacking disorder, describes small variations in the bilayer separation distances, where the lipid membrane moves with respect to its nearest neighbouring membrane. The crystalline long-range order is lost as a result of the thermal disorder of the second type, however *quasi*-long range order is maintained. There is a third type of disorder, and this originates from the increased bilayer bending fluctuations (38). The presence of stacking disorder leads to a loss in the ordering of the lipid system and one therefore speaks also of *quasi*-Bragg peaks being recorded in SAXS regime to highlight the absence of long range order, as presented in Chapter 3.

1.1.5 The Metastable Ripple Phase, P_{β}

An additional gel phase is observed when cooling PCs from the fluid phase to below T_M , known as the metastable ripple phase. This phase coexists with the stable ripple phase and is observed at 39 °C for DPPC. In comparison to the stable ripple phase, which is observed upon both heating and cooling, the metastable ripple phase displays a symmetrical modulation of the bilayer, approximately twice the length of the corresponding stable ripple phase. The bilayer thickness varies, compared to an almost constant bilayer for the stable ripple phase, with the maximum thickness at regions of low water content (23). In order to compensate for the change in bilayer thickness, the tilt angle of the hydrocarbon chains alters between 30-40°. The metastable ripple phase has approximately 30 % higher water content than the stable ripple phase, which is considered to be the reason why it is only accessible upon cooling from the high water content fluid phase (23). This increased water content in the metastable ripple phase is accommodated by the presence of water pockets within the bilayers. The metastable ripple phase is stable for a few hours until it dissociates in to the equilibrium form.

Sengupta *et al.* (30) attempted to produce an EDP for the metastable ripple phase whilst explaining why it is so difficult to achieve an accurate EDP and proposed three possible

structural models. Nevertheless all EDPs of the metastable ripple phase display higher water content than the stable form.

Table 1 provides a summary of the phase transitions which occur at different temperatures for fully hydrated PCs with different hydrocarbon chain lengths. The phase transition temperatures increase with increase in hydrocarbon chain length due to the increased van der Waals interactions between the chains.

Table 1: A summary of the phase transitions and their temperatures for fully hydrated, saturated diacyl PCs. Adapted from (14).

Hydrocarbon chain length	$L_C \rightarrow L_{\beta'}$ T (°C)	$L_{\beta'} - P_{\beta'}$ T (°C)	$P_{\beta'} - L_{\alpha}$ T (°C)
15	20.2 ± 3.0	22.0 ± 2.5	33.7 ± 0.8
16	18.8 ± 3.1	34.4 ± 2.5	41.3 ± 1.8
17	21.6 ± 3.8	42.7 ± 1.1	48.6 ± 0.6
18	26.3 ± 5.2	49.1 ± 2.9	54.5 ± 1.5
19	30.0 ± 4.3	57.2 ± 1.1	60.2 ± 1.1
20	36.9 ± 1.3	63.2 ± 0.8	65.3 ± 1.5
21	28.0	69.4 ± 0.9	70.7 ± 1.6
22	32.1	-	73.6 ± 0.1

1.1.6 Anomalous Swelling

In addition to the ripple phases, PCs have another unique characteristic known as anomalous swelling which is observed upon cooling from temperatures above the fluid phase to T_M . When approaching T_M , the d spacing increases non-linearly which is caused by an expansion in d_w , see Figure 12.

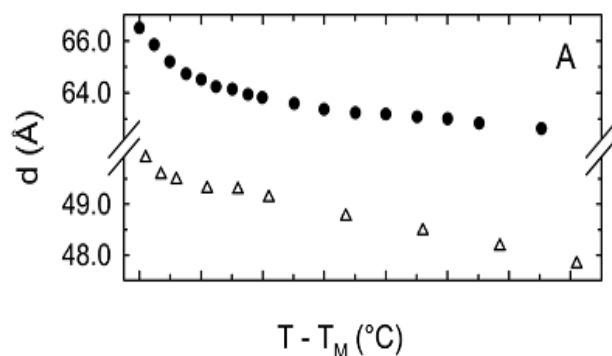


Figure 12: The temperature dependence of the lamellar d spacing. The circles are for 1,2-dimyristoyl-sn-glycero-3-phosphocholine and the triangles are for 1,2-dimyristoyl-sn-glycero-3-phosphoethanolamine bilayers. Taken from (20).

It was found (39) that this swelling behaviour is partially due to a drop in the bending rigidity upon approaching T_M . This in turn, causes an increase in bending fluctuations and consequently, an increase in bilayer repulsion and therefore an increase in d_w .

Studies carried out by Lemmich *et al.* (40) have shown that the anomalous expansion of d_w decreases as the hydrocarbon chain length increases and seems to hit at a maximum for C_{18} chain length. An extensive study into the anomalous swelling regime (41) illustrated this behaviour and showed that the shortest hydrocarbon chain length studied did indeed deviate the most from a linear increase in lamellar repeat distance, see Figure 13. Δd_{an} is defined as the anomalous swelling component, taken as the amount of deviation from a linear increase in the lamellar repeat distance.

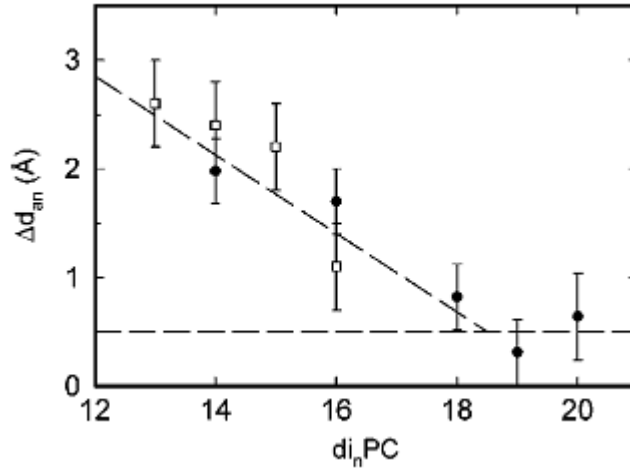


Figure 13: The chain length dependence of the anomalous swelling component, Δd_{an} . Taken from (41).

The increase in d_{HH} is the only cause for the observation of a slight increase in the d spacing for PCs with hydrocarbon chain lengths above 18 (i.e. no contribution from d_w to an increase in the d spacing is given), unlike the shorter chained lipids. Therefore Pabst *et al.* (41) concluded that the anomalous swelling for PCs with hydrocarbon chain length 18 and below are due to a combination of increase in d_w and d_{HH} , whereas those with a hydrocarbon chain length longer than 18 exhibit a small anomalous swelling due to only an increase in d_{HH} .

On a side note, there has been debate on whether the ripple phase and anomalous swelling are associated with each other. Richter *et al.* (42) suggested that the two phenomena are associated whereas Mason *et al.* (43) reported anomalous swelling behaviour in the absence of a ripple phase upon studying phosphatidylethanolamine and therefore suggested that the two phenomenon to exist independently. Pabst *et al.* (41) investigated further by studying the ripple amplitude to see if there is any correlation with the fluctuation amplitude above T_M . The authors showed that there was no correlation and that the ripple amplitude changes with the hydrocarbon chain length without depending on the temperature. Therefore, the conclusion is that the ripple phase forms independently to the anomalous swelling in the L_α phase.

1.2 Phosphatidylcholine Lipid Mixtures and their Thermal and Structural Properties

Mixtures of pure PCs can display different phase behaviours compared to their pure lipid phase behaviour. Garidel and Blume (44) studied two very similar lipids (DMPC and DPPC) and their mixtures; their structures are similar as they have the same headgroup and differ only by the chain length. They found that the miscibility of the lipid mixtures depends on their headgroup structures and charges, the difference in hydrocarbon chain length, and also the phase that is present. For example, they found that the miscibility of the lipid mixtures is higher in the fluid phase than in the gel phase. This is attributed to the increased thermal mobility and fluidity in the fluid phase. For the gel phase, substantial de-mixing and at times, complete immiscibility have been observed, with the largest contribution arising from steric effects, and a presence in chain tilt in the gel phase. Different lipid headgroups would result in different lipid mixture miscibilities; the authors found that lipids with headgroups that have the ability to form strong intermolecular attractive bonds with each other and form un-tilted gel phases. For example, phosphatidylethanolamine lipids would be more immiscible compared to those with less intermolecular forces between the headgroups and are tilted like PCs. The result of immiscibility in lipid mixtures leads to decreased cooperativity at the main transition temperature which can be well recorded by differential scanning calorimetry. The results from 1,2-dimyristoyl-*sn*-glycero-3-phosphocholine, DMPC, and DPPC are presented in Figure 14. The broadening of the main transition peak for the lipid mixtures, as shown in Figure 14a, is a clear visual evidence of the decrease in cooperativity. Figure 14b shows that the cooperativity hits a minimum at 50:50 mixture and leads to a “lens”-shaped plot due to the largest difference between the onset and offset temperatures of the peaks.

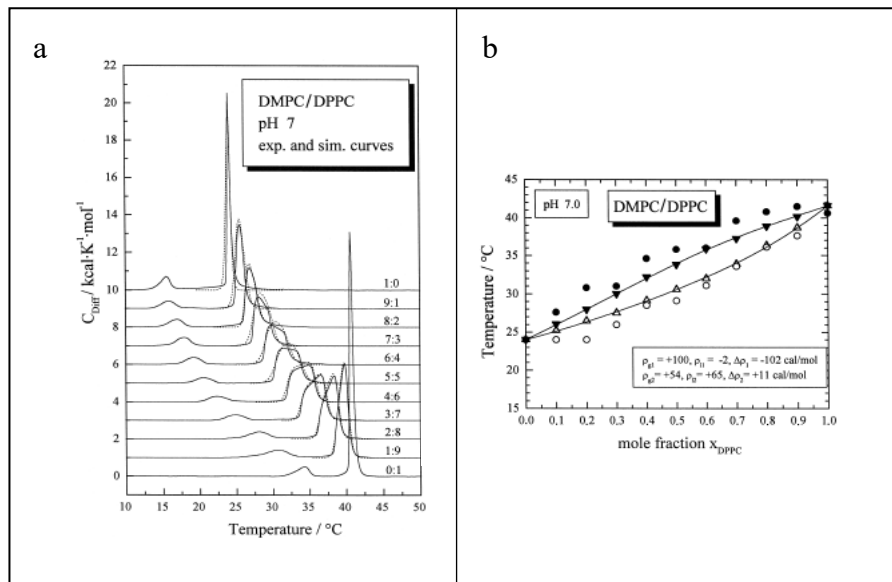


Figure 14: The DSC results of DMPC/DPPC lipid mixtures. a) The DSC thermograms for different molar ratios of the lipid mixtures. b) The change in cooperativity with change in lipid composition by plotting the onset (open) vs. offset (filled) temperatures of the main transition. The triangles are results from simulations and the circles are calculated from experimental results. Both figures taken from (44).

Shimshick and McConnell (45) studied the phase behaviour of DPPC with 1,2-distearylphosphatidylcholine, DSPC, where both lipids are also very similar in structure. DSPC has two extra methyl groups on both hydrocarbons chains compared to DPPC. The authors also found the presence of a two-phase separation of the gel phase and fluid phase at temperatures within the difference of the two PC melting temperatures, Figure 15.

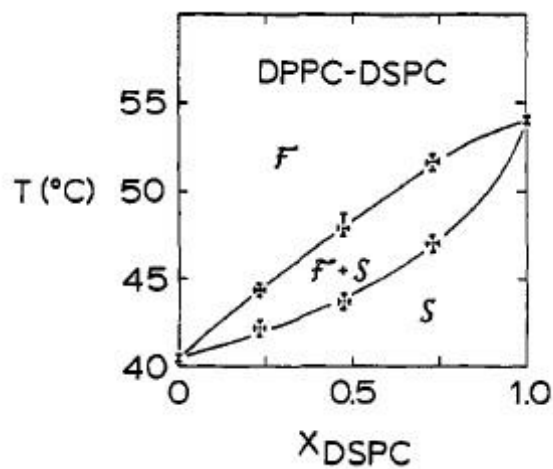


Figure 15: The phase diagram of DPPC/DSPC mixtures. Taken from (45).

If both PCs have diacyl linkages and are above both of the main transition temperatures, then the fluid lamellar phase is observed. However, when the temperature is lowered to below the T_M of the higher melting PC, then a phase separation into gel and fluid domains is observed, and depending on the temperature and composition, the gel phase can be observed as the stable ripple, lamellar gel or even lamellar sub-gel phase. Schmidt *et al.* (46) studied the phase behaviour of 1,2-dioleoylphosphatidylcholine, DOPC, and DPPC mixtures in excess water. The authors used ^2H NMR to study the phase behaviour of the mixture and observed the coexistence of a gel phase and fluid phase in DPPC rich mixtures at temperatures below the T_M of highest melting temperature component, DPPC. In fact, at 24 °C a range of phases are observed corresponding to different ratios of the PCs, see Figure 16. At 24 °C, pure DPPC is in the gel phase as expected, but when the DOPC content is increased a two-phase coexistence region is identified by the NMR spectra. When the DOPC content is above 50%, only the fluid phase is observed at 24 °C. The addition of a second component to the system can lead to the suppression of the T_{pre} , and hence, elimination of the ripple phase, which is observed with DOPC/DPPC mixtures with DOPC concentrations above 5 mol %. The gel phase is transformed into the sub-gel phase for pure DPPC at around 7 °C, although very slowly and it typically requires several days for the transition to complete (24). In comparison, the DOPC/DPPC mixture leads to the gel phase being metastable at temperatures below 16 °C and the sub-gel phase appears. This is reflected in the phase diagram in Figure 17.

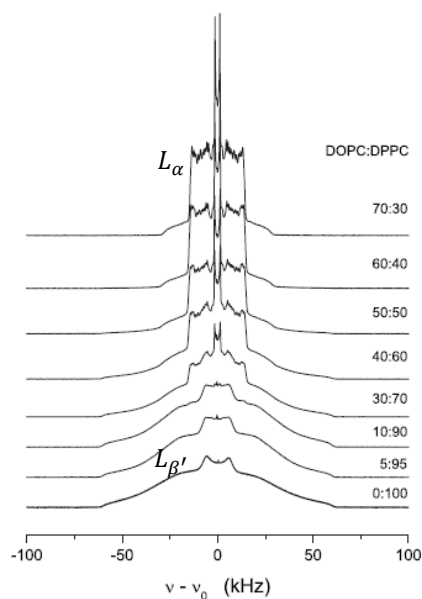


Figure 16: The phases of DOPC/DPPC mixtures at different ratios at 24 °C observed via ^2H NMR with deuterated DPPC. Adapted from (46).

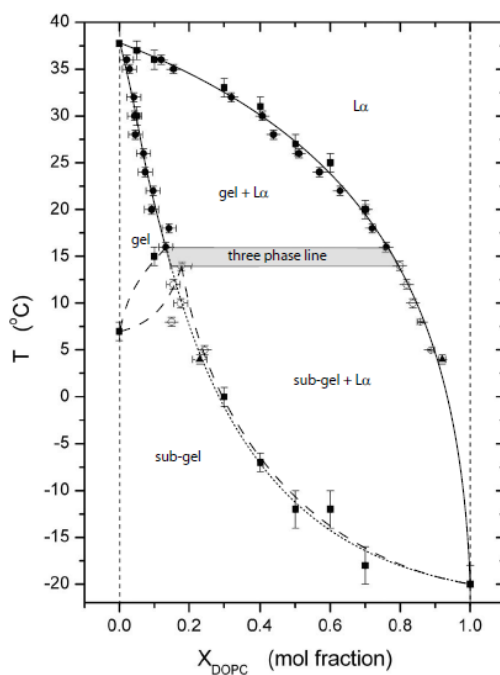


Figure 17: The phase diagram for DOPC/DPPC mixtures. Taken from (46).

Soloviov *et al.* (47) studied the behaviour of DPPC and 1-palmitoyl-2-oleoyl-*sn*-glycero-3-phosphocholine, POPC, mixtures at 3:1 (wt/wt) respectively in excess water and compared the phase transition temperatures and d spacing to pure DPPC. The authors found that the same phase transitions were observed but the d spacing of the

ripple phase was decreased from pure DPPC at around 73 Å to DPPC/POPC at 66 Å. No explanation was given as to why this was observed, but it is tempting to believe that the ripple height profile decreases within the binary mixture.

So how about mixtures of two PCs with different linkages? Lohner et al. (48) studied the phase behaviour of mixtures of DPPC with 1,2-*o*-dihexadecyl-*sn*-glycero-3-phosphocholine, DHPC. Both PCs have C₁₆ hydrocarbon chains and only differ in their linkages; DPPC has an ester linkage and DHPC has an ether linkage, the structure of DHPC is shown in Figure 18. It has already been discussed that at low temperatures DPPC exists in lamellar sheets with tilted lipid chains, whereas DHPC prefers an interdigitated phase, and it appears that the presence of DHPC strongly influences the structure of the mixture DHPC/DPPC. This is observed already at very low temperatures within the sub-gel phase, below the sub-gel transition temperature of DPPC. The presence of small amounts of DHPC in DPPC leads to a strong reduction of the sub-gel transition temperature, and at 15 mol % DHPC, the transition is completely abolished. Whereas the presence of small amounts of DPPC in DHPC does not influence the sub-gel transition and it remains until there are equal molar parts of both PCs, see Figure 19. The influence of the binary mixture on T_{pre} is remarkable. T_{pre} displays a minimum temperature reached at 50 mol% of each PC. Moreover, T_M increases linearly with increasing amount of DHPC added to DPPC. Consequently, the ripple phase is present over a larger temperature range than for pure DPPC, when DHPC is added.

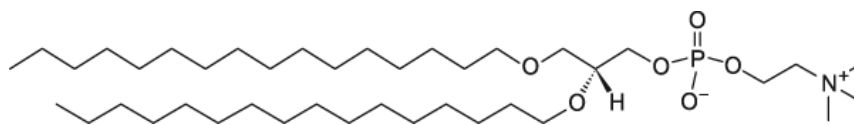


Figure 18: The structure of DHPC.

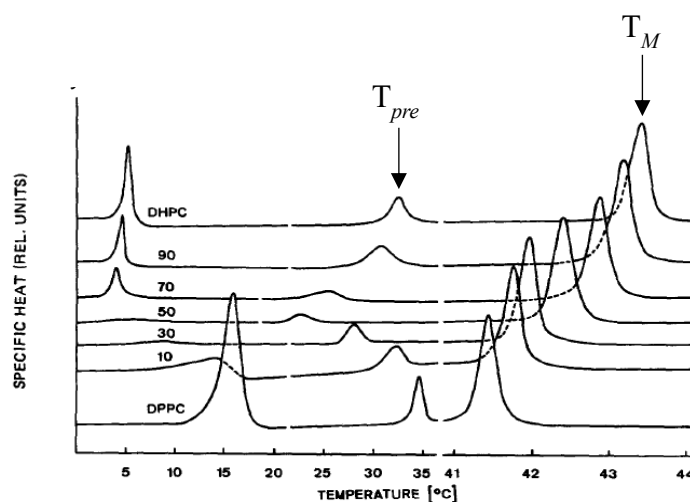


Figure 19: DSC thermograms of DPPC/DHPC mixtures in excess water with their mol % indicated. Adapted from (48).

At low temperatures, increasing amounts of DHPC to DPPC leads to a linear increase in the d spacing, whereas there is a very small effect on the d spacing when adding DPPC to DHPC, see Figure 20. The prominent smaller d spacing for DHPC rich mixtures reflects the interdigitated structure and the negligible effect of DPPC even at 40 mol %. Explanation to the behaviour observed in the mixtures originates from the structures of the pure PCs to start with. DPPC has very little effect on the low temperature DHPC interdigitated structure because the hydrocarbon chain packing is almost ideal (48), so changes to this structure are undesirable. On the other hand, the molecular interactions between the ester linkages in DPPC determine the bilayer lamellar structure. When a DHPC with an ether linkage is introduced, the existing hydrogen bonding network present in DPPC is already lost and so DHPC influences the structure of DPPC much more easily. Figure 21 displays the phase diagram of DPPC/DHPC mixtures.

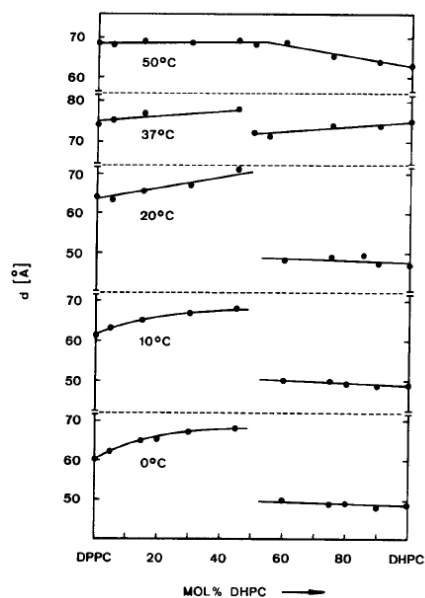


Figure 20: The change in d spacing as DHPC is added in increasing amounts to DPPC. Taken from (48).

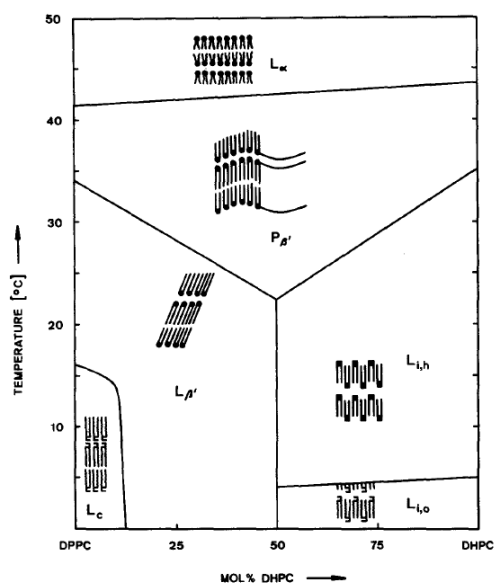


Figure 21: The phase diagram for DPPC/DHPC mixtures. Taken from (48).

Roy and Sarkar (49) studied DMPC/DMPE mixtures to look at the effect of headgroup structure to identical chain length lipids. The authors also observed a decrease in cooperativity for the lipid mixtures compared to their pure lipid behaviour. They found that the incorporation of DMPE to DMPC lead to increased intermolecular forces between the headgroups, as the ethanolamine headgroup is able to hydrogen bond more than the choline headgroup. Figure 22 shows the chemical structure of 1,2-dimyristoyl-

sn-glycero-3-phosphoethanolamine, DMPE. Consequently, the lipids are more tightly packed and aligned, leading to a smaller area per molecule and thus, the enthalpy for the main transition is increased, see Table 2.

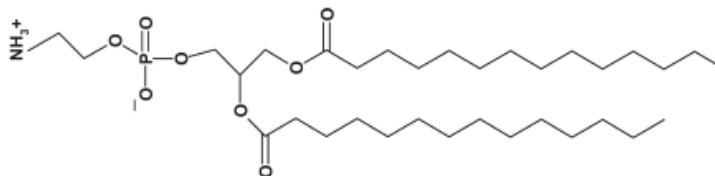


Figure 22: The structure of DMPE.

Table 2: The change in enthalpy for the main transition with change in DMPC/DMPE composition. Adapted from (49).

DMPC/DMPE composition	Enthalpy of main transition (kJ. mol ⁻¹)
100:0	10.24 ± 0.41
90:10	17.66 ± 0.13
80:20	24.14 ± 0.45
70:30	22.34 ± 0.34

The properties of lipid mixtures depend on a range of factors, but they all originate from the structure and properties of the pure lipid. It is found that lipid mixtures are more miscible, if the two lipids are similar in structure and if they are both in the same phase. If the temperature studied of the lipid mixture is below the T_M of one lipid and also below the T_M of the other lipid, then two phases will coexist. Furthermore, differences in the headgroup and the linkage affect the properties of the lipid mixtures. The literature on lipid mixtures has also highlights the variety of techniques that can be applied to the study of lipids; whilst DSC still dominates ((44, 48, 50-52)), new insights have been also achieved from other techniques such as NMR and IR spectroscopy ((46, 52)).

1.3 The Interactions of Phosphatidylcholine Lipid Bilayers with Hydrophilic Small Molecules

The study of interactions between phospholipid membranes is essential not only for applications but also to understand fundamental biological processes. More informed formulation developments can be made, if an in depth understanding on how each component in the formulation interacts with each other. Moreover, a variety of important bioactive, hydrophilic molecules are found in both mammalian and plant cell membranes. It is of deep interest to understand how these molecules that are found in cells affect the well understood structure and properties of phospholipid membranes.

1.3.1 The Influence of Kosmotropes

The introduction of solutes to an aqueous medium induces structural changes to water and, depending on their effects to the hydrogen-bonded networks within the water medium, they can be classified as kosmotropes i.e. “structure makers”, or chaotropes i.e. “structure breakers”. Studies in to the effect of kosmotropes on aqueous phospholipid systems have revealed that the most pronounced change concerns the stability of the lipid phases (53). Kosmotropes appear to favour the formation of high-temperature inverted hexagonal phase and low temperature lamellar gel phases, whereas the intermediate fluid phase is not favoured. This behaviour can be explained by the role of kosmotropes; they stabilise the structure of bulk water, so they tend to avoid lipid/water interfaces and reduce the amount of interfacial water. The fluid phase observes the highest area per lipid molecule due to their high fatty acid chain mobility and *trans-gauche* conformations, therefore kosmotropes tend to destabilise this phase and reduce its existence range. The presence of kosmotropes has shown to increase both the T_{pre} and T_M , with a more pronounced effect on the former. As a consequence of the greater sensitivity of the T_{pre} to kosmotropes, the pre-transition may merge with the main transition at high enough solute concentrations. Koynova *et al.* (53) attribute this greater pre-transition sensitivity due to a lower enthalpy compared to the main transition.

1.3.1.1 Sugars

Sugars are effective at preserving the structure and functional integrity of biological membranes against freeze-drying (54), this is because they replace the water molecules as the membranes are dehydrated. Concomitantly, the T_M of DPPC/sugar systems is similar to that of hydrated DPPC systems (55). But in fact, the effect of sugars to the lipid membrane depends on the hydration level of the lipid and as was investigated by Nagase *et al.* (56). The presence of sugars in DPPC lowers the T_M of DPPC by forming hydrogen bonds between the OH groups of the sugar with the polar headgroup (57), disaccharides have a larger effect on the T_M than monosaccharides due to the higher the number of hydrogen bonds. However, if water is present at 41 wt.% or higher, then the presence of a sugar will increase both T_{pre} and T_M . Nagase *et al.* (56) found that the inclusion of glucose to DPPC with 41 wt.% water, increased the T_{pre} and T_M values by 3.9 and 1.7 °C, respectively; thus exhibiting a typical behaviour of a kosmotrope.

Demé *et al.* (58) also looked at the structural effect of sugars but instead with DMPC. The authors studied different concentrations of glucose and fructose in the L_α phase of DMPC and it was found that already 5 wt.% of sugar compromises the ordering of the membrane where the Bragg peaks broaden and the second order Bragg peak disappears at 20 wt.%. Although the addition of sugar induces disorder to the lipid bilayer, the sample does remain lamellar even at the highest sugar concentration. In addition, the d spacing increases with increasing concentration of sugar and this is due to an increase in d_w . The authors do mention that small hydrosoluble molecules, such as glucose and fructose, will favour repulsive interactions between the membranes and lead to swelling which is also confirmed in (59), which is the most probable reason to an increase in d_w .

The mechanism to the effect of sugars on a lipid membrane also depends on the concentration of the sugar. Tian *et al.* (60) presented both opposing mechanisms; (i) the water replacement mechanism as described above and, (ii) the water entrapment mechanism; whereby the sugar is expelled from the interstitial water layer and concentrates the residual water molecules at the water layer. It appears that the water replacement mechanism dominates at low sugar concentrations and the water entrapment mechanism is preferred at high sugar concentrations (61), although there seems to be discrepancies to what concentration is determinant. Tian *et al.* (60) used molecular simulations to study the interaction of di-mannose with PCs. They found that the location of the sugar depends on the thickness of d_w . Di-mannose has little

interaction with the lipid interface and is easily desorbed from the interface, however, the smaller the water layer, the more chance of the sugar hydrogen bonding to the oxygen atoms below the headgroup of the lipid. Therefore, the thicker the water layer, the less chance of sugar interacting with the lipid. Tian *et al.* also looked at the enthalpy and entropy contributions to sugar-lipid interactions. They found that there is no preference for the sugar to be at the lipid interface or in the bulk water in terms of enthalpy. Whereas it appears that the location of di-mannose is entropy driven; there is an entropy gain, if the water molecules are expelled from the lipid-water interface and into the bulk water by the sugar substitution mechanism, hence this mechanism dominates first. However, there are a finite number of lipid binding sites, and when it becomes fully occupied, further addition of sugar has no other choice but to remain in the bulk of water. This saturation level is at 0.05 M- in other words, at concentrations higher than 0.05 M di-mannose, the water entrapment mechanism becomes preferential.

1.3.1.2 N-methyl Glycines

Betaine and sarcosine are both part of the group of N-methyl glycine derivatives; betaine is also known as trimethyl glycine and sarcosine as methyl glycine, see Figure 23. Rudolph and Goins (62) studied the effect of betaine on the transition temperature of DPPC and found that there is a linear relationship between the increase in both T_{pre} and T_M with the concentration of betaine. T_{pre} is affected more than T_M - the highest concentration of betaine studied was 3 M which increased T_M by 2.5 °C and increased T_{pre} so much that it was completely suppressed from the main transition. At 2 M betaine, the T_{pre} was increased by 5 °C. The effect of betaine on transition temperatures is also reproduced in (63), where the authors also showed that the transition peak broadens by using differential scanning calorimetry, suggesting that the presence of betaine lowers the cooperativity of the transition. Rudolph *et al.* (63) also mentioned that the inner lamellae may be dehydrated as a result of betaine added to the lipid as there have been suggestions that an increase in transition temperature is due to dehydrated lamellae (57).

Like sugars, betaine and sarcosine are also effective cryoprotectants against freeze/thawing of liposomes. Anchordoguy *et al.* (64) studied the effects of sarcosine and betaine and found that much higher concentrations of betaine and sarcosine (1 M and above) are required in order to be effective cryoprotectants compared to sugars.

Furthermore, the authors found that sugars and the two kosmotropes interact with the lipid bilayer differently. Sugars are effective by hydrogen bonding with the lipid headgroups, as mentioned above, by the water replacement mechanism. Betaine and sarcosine on the other hand, favour to remain in the bulk water over the interface, and thus for this reason are effective protein stabilisers by the preferential exclusion mechanism (65). They stabilise proteins by structuring the water in their solvation shells and thus making the water molecules less available to interact with the protein. Therefore, it suggests that betaine and sarcosine will produce the same effect to lipid bilayers by altering the structure of the water and making it less available at the bilayer interface, thus leading to a dehydrating effect on the bilayer.

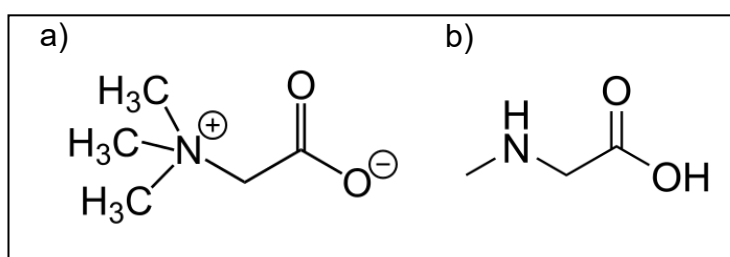


Figure 23: The structures of a) betaine and b) sarcosine.

Rudolph *et al.* (63) presented three possible interaction mechanisms for betaine with a lipid bilayer: (i) betaine interacts directly with the hydrocarbon chains, (ii) betaine alters the long range order of water near the polar residues of the lipid, leading to changes in the spacing between the headgroups and (iii) betaine forms coordinate linkages with either the polar headgroups or their hydration sphere, leading to changes in the packing density of the headgroups. The first hypothesis seems rather unlikely as betaine is hydrophilic and a known kosmotrope which is also supported by Rudolph *et al.* However the authors were not able to attribute their observed results to either hypothesis (ii) or (iii), therefore suggesting that there is a possible combination of mechanisms for interaction.

The effect of betaine on membrane fluidity has also been studied by Popova and Busheva (66). It was found that the incorporation of betaine into isolated thylakoid membranes led to a more rigid membrane, however, any concentration of betaine above 0.02 M did not increase the rigidity of the membrane any further. It was further suggested that the rigidity could be attributed to a decrease in motional freedom in the

headgroup with no change in the fluidity of the bulk lipid phase. Consequently, the permeability of the membrane decreases when betaine is incorporated. This also supports the work of Rudolph *et al.* (63), where their monolayer experimental results suggest that betaine may orient to the lipid headgroup region.

1.3.1.3 Other Kosmotropes

Trimethylamine-N-oxide, TMAO, appears to be the most widely studied kosmotrope and widely known as a “counteracting” osmolyte by stabilising proteins to counteract the denaturing effects of molecules such as urea (67, 68). As a result, the literature has focussed on understanding the mechanism for protein stabilisation and not the effect of TMAO on phospholipid membranes. Zou *et al.* (68) found that TMAO stabilises proteins due to the highly unfavourable interaction between TMAO and the peptide backbone on the protein and thus is excluded from the protein surface and is operating by the preferential exclusion mechanism.

Feng *et al.* (69) studied two urea derived kosmotropes named dimethylurea, DMU, and tetramethylurea, TMU. The X-ray diffraction results show that the addition of these two molecules to 1,2-dioleoyl-*sn*-glycero-3-phosphatidylcholine, DOPE, leads to a decrease in the d spacing, see Figure 24. From this, the authors suggest that both kosmotropes penetrate the bilayer and insert themselves within the interfacial headgroup region. It would be expected, therefore, that the addition of DMU and TMU would lead to an increase in A_C , however this has not been confirmed in any further studies.

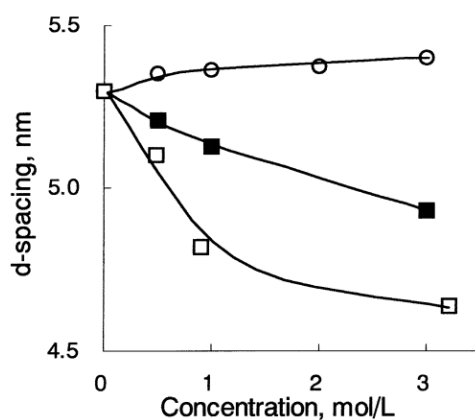


Figure 24: The change in d spacing at 7 °C of DOPE bilayers with increasing concentration of urea (circles), DMU (filled squares) and TMU (open squares). Taken from (69).

1.3.2 The Influence of Chaotropes

Koynova *et al.* (53) studied the influence of chaotropes, known as “water structure breakers”, on lipid phase behaviour. Sodium thiocyanate and guanidine were studied and it was found that they stabilise the fluid phase and expand the temperature range of fluid phase existence by lowering the main transition phase. Chaotropes favour the fluid phase because the area per lipid is larger compared to the gel phase and thus enabling the presence of the chaotrope at its preferred location within the interfacial water region. As a result, the authors found that the addition of both sodium thiocyanate at increasing concentrations leads to a decrease in the main transition temperature of 1,2-dihexadecyl-*sn*-glycero-3-phosphoethanolamine, DHPE.

Urea is a well-known chaotrope and protein destabiliser by interacting directly with the protein (67, 68). Despite some publications attributing urea’s effect on proteins and lipid membranes by an indirect mechanism of weakening the hydrophobic effect (70, 71) on proteins. There is increasing evidence in the literature showing urea interacting directly (72, 73). Feng *et al.* (74) addressed these conflicting arguments by using both experimental and theoretical techniques to study the interaction of urea with DPPC. Urea appeared to not only interact directly with the headgroup of DPPC by hydrogen bonding with the lipid’s amino group, phosphate group and glycerol backbone, but also the interactions are preferential over the interactions of water with lipid. As a result of the direct interaction and membrane penetration, the addition of urea leads to a lateral expansion of the lipid membrane, reflected by an increase in the area per lipid of DPPC, Figure 25. Moreover, the authors reported the fluid phase leads to more favoured hydrogen bonding interactions between urea and the phosphate group of the headgroup, compared to the gel phase.

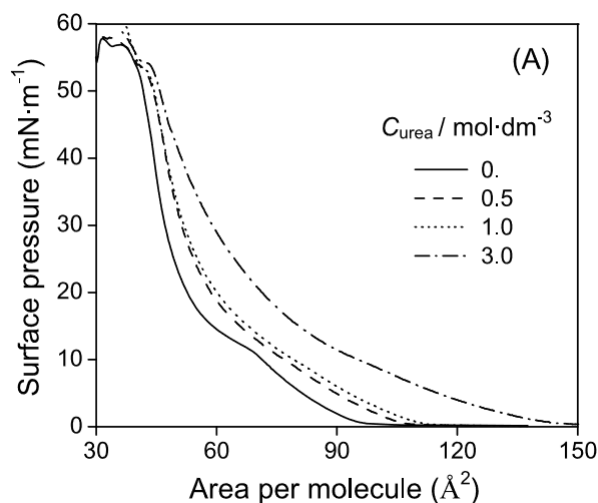


Figure 25: Langmuir isotherms of DPPC monolayers spread on different concentration of urea solutions. Taken from (74).

Sanderson *et al.* (75) found that the addition of urea leads to a decrease in T_M of palmitoleoylphosphatidylethanolamine, POPE and therefore stabilising the fluid phase. This was later confirmed by Feng *et al.* (69) who studied the effect of urea on DOPE who also found that the addition of urea leads to an increase in the d spacing which appears to be a result of a decrease in the van der Waals attractive forces between two bilayers, see Figure 24.

In summary, the addition of kosmotropes favours the gel phase as these molecules avoid the interface, leading to a decrease in the interstitial water thickness, d_w . As the gel phase is favoured in the presence of kosmotropes, they lead to an increase in both, T_{pre} and T_M . In comparison, the addition of chaotropes favours the fluid phase as they penetrate through to the interface and increases d_w . The addition of chaotropes leads to a decrease in T_M . Table 3 summarises the effects of the aqueous soluble molecules discussed above on the thermal and structural behaviour of phospholipids.

Table 3: A summary of the effect of aqueous soluble molecules on the thermal and structural behaviour of phospholipids.

Molecule	Thermal Effect	Structural Effect	Reference
Betaine	Increases T_{pre} and T_M	D_w decreases	(62)
Sodium thiocyanate	Decreases T_M	Unknown	(53)
DMU, TMU	Unknown	D spacing decreases	(69)
Urea	Decreases T_M	D spacing increases	(69, 75)
Sugars	Increases T_{pre} and T_M	In general: D_w decreases at low concentrations D_w increases at high concentrations	(53, 57, 58)

1.4 The Structure and Properties of Humectants

Betaine, sarcosine and acetaminde monoethanolamine, AMEA, are aqueous soluble molecules known as humectants. Humectants are hygroscopic substances used as a source of moisture by attracting and binding to water molecules. Smiatek *et al.* (76) have attributed this hygroscopic nature due to the zwitterionic ($N^{(+)}$ and $O^{(-)}$) groups in their structure, see Figure 23.

Humectants are known to be used in many personal care products, particularly skin creams and haircare products (77). When used in dermatological formulations, humectants work by attracting water to the stratum corneum, therefore providing rehydration and a moisturising sensation to the user. For haircare products, humectants work by softening the hair, making the texture of the hair feeling smoother. Aside from personal care products, humectants are also found in other products due to their unique properties. Humectants have the ability to alter the freezing point of some molecules leading them in to anti-freeze products, they can also be used as preservatives or emulsion stabilisers as they can alter the viscosity and retard the evaporation water of a given system (77). These molecules are also examples of kosmotropes, which support the bulk water hydrogen bonding network and hence are favoured to be in the bulk of the water and be excluded from interfacial regions. As a consequence, in fully hydrated

lipid systems, kosmotropes would favour gel, L_{β} , and hexagonal, H_{II} , phases over the fluid phase, L_{α} , as the fluid phase has the largest area per lipid (53).

Betaine and sarcosine are known to be osmolytes (66, 78-82), which are molecules that are osmotically active and have the ability to protect microorganisms against stresses such as dehydration, as well as acting as cryoprotectants. Osmolytes are also well known to be effective protein stabilisers (78, 83, 84) by means of the “preferential exclusion” mechanism, whereby they are excluded from the protein hydration sphere or protein surface in solution, eliminating any unfavourable interactions between the osmolyte and the protein. As a result, the concentration of osmolyte close to the protein is lower compared to the bulk (76). Furthermore, betaine is effective in maintaining membrane integrity and retention of water within the cell (78, 85), as well as being a methyl donor in biological functions such as converting homocysteine to methionine (78, 82) and evidence on its role in the human health and possible ability to improve athletic performance have been published (86). Sarcosine has many similar traits as betaine due to its similar chemical nature. In addition to being an osmolyte, sarcosine has shown evidence for improving the memory of patients with schizophrenia (87), and it is also found to accelerate the rate of photosynthesis (88).

The addition of betaine or sarcosine to water effects the properties of water by supporting its tetrahedral hydrogen bonding network (80); Thoppil *et al.* (78) found that the enthalpy of dilution for betaine is an exothermic process. Furthermore, the density of water increases with addition of increasing amount of betaine or sarcosine to water (80, 84). There have been various studies in to the first hydration sphere of betaine both by experimental and computational methods. Venkatesan and Lee (89) found that there are five regions surrounding betaine which would exhibit hydrogen bonding interactions of water with betaine, with three relatively strong interacting regions and two weaker interacting regions. Furthermore, they found that the interaction of seven molecules with one betaine molecule lead to the most stable system, with four water molecules hydrogen bonding directly with betaine and three water molecules forming a water-water ring network around betaine, Figure 26a. Similarly for sarcosine, three hydrogen bonds between water and sarcosine are formed (87, 88) and four water molecules forming a ring of water-water hydrogen bonds around sarcosine, Figure 26b. In addition, the formation of sarcosine-water hydrogen bonds increases the hydrogen bond lifetime from 1.56 ps for pure water to 3.81 ps for a sarcosine-water hydrogen bond (80).

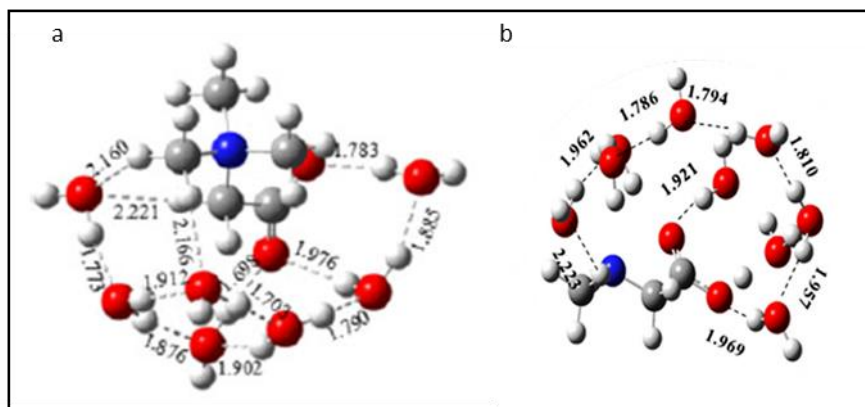


Figure 26: The hydrogen bond interactions in the first hydration shell of a) betaine with 7 water molecules and b) sarcosine with 9 water molecules. Taken from (89) and (87), respectively.

This review has covered the properties of pure fully hydrated phosphatidylcholines, their mixtures and also their interactions with bioactive molecules with a main focus on chaotropes and kosmotropes. It is clear that the literature holds a wealth of information on pure phosphatidylcholine systems, however the ripple phase remains inconclusive. The origin of the ripple phase and the detailed structure of the metastable ripple phase are yet to be identified. Further, the properties of lipid mixtures have been studied by a variety of experimental techniques. Koynova and Caffrey have provided a very useful index summarising the publications on phospholipids as of 2002 (90). It has been noted however, an apparent lack of X-ray and or neutron scattering results to reveal the nanostructure of lipid mixtures. Finally, the interaction of PCs with hydrophilic molecules has been reviewed. The change in properties to the lipid depends on the nature of the molecule, for example, whether they are a kosmotrope or a chaotrope. Determining the mechanism of interaction has proven difficult and subject to debate for various systems and the interaction of kosmotropes with lipid bilayers remains greatly unknown.

1.5 Research Aims

The objective of this thesis is to investigate the structure and stability of phospholipid membranes, specifically PCs, to temperature change and interactions with other components found typically in dermatological formulations. Different systems of differing complexity will be studied to suit their aims.

Firstly, humectants are used widely in skin creams due to their hygroscopic properties, thus their influence on the nanostructure and phase behaviour of DPPC will be studied. It is envisaged that their effect on DPPC will elucidate their interactions with DPPC. DPPC has been chosen as the model membrane not only due to the wealth of existing literature available for reference, but also due to its vast use as a main structural component in commercial formulations. The outcomes of this study will provide information on the fundamental effects of humectants and their interactions with phospholipids; two typical components in dermatological formulations. Furthermore, it may also provide insights commercially; for example, typical formulations may comprise more than one humectant, formulators may wish to decrease the number of humectants for economical reasons and the outcomes of this study may identify which humectant is the best performing and worst performing.

Secondly, commercial lipid samples are typically used in dermatological formulations to save manufacturing costs. Commercial lipid samples may consist of a mixture of lipids as well as containing impurities such as residual solvents and free fatty acids. Therefore, the nanostructure and thermal properties of a commercial lipid sample containing DPPC and DSPC will be compared to its equivalent higher purity lipid mixture, to assess its comparability to pure lipid systems. Additionally, the properties of lipid mixtures of DPPC and DSPC at different compositions will be studied. The outcomes of this study would indicate how representative the higher purity phospholipids are compared to commercial lipids. Thus, formulators would be able to understand better the behaviour of the commercial lipid mixture and how it compares with model lipid mixtures used mainly in research publications.

Thirdly, more complex oil-in-water emulsions will be investigated, containing three main components: a commercial lipid, an oil and a polymer. The stability of the lipid in such a multi-component formulation will be understood and offer insights on how the overall structure of a skin cream formulation in the bottle may be found. Furthermore, information on what structure the multi-component formulation forms after being applied to the skin will be studied. To achieve this, a “drying” procedure has been performed to simulate conditions of the film formed after a user applies the skin cream. This study will provide information on the structure and thermal behaviour of formulations more similar to that of commercial products which can be compared to that of the first two studies to see how the increase in number of components affects the stability of the main structural component - the lipid.

The outcomes of these three objectives will not only offer new insights on fundamental interactions of small aqueous soluble molecules (humectants) with model lipid membranes and further enhance the scientific literature and understanding on lipid mixtures. The learnings will also enrich industry and enable enhanced and more informed decisions to be made on how to develop upon formulations. For instance, phospholipids are used in dermatological formulations to deliver tightly packed lipid systems mimicking the packing of the ceramide lipids found in the skin. The packing of PCs to achieve this property is in the lamellar gel phase, thus it is of interest to stabilise this phase. The outcomes of this thesis will enable industry to understand how formulations can be developed to ensure the lamellar gel phase is delivered to the skin.

Chapter 2 Materials and Methods

2.1 Materials

DPPC and DSPC were both purchased from Avanti Polar Lipids, Inc. (Alabama, U.S.) and used without further purification. Betaine was purchased from Amino GmbH (Frellstedt, Germany), sarcosine was purchased from Chengdu Chengnuo New-Tech Co. Ltd (Chengdu, China) and AMEA (commercial name as Incromectant AMEA 70-LQ-(MH)) from Croda (Goole, U.K.). Phospholipon 90H, P90H, was purchased from Phospholipid GmbH (Cologne, Germany). The solvents chloroform and methanol were from VWR International Ltd. (Lutterworth, U.K.). Filtered MilliQ water (filtered and deionised water 18.2 MΩcm at 25 °C) is referred to as water from hereon. Samples for the novel multi-component formulations were supplied by GSK Ltd. already prepared.

2.2 Sample Preparation

2.2.1 Preparation of Pure DPPC and DSPC Liposomes

5 wt.% fully hydrated DPPC or DSPC pure liposomes were prepared with water. The lipid/water mixtures were then heated to 55 °C and 65 °C, for DPPC and DSPC respectively, and vortexed repeatedly to achieve homogenous mixtures. The samples were then left to incubate at 4 °C overnight.

2.2.2 Preparation of DPPC Liposomes with Humectant

Weighted amounts of DPPC were dissolved in chloroform/methanol (2:1 ratio) solvent. Solutions of the humectants were made by dissolving an appropriate amount of the humectant with milliQ water. In order to guarantee homogeneous concentrations of the humectants within the forming of multilamellar vesicles, MLVs, and in bulk, (i) the humectant solution was then added to the DPPC dissolved in chloroform/methanol resulting in a concentration of DPPC of 5 wt.%. (ii) The mixture was then vortexed and heated to 55 °C, subsequently placed under vacuum for 15 minutes. (iii) This procedure was repeated three more times and then the sample was left under vacuum until a thin, dry film remained. (iv) The sample was then rehydrated with filtered milliQ water,

keeping DPPC at 5 wt.%. (v) Finally, the sample was repeatedly heated at 55 °C and vortexed, ensuring a homogenous mix. The sample was then left to incubate at 4 °C overnight.

2.2.3 Preparation of Phospholipon 90H Liposomes

5 wt.% of P90H was hydrated with water and heated to 65 °C. The mixture was heated and vortexed repeatedly to achieve a homogenous mixture. The sample was then left incubate at 4 °C overnight.

2.2.4 Preparation of DPPC/DSPC Mixture Liposomes

An appropriate amount of each lipid was weighed to reflect the corresponding composition and dissolved in chloroform:methanol (2:1) solvent. The sample was then placed under vacuum so that the solvent was evaporated to leave a thin film. The film was hydrated with water to achieve 5 wt.% total lipid concentration. The lipid mixture was then heated to 65 °C and vortexed repeatedly to achieve a homogenous mixture. The sample was then left incubate at 4 °C overnight.

The compositions of the lipid mixtures are in wt.% to be easily comparable with the P90H lipid sample. The 50 wt.% DSPC sample is equivalent to 48 mol% DSPC, therefore, with a 2 % difference, the wt.% samples are comparable to mol% compositions.

2.2.5 Preparation of Novel Multi-Component Formulations

The preparation of the novel multi-component samples was conducted at GSK and used as received. Details of the formulations are provided in Table 4.

Two types of samples were measured for the each novel multi-component formulation. “Wet” samples are referred to as measurement of the sample taken directly from the bottle with no modification. “Dried” samples refer to the multi-component formulation sample having undergone a drying protocol. Each sample was loaded into both sides of an Anton Paar paste cell, see Figure 27, then without closing the paste cell, was placed in to a vacuum desiccator over colour indicating silica gel for 1 hour. The relative humidity and temperature were recorded using a dial thermohygrometer (Shanghai

QualityWell Industrial Co Ltd, China) for each sample which ranged between 6-18 % R.H. and 19-23 °C, respectively. The dried samples were prepared by the described method to simulate conditions of when the cream would be applied on to the skin by a user and left to dry (91).

Table 4: The list of structuring components and their concentration (wt.%) in each formulation studied as novel multi-component samples.

Platform	Material	Formulation code							
		0,0,0	0,1,0	0,0,1	0,1,1	1,0,0	1,0,1	1,1,0	1,1,1
Lipid structuring	Alcohol 1	0.375	0.375	0.375	0.375	1.500	1.500	1.500	1.500
	Acid	0.225	0.225	0.225	0.225	0.900	0.900	0.900	0.900
	Alcohol 2	1.063	1.063	1.063	1.063	4.250	4.250	4.250	4.250
	Phospholipon 90H	0.313	0.313	0.313	0.313	1.250	1.250	1.250	1.250
	Isostearyl isostearate	0.225	0.225	0.225	0.225	0.900	0.900	0.900	0.900
Shea triglycerides	-	0.000	0.000	15.000	15.000	0.000	15.000	0.000	15.000
Polymer	-	0.200	0.500	0.200	0.500	0.200	0.200	0.500	0.500



Figure 27: A photograph showing both sides of an Anton Paar paste cell filled with sample before being placed inside a vacuum desiccator.

2.3 X-ray Scattering

X-ray scattering is a non-invasive technique in which planar lipid model membrane systems are commonly investigated with unilamellar vesicle, ULV, and MLV dispersions. Specifically, phospholipid MLVs are generally spherical in shape and consist of stacks of bilayers giving rise to a *quasi* long-range order, see Figure 28. Note that these liquid crystalline phases are known as the smectic phase, in which the bilayer stacks display a stacking disorder of second type (37), i.e. the crystalline long range order is not conserved, see Section 1.1.4 for more details. The overall size and the liquid crystalline order of phospholipid bilayers make both X-ray and neutron scattering suitable methods to study their nanostructure.

X-rays are scattered by electrons present in an atom and the scattering power is proportional to the number of electrons (92). The principles of X-ray scattering have been thoroughly explained by Glatter and Kratky (93), and Bragg's Law (94) specifies that the special case of X-ray diffraction, in which coherent scattered waves from the sample interfere constructively leading to a diffraction peak, or Bragg peak, and satisfy the equation:

$$2d\sin\theta = n\lambda \quad (1)$$

where d is the lattice spacing of the sample, 2θ is the scattering angle, n is an integer and λ is the wavelength of the incident and scattered wave. Equation 1 expresses that for scattered waves to interfere constructively, they must remain in phase and the difference in path length of two parallel waves is equal to an integer multiple of the wavelength. Due to the stacking disorder of second type, application of X-ray scattering on regular stacks of phospholipid bilayer sheets gives rise to *quasi*-Bragg peaks at constantly separated scattering angles (once more, MLVs produce *quasi*-long range ordered structures and not infinite long range order). When expressing the position of the *quasi*-Bragg peaks in form of the wave vector q_h , we can write:

$$q_h = \frac{2\pi h}{d} \quad (2)$$

where h is the diffraction order (Miller index) and d is the lattice spacing, as defined in Figure 28. Therefore, using X-ray scattering easily yields information on the d spacing from the position of the Bragg peaks. Furthermore, other structural information such as the head-to-headgroup distance, d_{HH} , and the interstitial water layer thickness, d_w , can

be gathered from X-ray data via less-trivial data analysis methods to generate EDPs. D -spacing, d_W and d_{HH} are related by the following equation:

$$d = d_{HH} + d_W \quad (3)$$

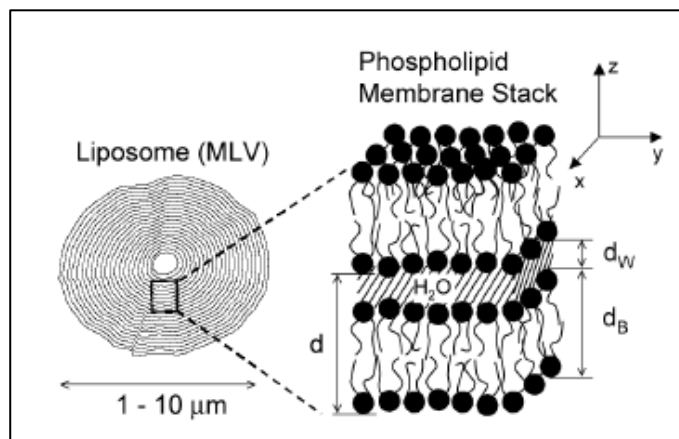


Figure 28: An illustration of the structure of phospholipid bilayers in multilamellar vesicles and definition of their structural parameters. Taken from (20).

2.3.1 X-ray Measurement

Both SAXS and WAXS were performed using a SAXSpace instrument (Anton Paar GmbH, Graz, Austria) equipped with a sealed-tube Cu-anode operating at 40 kV and 50 mA ($\lambda = 0.154$ nm). 1D scattering patterns were recorded with a Mythen micro-strip X-ray detector (Dectris Ltd, Baden, Switzerland). For the experiments, the detection range spans from a minimum scattering vector of $q_{min} = 0.1$ nm⁻¹ to $q_{max} = 18$ nm⁻¹ ($q = (4\pi/\lambda) \sin\theta$), where 2θ is the scattering angle. All samples apart from the novel multi-component samples were loaded in 1 or 1.5 mm diameter quartz capillaries and were then placed in to the temperature controlled sample stage equipped with a Peltier element (TCStage 150, Anton Paar, Graz, Austria). The novel multi-component samples were loaded into a paste cell assembled with thin Kapton windows and SAXS only measurements were conducted. An illustration of the X-ray set-up is presented in Figure 29. The temperature protocol of each experiment is detailed in Table 5. The temperature was held for 10 minutes before a measurement was taken by X-ray exposure for 30 minutes.

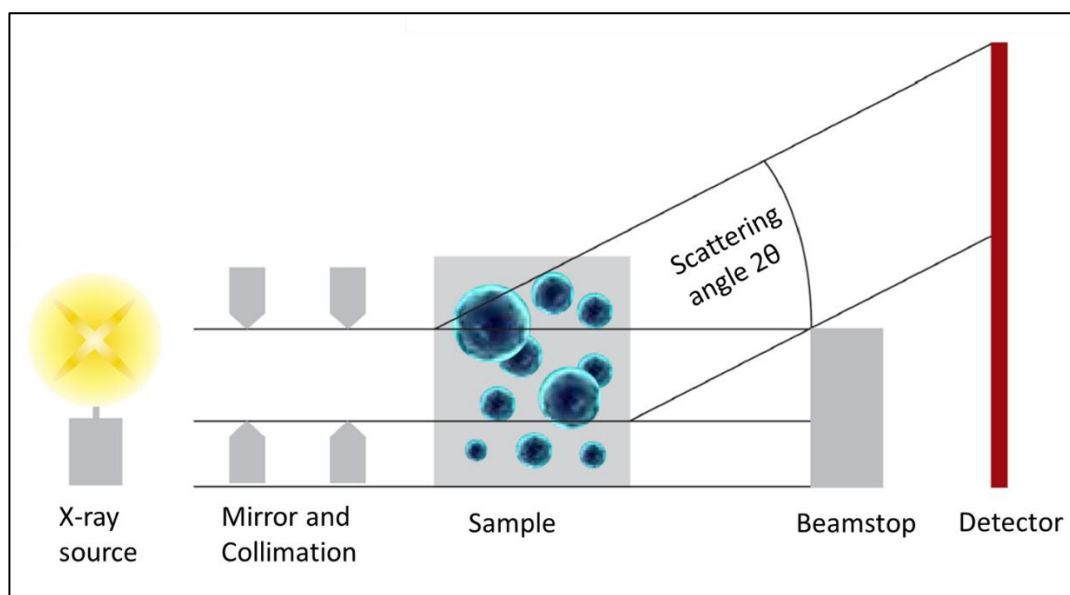


Figure 29: An illustration of the X-ray beamline set-up for measurements.

Table 5: The temperature protocol for X-ray experiments conducted on each sample type.

Sample name	Temperature protocol
DPPC liposomes	X-ray exposures were taken at every 2 °C from 25-51 °C.
DPPC liposomes with humectant	X-ray exposures were taken at every 2 °C from 25-51 °C. The X-ray exposure was increased to measure at every 0.5 °C between the temperatures 40-45 °C,
P90H liposomes	X-ray exposures were taken at every 5 °C from 25-60 °C.
DPPC/DSPC mixture liposomes	X-ray exposures were taken at every 2 °C from 30-60 °C.
Novel multi-component formulations	The wet samples were measured at every 5 °C from 25-70 °C. The dried samples were measured at the same temperatures as the wet samples with the addition of a measurement at 32 °C.

2.3.2 Data Reduction

Background measurements were taken for SAXS and WAXS data in order to perform the data reduction. Data were obtained for the empty capillary, the empty paste cell, the capillary filled with the relevant humectant concentration solution and paste cell filled with water at 25 °C with 30 minutes X-ray exposure. The position of the primary beam was corrected for all data using SAXStreat software (Anton Paar GmbH, Graz, Austria) and the intensity of the primary beam was normalised for all data using SAXSQuant software (Anton Paar GmbH, Graz, Austria) to account for the transmission correction

(95). Then subtraction of the empty capillary or paste cell from all data, including the appropriate sample holder filled with aqueous solution, was performed. To obtain the final reduced scattering curve of the sample, subtraction of the capillary or paste cell filled the relevant aqueous solution is required. To account for the excluded aqueous background volume in the sample, a multiplication factor is implemented (93) and reflect the 95 wt.% of aqueous solution present in the sample for my studies. The multiplication factor not only reflects the 95 wt. % ($\times 0.95$) of aqueous solution present in the sample but also accounts for interactions between water, the humectant and DPPC. This scaling factor results in the sample curve being shifted vertically such that the curve of the sample holder filled with aqueous solution fits just under the baseline of the sample curve, see Figure 30.

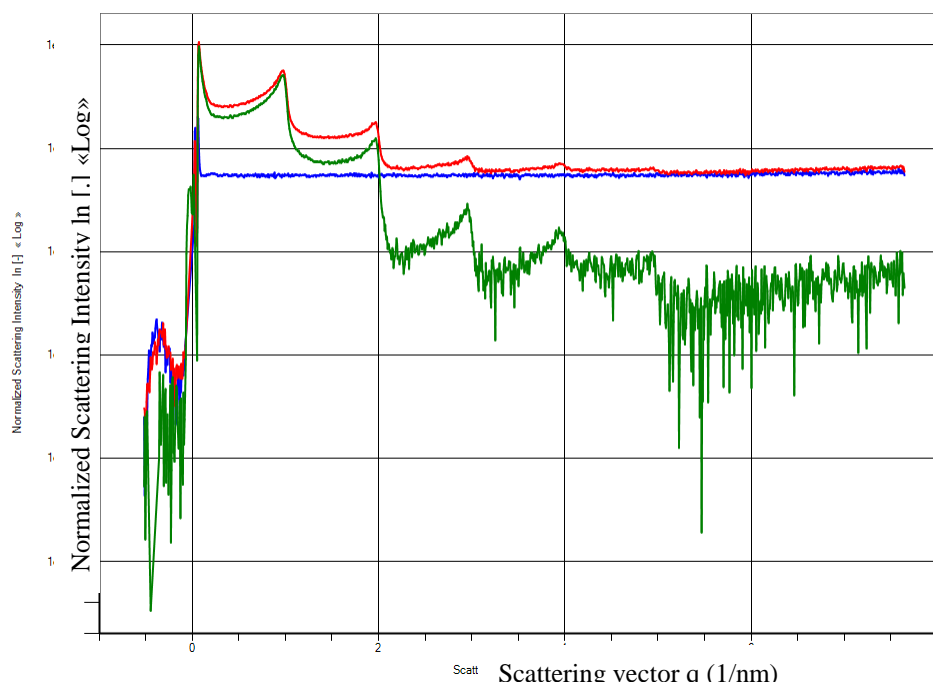


Figure 30: Example of subtracting a capillary filled with MilliQ water from the DPPC sample curve. The red line is the DPPC curve after subtraction of the empty capillary curve. The blue line is the capillary filled with water curve after subtraction of the empty capillary curve. The green line is the DPPC curve after subtraction of the capillary filled with water curve after using a multiplication factor.

In Figure 30 it can be further seen, that the recorded Bragg peaks are not symmetrical, but smeared on their low q side. This smearing effect is a result of the machine set-up with a line collimation system. In order to fit the Bragg peaks properly for data analysis, the scattering pattern needs to be either (i) de-smearred beforehand or (ii) the applied

peak-fitting function needs to be smeared to fit the scattering data. Details on smearing and de-smearing can be found in (93). When fitting globally the fluid lamellar phases the model function is smeared, while de-smearing was performed for the gel phase when calculating the electron density profiles, EDPs, as described in Section 2.3.4. De-smearing was also performed by using the SAXSQuant software before analysing the WAXS data of the DPPC liposomes and DPPC liposomes with humectants, to enable the appropriate calculation of A_C in the gel phase, as described in Section 2.3.5.

2.3.3 Determining the d spacing

For the the gel phase of the PC-liposomes and the novel multi-component samples, the d spacings were determined by plotting the SAXS results and taking the peak position of each peak by cursor in OriginPro (Origin lab, Silverdale Scientific Ltd., Buckinghamshire, U.K.), followed by fitting the linear regression of peak position vs the order of the peak, see Figure 31. The d spacing is then calculated by the following equation:

$$d \text{ spacing} = \frac{2\pi}{\text{slope}} \quad (4)$$

Where $slope$ is the gradient of the linear regression.

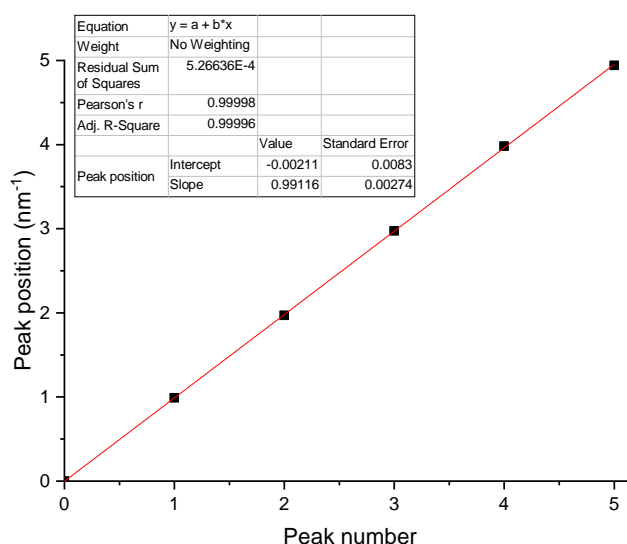


Figure 31: Example of performing a linear regression of the peak positions to calculate the d spacing in the gel phase.

For the fluid phase of the liposomes, the d spacing was determined by the global fitting analysis of the SAXS curve, described in the next section.

2.3.4 Calculating Electron Density Profiles

There are several methods to obtain the EDP of the lipid bilayer perpendicular to the planes, which have been reviewed in (96). As long as at least four *quasi*-Bragg peaks are recorded by X-ray scattering of non-swollen phospholipid water systems, then reasonable EDPs can be generated by performing a Fourier transform on the intensities of the peaks (97, 98). This is the case for the gel phase of DPPC, whereas for the less ordered fluid phase, an alternative method of performing global fitting analysis for the full- q range is required.

EDPs were calculated for both the gel phase and the fluid phase. For the gel phase, fitting of each peak is performed to collect information on the peak position, amplitude of the peak, and the peak area. The fitting of the peaks is conducted in Matlab (MathWorks, Cambridge, U.K.) where after firstly de-smearing the peak, peak fitting by a Lorentzian function is performed. Once these parameters are calculated, a Fourier transform can be performed to obtain the electron density contrast:

$$\Delta\rho(x) = \sum_{h=1}^{h=\max} \alpha_h F_h \cos\left(\frac{2\pi x h}{d}\right) \quad (5)$$

where, α_h are the phase factors, x is the distance in real space, d is the repeat distance or lattice spacing and F_h are the form factors for each peak that have been determined by:

$$F_h = \sqrt{I_h \cdot h^2} \quad (6)$$

The intensity, I_h , is hereby identified as the peak area of the Bragg peak and is multiplied with the squared Miller index (peak order), h^2 , considering the Lorentzian correction (this is a geometrical correction and details can be found in (99)). The phase factors, α_h , of each form factor for centrosymmetric structures are either +1 or -1 and are well known in literature for DPPC and DSPC (22) as -1, -1, +1, -1 for $h = 1, 2, 3, 4$.

For the fluid phase, a global fitting method according to the modified Caillé theory was adopted to account for the lattice disorder in fluid smectic phases, which is well described in (97, 100). The model fits the full q -range of the SAXS curve by using the following equation:

$$I(q) = (1 - N_{diff}) \frac{S(q)|F(q)|^2}{q^2} + N_{diff} \frac{|F(q)|^2}{q^2} \quad (7)$$

where $S(q)$ is the 1D lattice structure factor (based on the Caillé theory (38)), $F(q)$ is the form factor, whereby the bilayer model used has been described elsewhere (101), N_{diff} is a scaling constant considering different fractions of MLVs compared to ULVs present in the system and $1/q^2$ is the Lorentz correction. Structural parameters d , d_{HH} and d_W are obtained directly from the fits to the scattered intensities ($d = d_W + d_{HH}$). Mean fluctuations of the membrane position, σ , were derived from the Caillé parameter, η (102), which is obtained directly from the fit:

$$\sigma = \sqrt{\eta} \frac{d}{\pi} \quad (8)$$

The Caillé parameter is a measure of the membrane fluctuations, which are increased in the fluid phase compared to the gel phase. The Caillé parameter is defined as:

$$\eta = \frac{\pi K_B T}{2d^2 (BK_C)^{1/2}} \quad (9)$$

where B is the compression modulus and K_C is the bending rigidity of the membrane.

2.3.5 Calculating the Area per Lipid Chain

A_C is calculated for both the gel and the fluid phase. For the gel phase, the de-smearred WAXS peak at 25 °C was taken and a peak fit was performed using OriginPro software, see Figure 32. The two values of the peak centres obtained from fitting the WAXS peak were taken and used to calculate A_C of the gel phase by Equation 10 (103):

$$A_{C(gel)} = \frac{d_{20}d_{11}}{\sqrt{1 - \left(\frac{d_{11}}{2d_{20}}\right)^2}} \quad (10)$$

where d_{20} is the corresponding d spacing for the centre of the first peak (q_{20}) and d_{11} is the corresponding d spacing for the centre of the second peak (q_{11}). For the fluid phase, a peak fit using OriginPro of the WAXS data at $T_M + 2$ °C (for the X-ray results) was executed and the peak centre value was used as q in Equation 11 (104).

$$A_{C(fluid)} = 1.32 \left(\frac{9\pi}{4q}\right)^2 \quad (11)$$

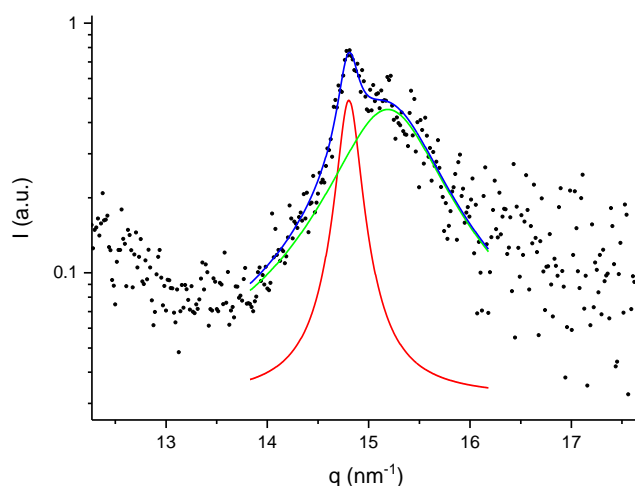


Figure 32: The de-smear WAXS curve of the gel phase of DPPC with peak fitting performed by OriginPro. The red and green curves are the fit results of peak 1 at q_{20} and 2 at q_{11} , respectively. The blue curve is the cumulative peak fit result.

2.4 Differential Scanning Calorimetry

DSC is another non-perturbing experimental technique which measures the change in heat flow for the sample as it undergoes a thermal treatment and compares it to a reference sample (usually water or air). The difference in the heat change can give information on the thermal behaviour of the sample. For instance, any thermal events such as phase transitions can be monitored by DSC; whenever a thermal event occurs, there will be a change in the difference in the heat flow of the sample compared to the reference and this is recorded. Phospholipids in excess water undergo transitions to different liquid crystalline lyotropic phases; for the case of the hydrated phosphatidylcholines studied, they will self-assemble in to the lamellar phase of which, there are different sub-phases, see Chapter 1. The phase transition temperatures and their corresponding enthalpy values have been recorded by DSC.

2.4.1 Differential Scanning Calorimetry Measurements

DSC was performed on a DSC 8000 (Perkin Elmer, Massachusetts, U.S.A.), calibrated with Indium and Zinc. The temperature protocol for each sample is displayed in Table 6, 1 °C/min scan rate was used for each experiment. The mass of each sample was

recorded as it was filled into hermetically sealed aluminium pans. The reference cell used is a sealed aluminium pan containing only air.

Table 6: The DSC temperature protocol for each sample type.

Sample name	Temperature protocol
DPPC liposome	The sample was heated from 25-51 °C
DPPC liposome with humectant	The sample was heated from 25-51 °C
P90H liposome	The sample was heated from 25-65 °C
DPPC/DSPC mixture liposome	The sample was heated from 25-65 °C

2.4.2 Determining the Transition Temperatures and Enthalpy Values

For the liposome samples, two phase transitions are observed through the temperature range studied, T_{pre} and T_M . The transition temperatures and the corresponding enthalpy values are deduced from the DSC results. The temperature for both transitions was determined by taking the onset value of the peak as shown in Figure 33. The enthalpy of each transition is taken as the integrated area under the peak. A minimum of three runs for each sample type was performed to assess the reproducibility of the recorded result.

The reliability of the enthalpy values determined by the Pyris 13.3 thermal analysis software (Perkin Elmer, Massachusetts, U.S.A.) was assessed by using two alternative methods, in addition to the thermal analysis software. The determined area of the peak was then compared between each method. One of the alternative methods can be best described as the “cut and weigh method” which involved weighing the mass of the peak as a print out and a reference mass of known enthalpy, thus deducing the enthalpy of the peak by using the ratio of the masses between the cut out peak and the reference area. The second alternative method is to determine the area of the peak by using the peak analysis function in OriginPro software. The enthalpy values were determined by all three methods for one experiment and for different concentrations of DPPC with sarcosine. The enthalpy values determined from all three methods gave repeated agreeable results for six different experiments with ± 0.2 kcal/mol difference, from this, it can be assured that the enthalpy results deduced from the Pyris 13.3 thermal analysis software and presented in Chapter 3 are reliable.

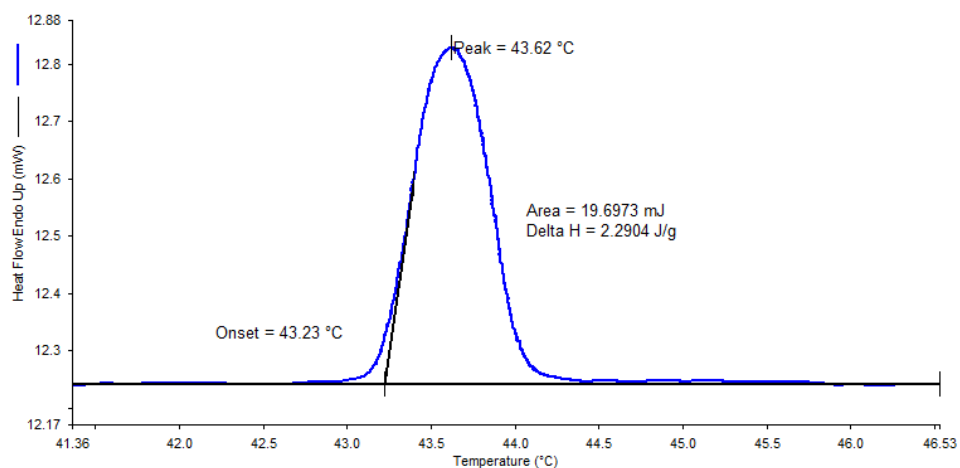


Figure 33: A DSC curve showing the T_M peak where the determined onset of transition temperature and enthalpy from the Pyris 13.3 software.

2.4.3 Determining the FWHM and Offset Values

The full width half maximum, FWHM, and peak offset values of each transition peak were determined by the peak analyser tool in OriginPro. By selecting the x-axis range required to analyse, the peak analyser tool is able to identify various properties of the peak including the peak FWHM and peak offset, as shown in Figure 34.

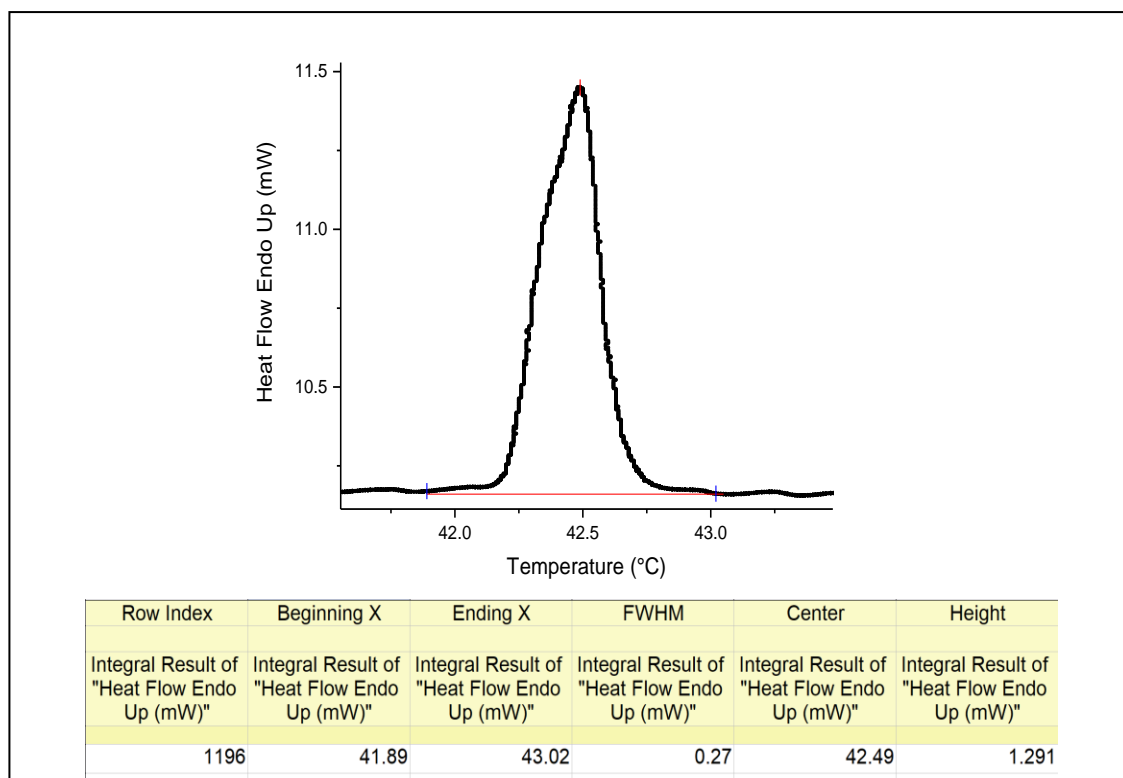


Figure 34: The main transition peak of DPPC collected by DSC where the range selected for peak analysis is shown by the two blue vertical lines either side of the peak. The results from the peak analyser tool in OriginPro are displayed below the curve.

2.5 Isothermal Titration Calorimetry

Isothermal titration calorimetry, ITC, is a technique used commonly to determine the binding enthalpies between two components, general overviews of ITC can be found in (105, 106). The heat change as a result of adding solute A in to a cell containing solute B is recorded by monitoring the change in power required to maintain a constant temperature within the cell. The heat change is the used to calculate the enthalpy of interaction between the solutes. In this study, solute A is the humectant solution and solute B is water and ITC was performed to understand the enthalpy of binding between each humectant and water.

2.5.1 Isothermal Titration Calorimetry Measurements

ITC measurements were carried out on a MicroCal ITC200 (Malvern Panalytical, Malvern, U.K.) with water as the reference sample. The titration cell, installed with a

mechanical stirrer set at 750 rpm stirring speed, was filled with 200 μl of water and the temperature of the cell was controlled at 25 $^{\circ}\text{C}$ with the reference power set to 10 $\mu\text{Cal/s}$. After an initial injection of 0.5 μl 0.4 M humectant solution into the titration cell at 60 seconds, 2 μl injections were introduced at every successive 90 seconds 19 times. A total of 20 injections are introduced in to the cell during one experiment.

2.5.2 Background Subtraction

To eliminate any solvent mixing interactions between water-water molecules, a background measurement of injecting water in water was performed and the ITC curve subtracted from the sample curve.

2.5.3 Determining the Enthalpy of Interaction

The enthalpy of binding of humectant with water is calculated by the below equation:

$$\Delta H = \frac{q}{c V} \quad (12)$$

where q is the heat change, c is the concentration of the injected solute and V is the injected volume.

Chapter 3 Results

3.1 The Influence of Humectants on the Thermotropic Behaviour and Nanostructure of DPPC

3.1.1 Introduction

It is of interest to study the effect of water-structuring components, found in typical dermatological formulations, on the structure and stability of the phospholipids used as the main structural component. Humectants are hygroscopic substances used as a source of moisture by attracting and binding to water molecules. Humectants are used in many personal care products, particularly skin creams and haircare products (77). In dermatological formulations, humectants work by attracting water to the stratum corneum, therefore providing a rehydration and moisturising sensation to the user. These molecules provide these sensations as they are examples of kosmotropes, which support the bulk water hydrogen bonding network (80). Understanding the effect of humectants on the structure and thermal behaviour of PCs will enable the formulator to make more informed decisions when developing formulations. Three different humectants will be studied: betaine, sarcosine and acetamide monoethanolamine, AMEA, see Figure 35.

Studies in to the effect of kosmotropes on phospholipid membranes have shown that they are favoured to be in the bulk of the water and are excluded from interfacial regions. As a consequence, in fully hydrated lipid systems, kosmotropes would favour gel, L_{β} , and hexagonal phases over the fluid phase, L_{α} , as the fluid phase has the largest area per lipid (53), i.e. displaying the largest number of waters per lipid.

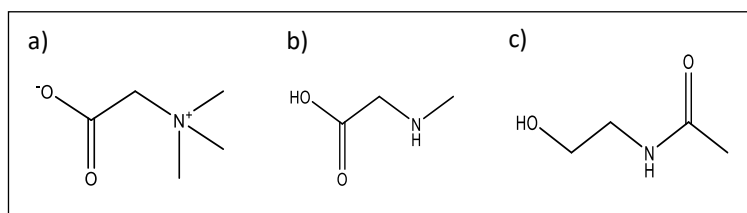


Figure 35: The structure of a) betaine b) sarcosine and c) AMEA.

The mechanism by which humectants interact with the lipid bilayer remains in question. Rudolph *et al.* (63) presented three possible interaction mechanisms for betaine with a lipid bilayer: (i) betaine interacts directly with the hydrocarbon chains, (ii) betaine alters the long range order of water near the polar residues of the lipid, leading to changes in the spacing between the headgroups and (iii) betaine forms coordinate linkages with either the polar headgroups or their hydration sphere, leading to changes in the packing density of the headgroups. The first hypothesis seems rather unlikely as betaine is hydrophilic and a known kosmotrope which is also supported by Rudolph *et al.* However the authors were not able to attribute their observed results to either hypothesis (ii) or (iii), therefore suggesting that there may be a possible combination of mechanisms for interaction. There are a growing number of studies (64, 107, 108) supporting hypothesis (ii) which briefly described the preferential exclusion mechanism by which the humectant does not interact with the lipid bilayer directly.

Rudolph and Goins (62) found that the phase transition temperatures of DPPC increase with increasing concentration of betaine. Rudolph and Goins also found that the transition from gel to ripple phase, T_{pre} , was susceptible to a larger increase than the transition from ripple to fluid phase, T_M . Furthermore, if the concentration of betaine is 3 M or higher, then T_{pre} completely disappears and merges with T_M . Rudolph and Goins studied betaine at four concentrations: 0, 1, 2 and 3 M, which resulted in a linear increase in the transition temperatures as the betaine concentration was increased.

This study aims to explore the effects of humectants on DPPC at much lower concentrations than previous studies by using a combination of X-ray scattering and differential scanning calorimetry, DSC. These techniques will also reveal, for the first time, the nanostructural effects of humectants on the DPPC bilayer as well as tracking the thermal changes, therefore providing further insights into the interaction between humectants and DPPC.

3.1.2 Thermotropic Changes

DPPC self-assembles into lamellar lyotropic liquid crystalline phases when in excess water. Three phases are observed from 25 to 50 °C, the lamellar gel phase, L_{β} , the ripple phase, P_{β} , and the lamellar fluid phase, L_{α} , and can be well documented by SAXS, see Figures 36 and 37. Note that PCs self-assemble into liquid crystalline structures of the Smetic phase when hydrated, i.e. the fluid phase is not the only liquid

crystalline phase, but all phases are liquid crystalline (20). In fact, the gel phase is the smectic B phase and the fluid phase is the smectic A phase (109). The transition from gel phase to ripple phase is called the pre-transition temperature, T_{pre} , and is observed at 35 °C, see Figure 37, which agrees well with literature (14). The transition from ripple to fluid phase is called the main transition temperature, T_M , is observed at 42 °C which also agrees well with literature (14). The d spacing of DPPC changes when a phase transition occurs, reflecting the different chain conformations present for each phase, see Figure 38. In the gel phase the chains are in all-*trans* conformation, followed by an intermediate ripple phase with asymmetric saw-tooth like height modulation of the bilayers which increases the d spacing in stacking direction, followed by melting of the chains to *trans-gauche* conformation and a decrease in the d spacing, for more information refer to the Introduction Chapter 1.1.

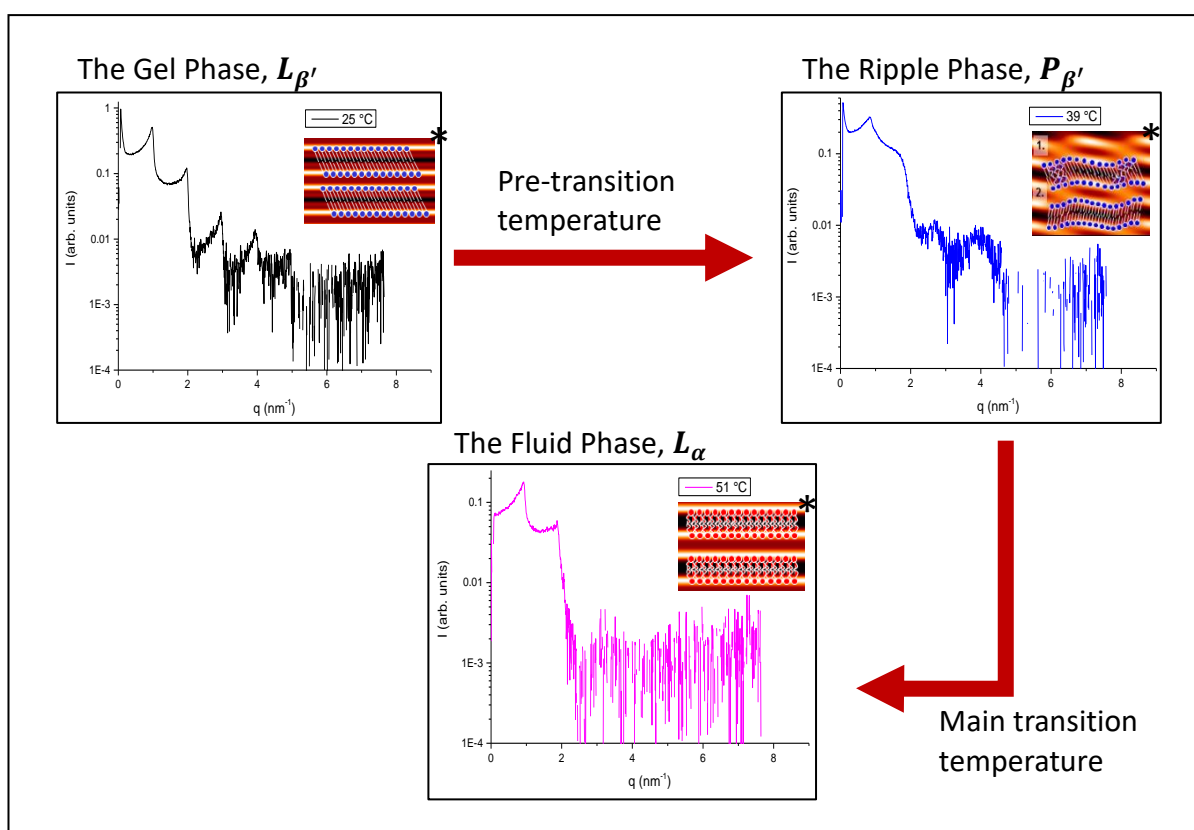


Figure 36: The SAXS curves for the gel, ripple and fluid phase and the structures of the lipid bilayers shown in the inset of each phase. *Insets taken from (20).

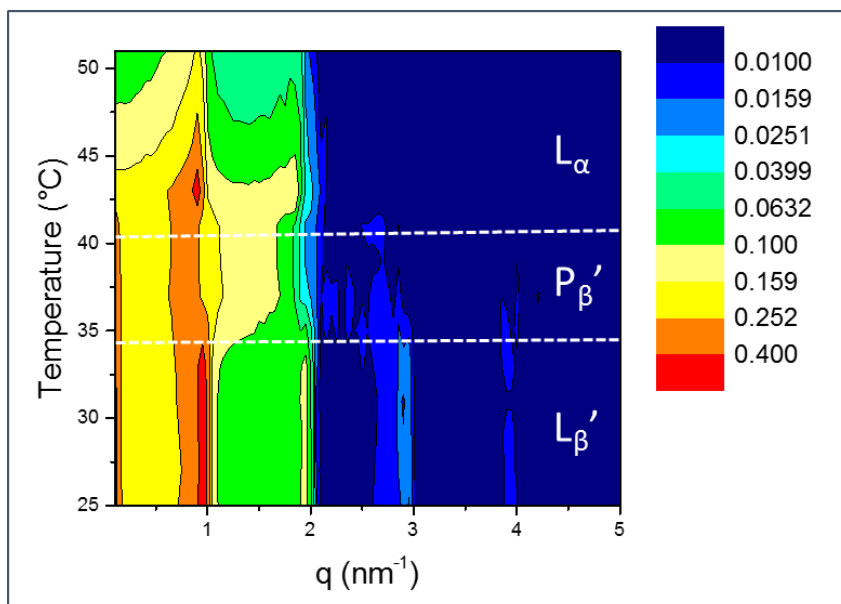


Figure 37: The structural changes of DPPC observed between 25 to 50 °C by small angle X-ray scattering. The z axis is Intensity (a.u.) where the dark blue areas are lowest in intensity and the red areas are highest.

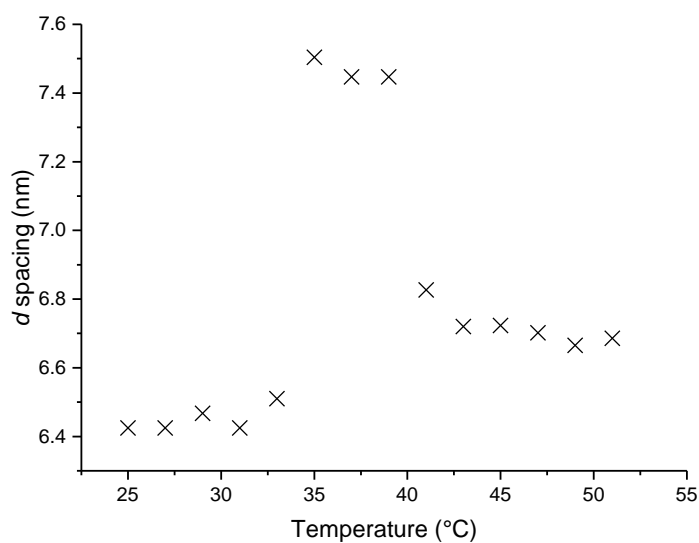


Figure 38: The change in d spacing of DPPC with increasing temperature.

Figure 39 shows the relationship between the phase transition temperatures and the concentrations of each humectant. The results of betaine are in agreement with previously published results (53, 62, 63) displaying a higher increase in T_{pre} than T_M . The reason behind a greater observed increase in T_{pre} than T_M is, due to a reflection on the lower enthalpy of the pre-transition to the ripple phase than the main transition to

the fluid phase (53). This will be elaborated later in the discussion, as this can be expressed as an inverse proportionality of the transition temperature to enthalpy changes; i.e. it can be shown that phase transitions with lower enthalpies are more susceptible to transition temperature changes. The results for betaine show that, T_{pre} follows an almost linear increase with increasing concentration of betaine, similar to Rudolph and Goin's (62) findings. T_M does not however, follow a linear increase as previously described by Rudolph and Goins, when including also low concentration data points as in this study. In fact, at low concentrations ($<0.4\text{M}$) all three humectants display a steep increase in T_M at low concentrations which then plateaus at high concentrations ($>0.4\text{ M}$), an observation that previously has been overlooked. It is noticeable from Figure 39 that sarcosine behaves very similarly to betaine, which can be attributed to their alike structures, see Figure 35. For AMEA, the trend in T_M is not as pronounced as for betaine and sarcosine. Equally, also for T_{pre} only a slight increase is observed for increasing concentrations of AMEA, compared to betaine and sarcosine. The results of DSC measurements are summarised in Table 7.

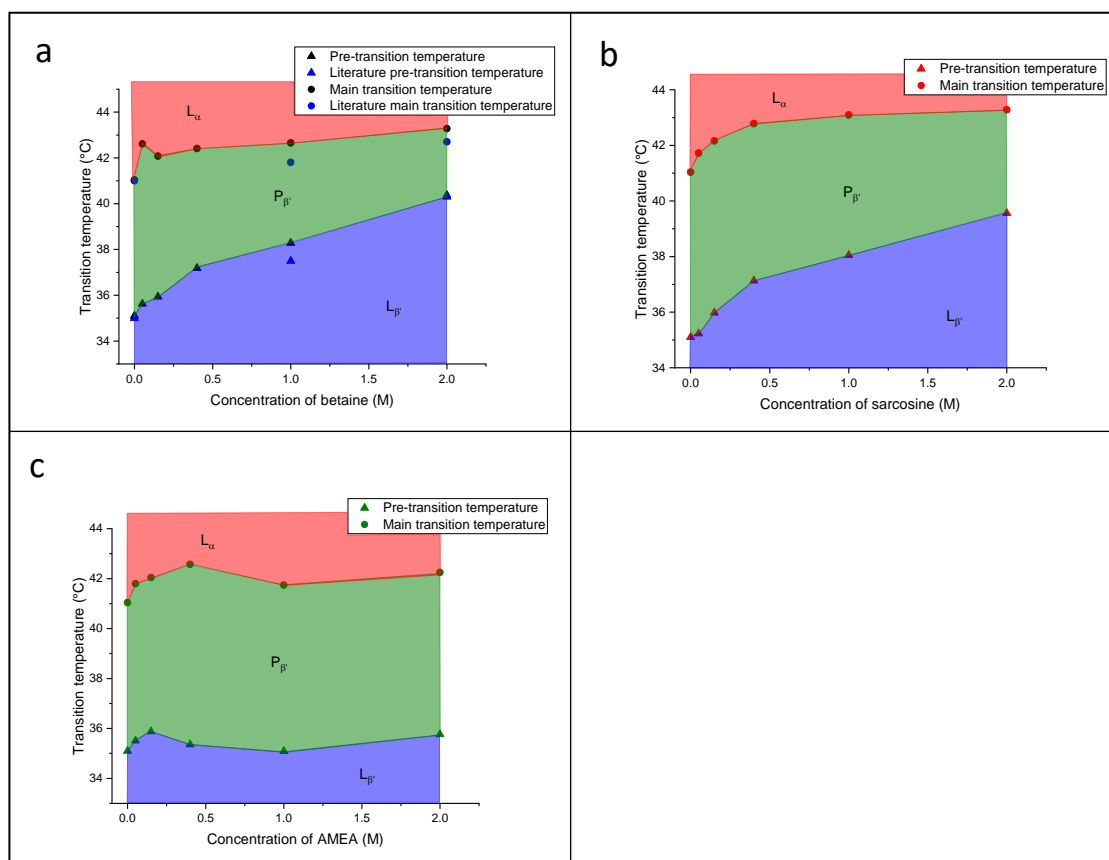


Figure 39: The phase diagrams of DPPC with increasing concentrations a) betaine b) sarcosine and c) AMEA.

Table 7: The Phase Transition Temperature and Enthalpy values of fully hydrated DPPC with:

a) Betaine

Concentration of Betaine (M)	Pre-transition		Main transition	
	Temperature (°C)	Enthalpy (kcal/mol)	Temperature (°C)	Enthalpy (kcal/mol)
0.00	35.1	1.33	41.0	7.52
0.05	35.6	0.91	42.6	6.51
0.15	35.9	1.72	42.1	8.64
0.40	37.2	0.95	42.4	7.30
1.00	38.3	0.87	42.7	6.06
2.00	40.4	0.88	43.3	9.48

b) Sarcosine

Concentration of Sarcosine (M)	Pre-transition		Main transition	
	Temperature (°C)	Enthalpy (kcal/mol)	Temperature (°C)	Enthalpy (kcal/mol)
0.00	35.1	1.33	41.0	7.52
0.05	35.2	0.91	41.7	7.75
0.15	36.0	1.13	42.2	8.05
0.40	37.1	0.75	42.8	5.25
1.00	38.1	0.76	43.1	6.09
2.00	39.6	0.86	43.3	5.89

c) AMEA

Concentration of AMEA (M)	Pre-transition		Main transition	
	Temperature (°C)	Enthalpy (kcal/mol)	Temperature (°C)	Enthalpy (kcal/mol)
0.00	35.1	1.33	41.0	7.52
0.05	35.5	0.89	41.8	9.78
0.15	35.9	0.98	42.0	7.42
0.40	35.4	0.99	42.6	7.22
1.00	35.1	0.83	41.7	6.37
2.00	35.8	0.74	42.3	5.67

The corresponding enthalpy values for both transitions have been determined and are shown in Table 7 and Figure 40. For the pre-transition, despite a possible outlier at 0.15 M betaine, the addition of all three humectants leads to a decrease in the pre-transition enthalpy. The addition of sarcosine or AMEA leads to a distinct decrease in the pre-transition enthalpy with increasing concentration. For the main transition, the addition of betaine does not alter significantly the enthalpy value as the values fluctuate around the enthalpy of pure DPPC at 7.52 kcal/mol. Whereas for sarcosine and AMEA, the

main transition enthalpy values also decrease with increasing concentration for the main transition, in the same manner as for the pre-transition.

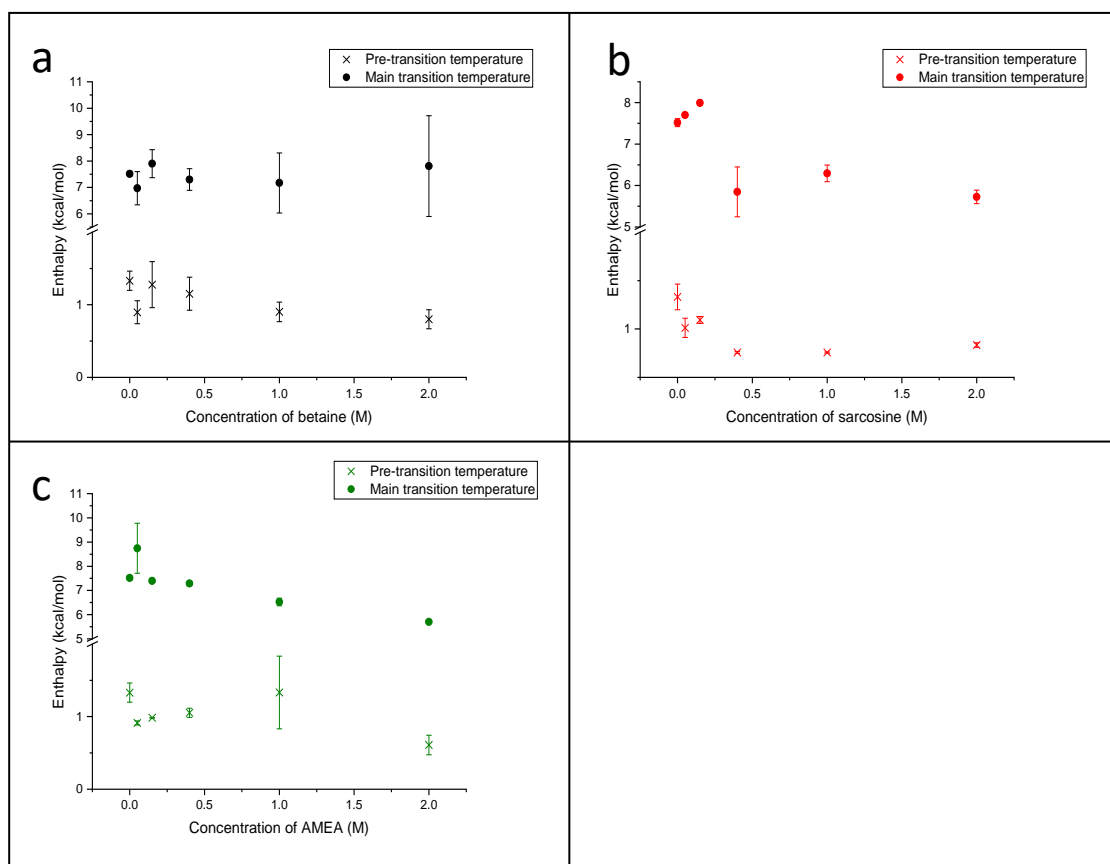


Figure 40: The enthalpy values for the phase transitions of DPPC with addition of a) betaine b) sarcosine and c) AMEA.

Isothermal calorimetry, ITC, was performed to assess the contribution of the binding energy between the humectant and water when they are both mixed. It can be seen from Figure 41 that the addition of each humectant to water leads to a different enthalpy of interaction. The addition of betaine leads to both an endothermic and exothermic contribution, the addition of sarcosine leads to an endothermic contribution and the addition of AMEA leads to an exothermic contribution. However, the results from ITC also show that the enthalpy of mixing between the three humectants is very small compared to the enthalpy of the phase transitions, as presented above. Therefore, it can be concluded that the change in enthalpy values observed by the addition of humectant to DPPC, is virtually independent of the humectant binding with the water molecules or on the changes of humectant partitioning into or out of the inter-lamellar water region.

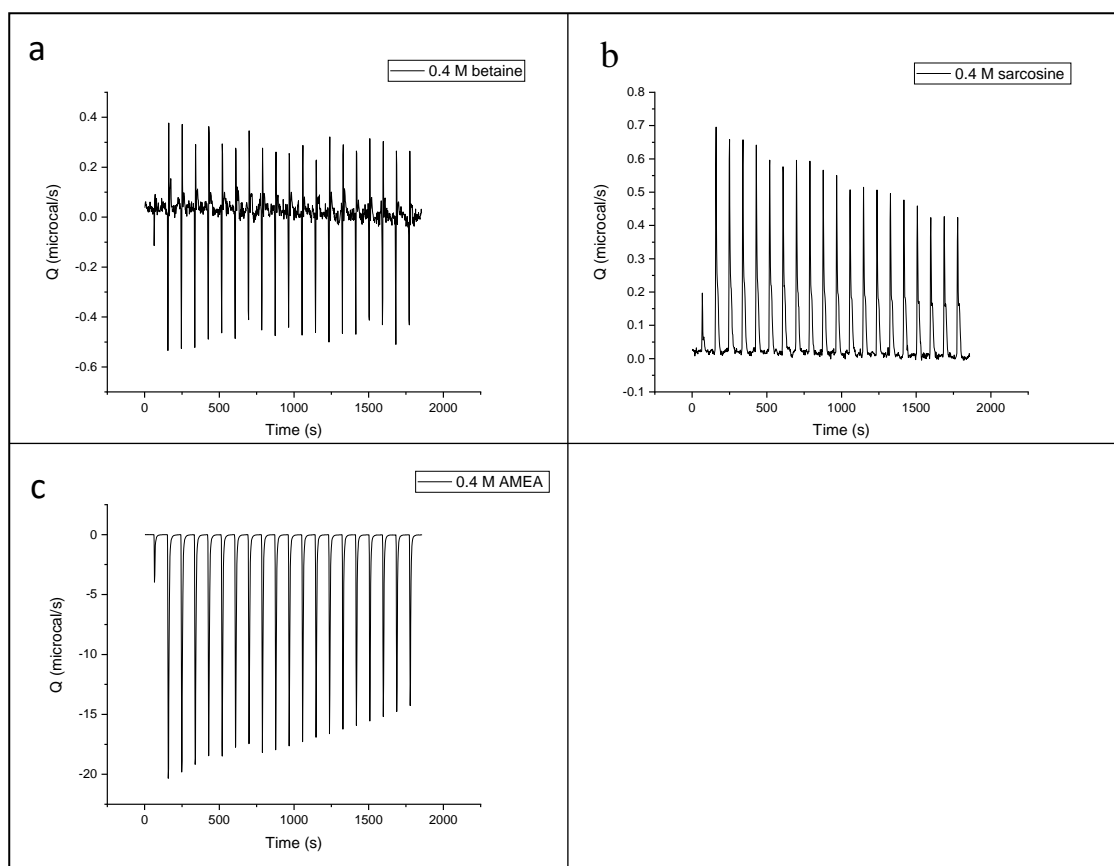


Figure 41: The ITC results for a) 0.4 M betaine b) 0.4 M sarcosine and c) 0.4 M AMEA injections to water.

Analysis on the main transition peak full width half maximum, FWHM, gives information on the change in cooperativity; the larger the FWHM the lower the cooperativity. It can be seen from Figure 42 that the FWHM is increasing with increasing concentration of humectant, this suggests that the cooperativity is decreasing. This observation suggests that the humectants may be coordinating with the lipid headgroup and its hydration sphere, or even penetrate into and interact with the lipid bilayer (63) at least at very high humectant concentrations, and thus rendering the transition less cooperative.

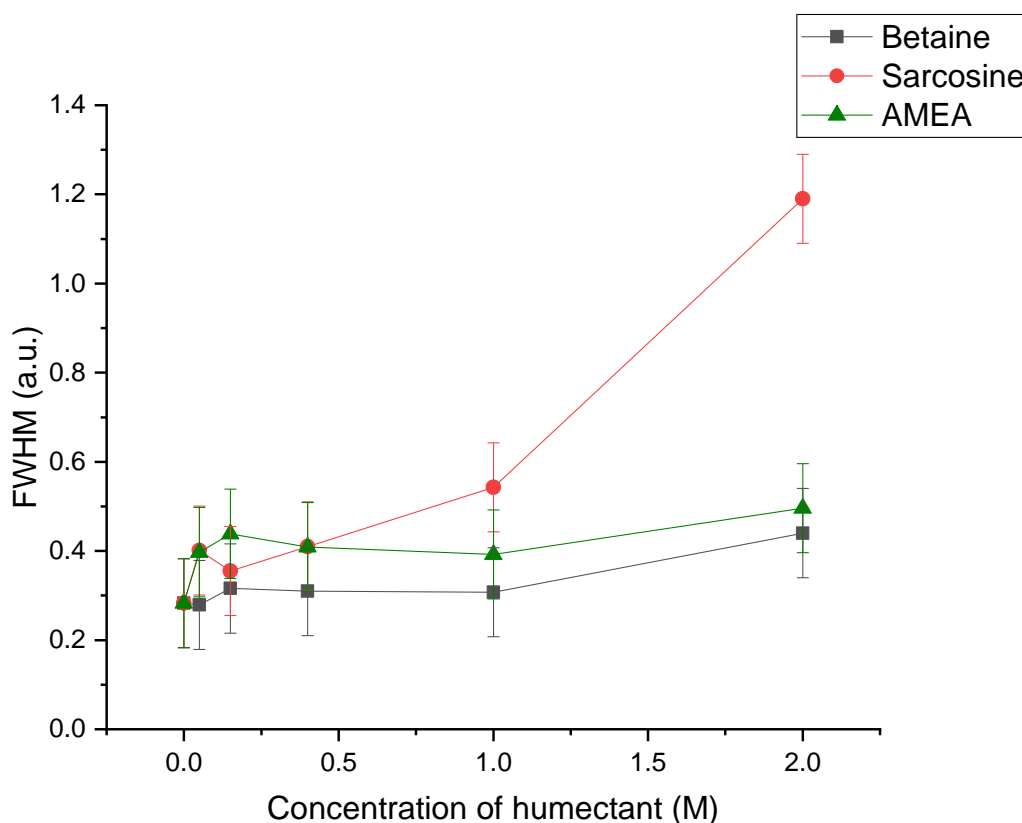


Figure 42: The change in FWHM for the main transition of DPPC with change in concentration of humectant.

3.1.3 Nanostructural Changes

Changes in the nanostructure of DPPC can be monitored with X-ray scattering.

Determined electron density profiles, EDPs, from the SAXS results reveal various structural information, see Figure 43. Here, d_{HH} and d_w are displayed, where $d = d_{HH} + d_w$. Note that the resolution of the EDP is within 8 Å as the EDP of the gel phase is calculated with 4 diffraction orders (101). The influence of the humectants on the bilayer for the gel phase is shown in Figure 44. The addition of each humectant results in a slight overall increase in d_{HH} (0.15 nm increase for betaine), but more distinctly, d_w decreases with increasing concentration of humectant (0.43 nm decrease for betaine).

As d_w decreases almost three times more than the increase of d_{HH} , an overall decrease in the d spacing is observed. The overall change in the bilayer due to the addition of betaine is illustrated in Figure 45.

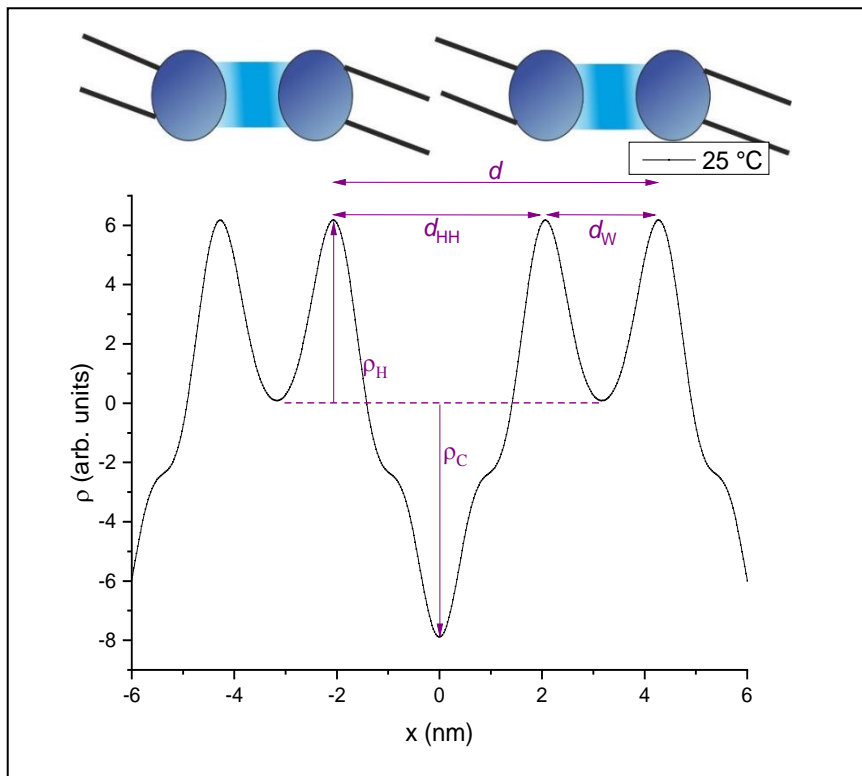


Figure 43: The electron density profile of fully hydrated DPPC in the gel phase. The parameters d , d_{HH} , and d_W are indicated in relation to the EDP. An illustration of two lipid bilayers is presented above the EDP to facilitate interpretation of the EDP.

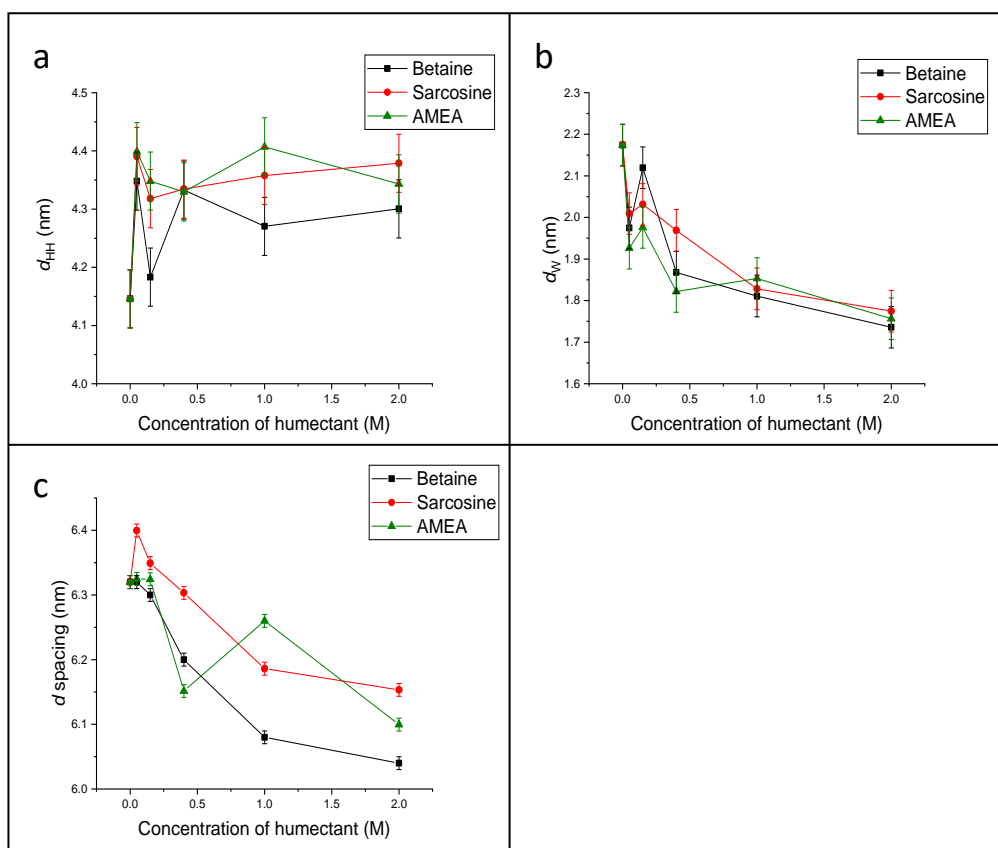


Figure 44: The change in a) d_{HH} b) d_W and c) d spacing of gel phase DPPC at 25 °C with increasing concentration of humectant.

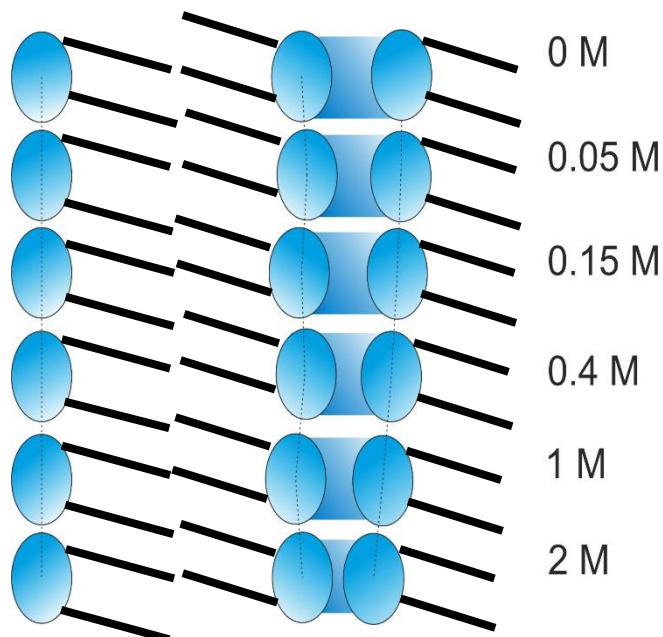


Figure 45: An illustration of the effect of betaine on the nanostructure of fully hydrated DPPC in the gel phase.

The fluid phase SAXS curves for betaine with DPPC and their global fitting results are presented in Figure 46. Good fits are achieved with the global fitting analysis and the results of the structural parameters are presented in Figure 47. The change in structural parameters of DPPC with betaine with increasing temperature reflects the typical thermal behaviour of phosphatidylcholines in the fluid phase (41). The d_{HH} decreases with increasing temperature as there are increasing number of *trans-gauche* conformations. There is very little change for d_w with increasing temperature, therefore the combination of d_{HH} and d_w leads to an overall decrease in the d spacing with increasing temperature. The anomalous swelling regime (110) has been reproduced here with the d spacing trend, where the d spacing increases non-linearly, when cooled from above T_M and approaching closer and closer to T_M , see Section 1.1.6 for more details. The change in the Caillé parameter, η , which gives information on the fluctuations of the bilayers, shown in Figure 47d, however, displays no clear trend for η with increasing temperature, which most likely due the simultaneous enhancement of membrane undulations near T_M caused by the anomalous swelling phenomena for medium chain-length PCs (110), see Chapter 1.1.5 for more information. It is noted, that for high temperature trends above T_M (not covered in this study), η is expected to increase clearly with temperature.

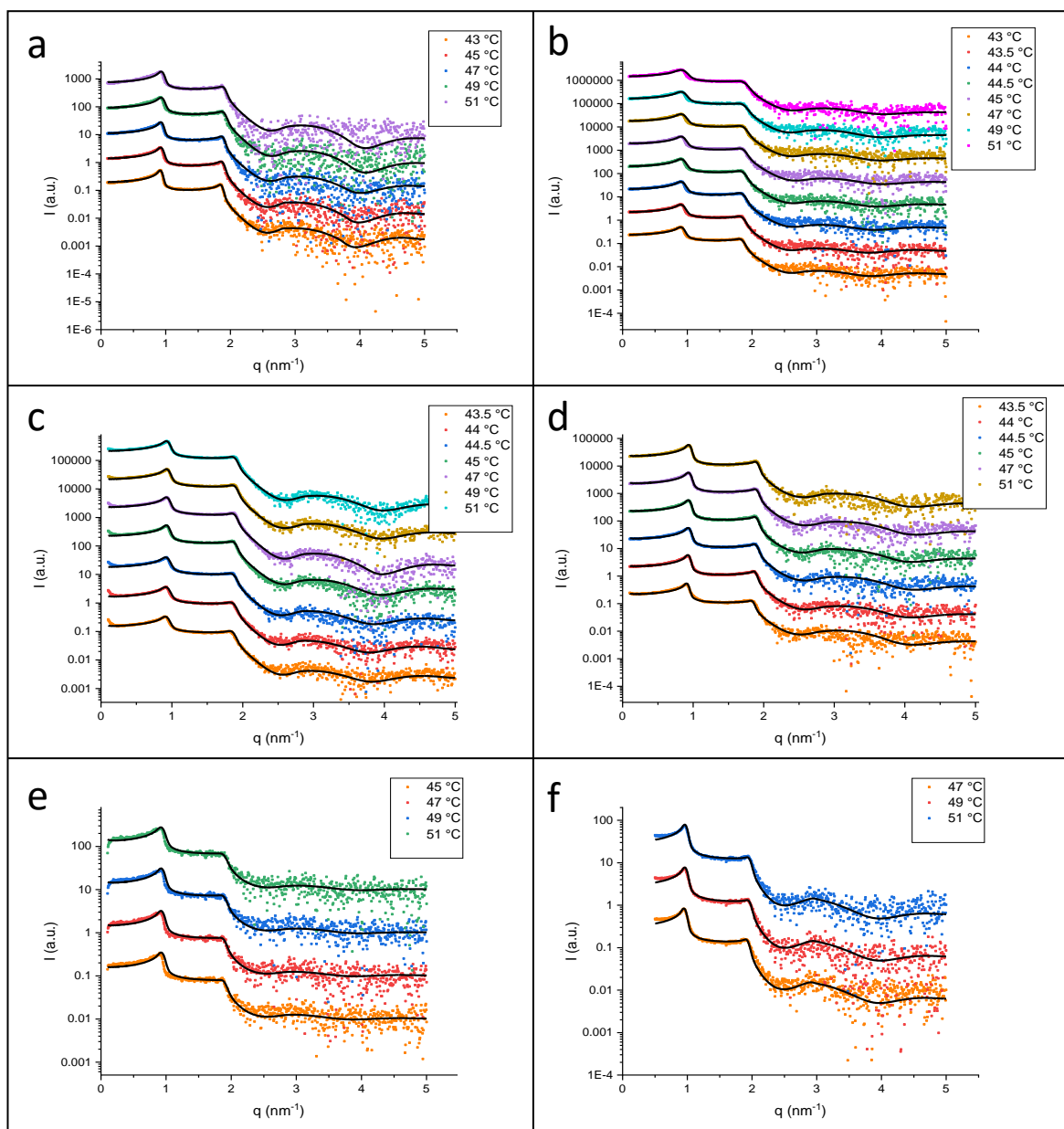


Figure 46: The SAXS curves for the fluid phase of DPPC with a) 0 M betaine b) 0.05 M betaine c) 0.15 M betaine d) 0.4 M betaine e) 1 M betaine and f) 2 M betaine. The global fitting results are presented by the black lines (for details of the fitting method see Section 2.3.4) for each concentration and temperature. The SAXS curves have been stack-plotted for clarity.

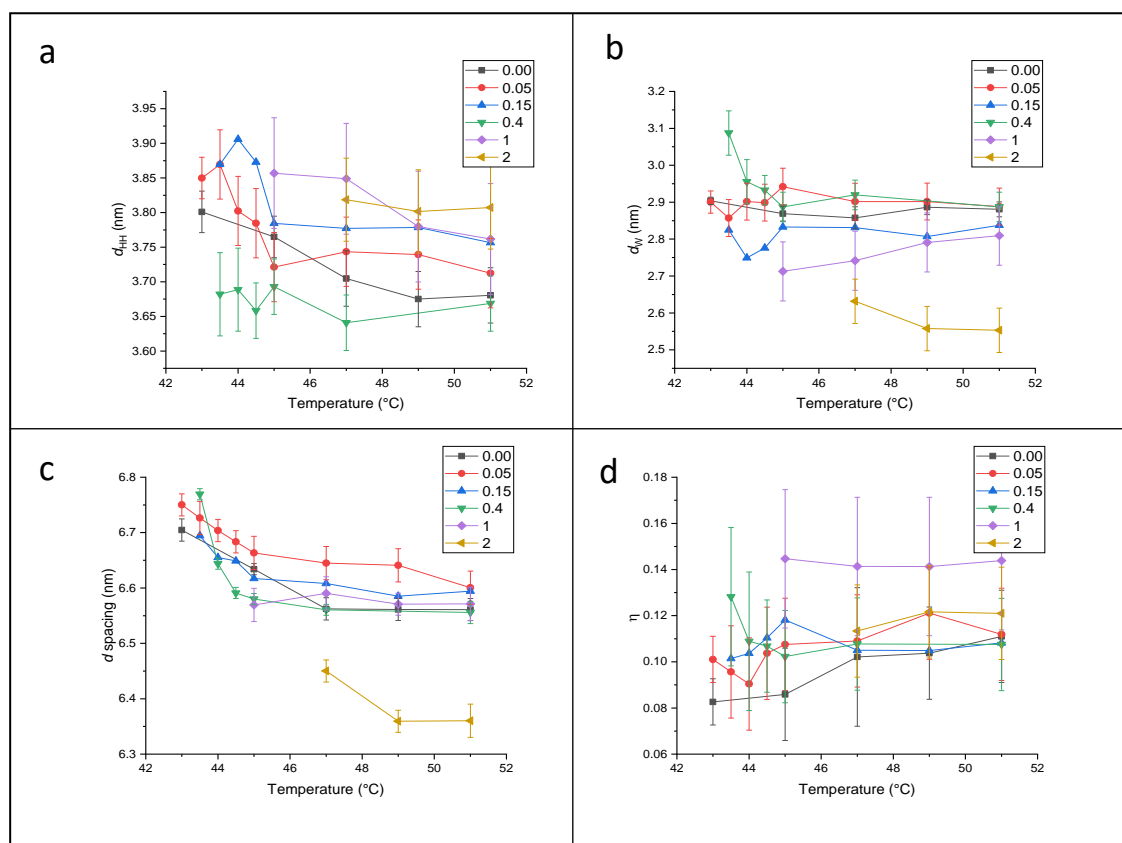


Figure 47: The change in a) d_{HH} b) d_W c) d spacing and d) η of DPPC with temperature in the fluid phase at different concentrations of betaine.

The change in the nanostructure of DPPC with concentration of each humectant is presented in Figure 48. To account for the different T_M for different concentrations of humectant, the results presented are for temperatures, where $T = T_M + 2$ °C. Overall, the trends are similar to those observed for the gel phase. D_{HH} increases slightly at 1 M concentration and above, but more dominantly, as compared to the gel phase, is the decrease in d_W for both betaine and sarcosine. It is noted that AMEA does not lead to a decrease in d_W in the fluid phase. A very slight increase in η with increasing concentrations of humectant is observed.

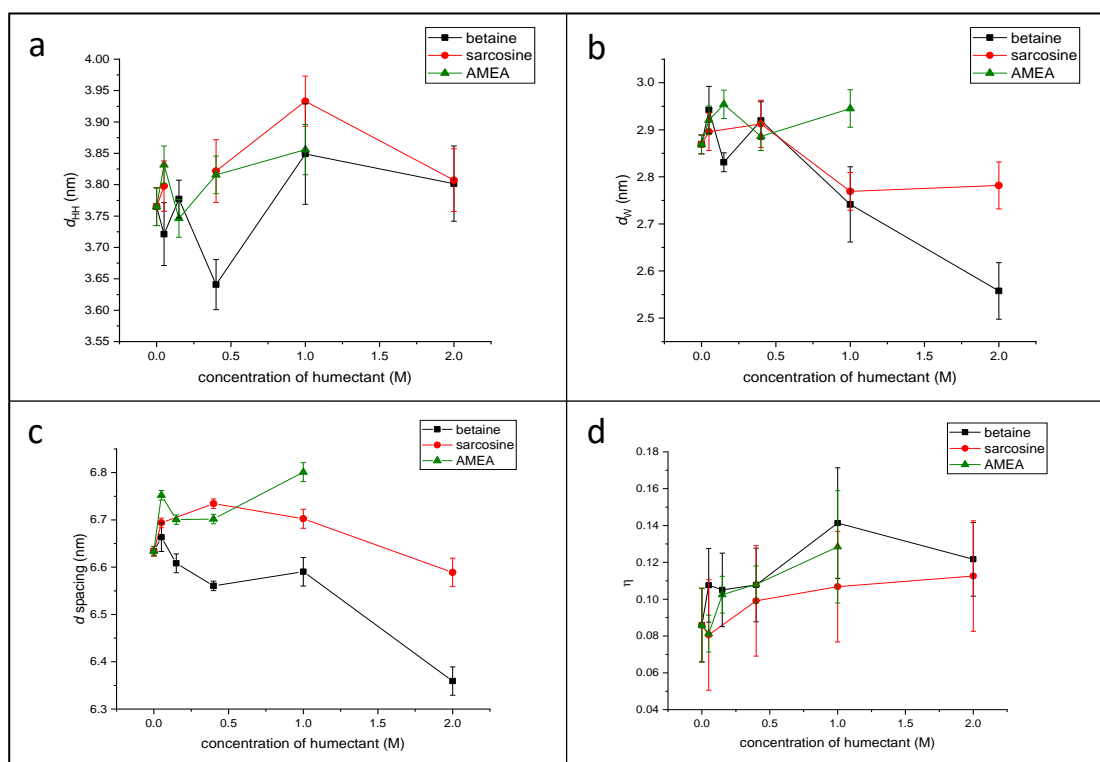


Figure 48: The change in a) d_{HH} b) d_W c) d spacing and d) η of DPPC with increasing concentration of humectant. Temperature is equal to $T_M + 2$ °C.

The results from WAXS offer additional insights, specifically to the lateral packing of the lipid chains. In Figure 49, the peak at $q = 14.8 \text{ nm}^{-1}$ for the gel phase is sharper and narrower compared to the ripple and liquid lamellar phases. The different shapes in the curves in the WAXS regime reflect the different packing orders of the lipids in the different phases. These differences are also illustrated in the WAXS contour plots in Figure 50. For instance, from Figure 50a, it is clearly seen that the most intensive diffraction peak in the gel-phase regime becomes broader with increasing temperature. The addition of betaine results in a change in the shape of the gel phase diffraction peaks. For example in the gel phase at 25 °C, it can be seen that the peak becomes narrower upon addition of betaine (cp. Figure 50a to panels b-f), when compared to that of pure DPPC. The same changes are observed for sarcosine and AMEA.

Taking a closer look at the gel phase WAXS curve, in Figure 49, two overlapping diffraction peaks are observed, one intense and narrow peak at $q = 14.8 \text{ nm}^{-1}$ and a second, less intense and broader peak at $q = 15.1 \text{ nm}^{-1}$. These peaks refer to the 20 and 11 Miller indices of orthogonally packed chains, see Figure 51. The $q_{20} = 14.8 \text{ nm}^{-1}$ peak corresponds to $d_{20} = 0.424 \text{ nm}$ and the $q_{11} = 15.1 \text{ nm}^{-1}$ peak corresponds to $d_{11} =$

0.416 nm, which agrees well with literature (103). For the determination of the area per lipid chain, A_C , refer to Equation 10 in Section 2.3.5.

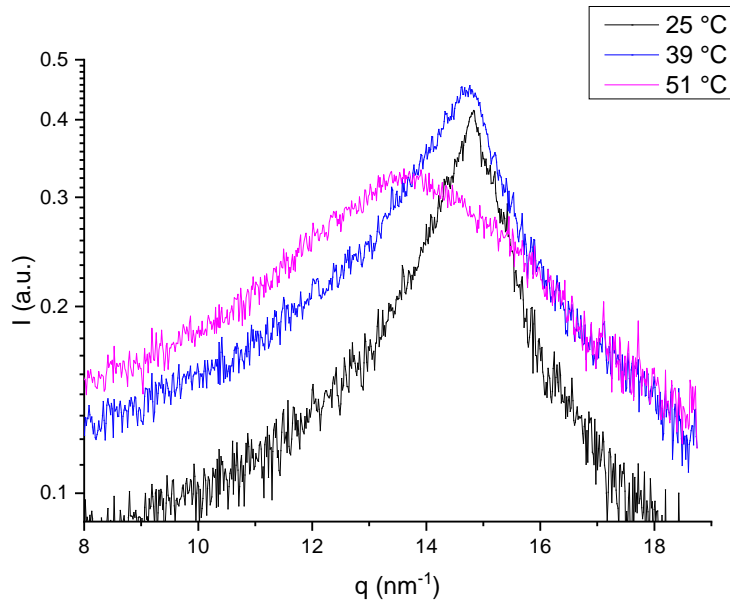


Figure 49: The different phases of pure DPPC as seen by WAXS at different temperatures. The black curve is the gel phase, the blue curve corresponds to the ripple phase and the pink curve is the fluid phase.

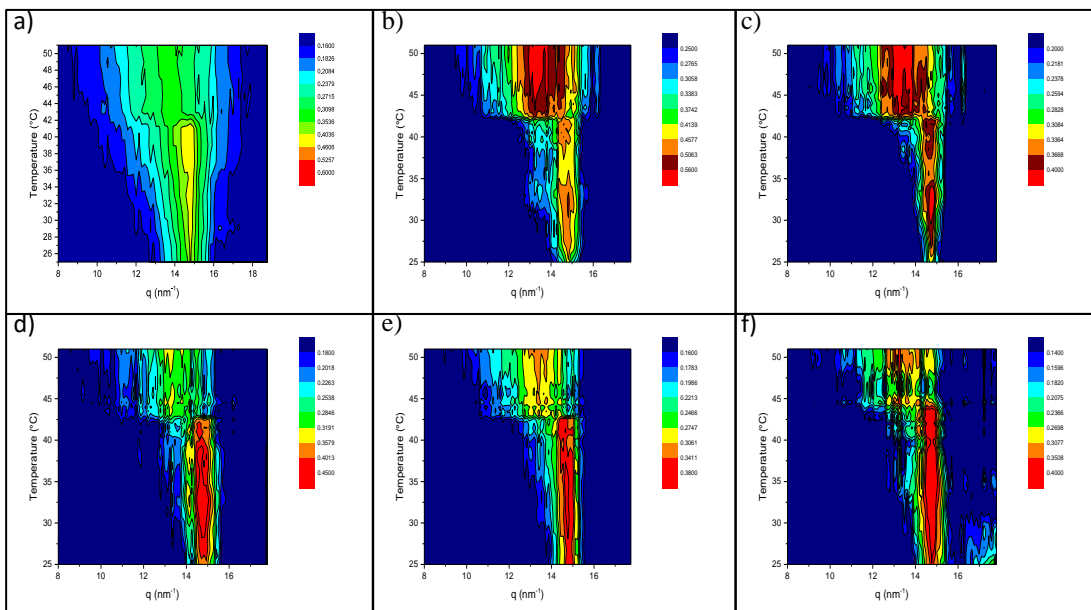


Figure 50: The change in the WAXS pattern of fully hydrated of DPPC with temperature for a) pure DPPC b) with 0.05 M betaine c) with 0.15 M betaine d) 0.40 M betaine e) 1.00 M betaine and f) 2.00 M. The z axis is the Intensity (a.u.) of the counts.

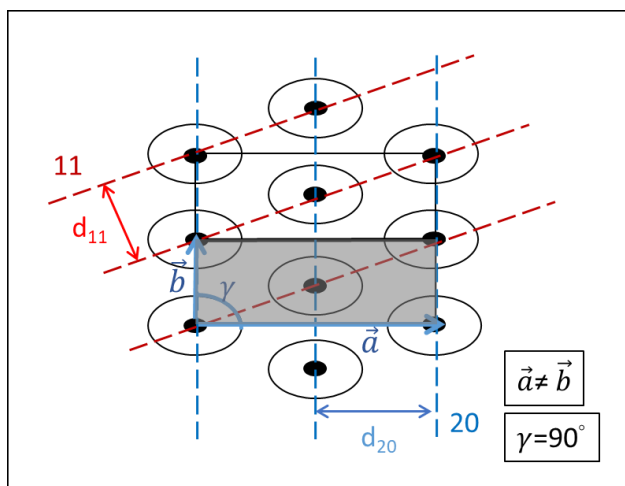


Figure 51: The unit cell and Miller Indices of the orthogonal lattice of the gel phase DPPC.

The change A_C has been calculated for both the gel and fluid phase, see Figure 52. For the gel phase, a slight decrease in A_C is observed for all humectants, apart from 2 M betaine, which shows a distinct increase in A_C . For the fluid phase, marginal effect of the humectant on A_C is observed.

Taking a closer look at the WAXS pattern observed for 2 M AMEA at 25 °C, there is a change in the electron density contrast as the intensity ratio between q_{20} and q_{11} switches, see Figure 53. Already at 1 M AMEA, this peak ratio is changing from a dominant q_{20} peak at 0.00 M AMEA to almost equal intensities of both peaks. At 2 M AMEA the q_{11} peak is even more intense as the q_{20} peak. This effect is not observed for betaine and sarcosine where the peak ratio remains the same at all concentrations with q_{20} being the more dominant peak. Figure 54 displays a plot to show the change in the ratio of the intensity between q_{20} and q_{11} with increasing concentration of humectant. The intensity values were taken directly from the raw data. This reaffirms the visual observation that the WAXS peak shape is independent of concentration for betaine and sarcosine, whereas for AMEA, the $q_{20}:q_{11}$ ratio < 1 reflects a more dominant q_{11} peak, at concentrations higher than 1 M.

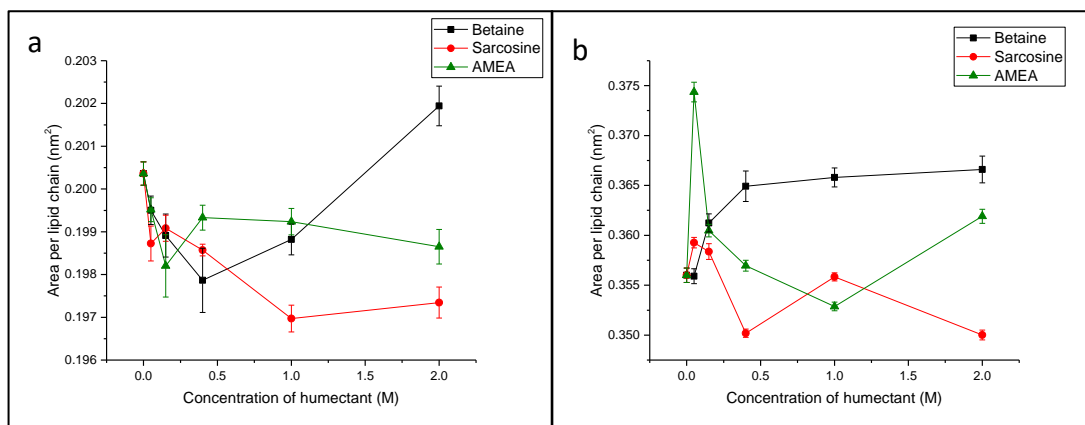


Figure 52: The change in area per lipid chain for a) the gel phase and b) the fluid phase of fully hydrated DPPC with each humectant.

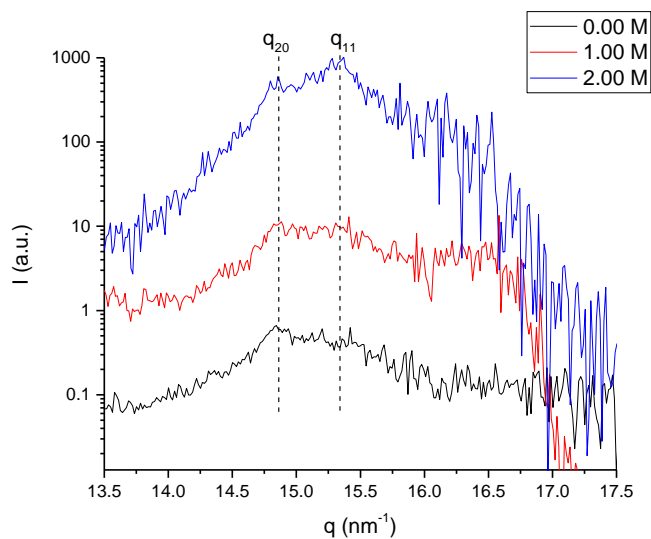


Figure 53: The change in peak shape of the WAXS peak for DPPC with AMEA at 25 °C.

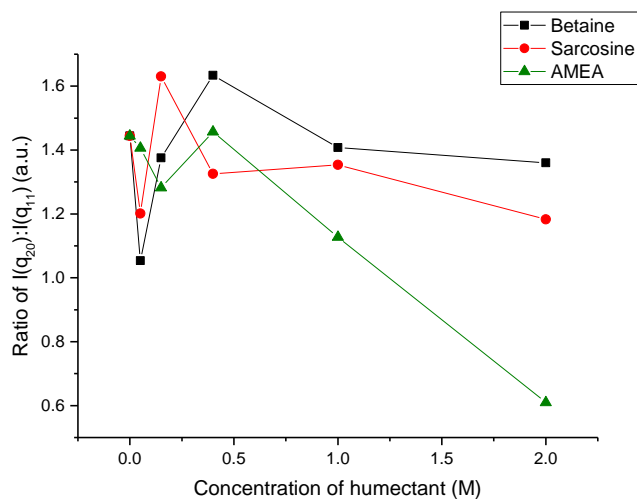


Figure 54: The change in ratio of the DPPC WAXS gel phase peak $I(q_{20}):I(q_{11})$ ratio with increasing concentration of humectant at 25 °C.

3.1.4 Discussion

3.1.4.1 Thermotropic Changes

The observed thermotropic effect of humectants on fully hydrated DPPC show that in general, the addition of humectant leads to an increase in both phase transition temperatures, and moreover T_{pre} is affected more so than T_M . This is typical behaviour of kosmotropes which tend to dehydrate lipid/water interfaces and hence stabilise low water phases on the cost of adjacent higher water phases (53). The behaviour of kosmotropes is depicted in Equation 13 which describes the thermotropic changes caused by solute effects on the basis of thermodynamic principles deduced by Koynova *et al.* (53). Here, it clearly shows that dT_{tr}/dc , the change in transition temperature with change in concentration, is inversely proportional to the transition enthalpy (the first term in Equation 13). The results presented above are in agreement with previous literature (53): the pre-transition temperature with a lower enthalpy value, shows a greater solute effect on the transition temperature when compared to the main transition with a higher enthalpy.

$$\frac{dT_{tr}}{dc} = \frac{RT_{tr}^2}{\Delta H} (x' - x'')(1 - c_L/c), \quad (13)$$

In Equation 13 shown above, dT_{tr}/dc is the solute dependent change of the transition temperature (humectant in this case), R is the gas constant, ΔH is the transition enthalpy, x is the fraction of inter-lamellar water per lipid molecule, where the prime and second

prime denotes the fluid and gel phase, respectively, c_L is the solute concentration in the inter-lamellar water region and c is the solute concentration in bulk (excess water region). The equation assumes that the solute concentration at the interfacial water region is equal in both gel and fluid phases. The second term ($x'-x''$) for the main transition is positive, since the fluid phase is more hydrated than the gel phase. The third term of the equation ($1 - c_L/c$) describes the influence of the uneven humectant concentration between bulk and inter-lamellar water. Since kosmotropes are defined by the inequality $c_L < c$ (caused by the dehydration effect of lipid/water interface), the overall value for dT_w/dc will be positive as clearly seen for sarcosine and betaine.

The betaine results are in agreement, in general, with previous results (62), especially for T_{pre} . However, despite the conclusions of Rudolph and Goins (62), the increase in T_M is only apparently linear, when considering solely high humectant concentrations (1 and 2 M). This study clearly shows for all humectants a nonlinear increase of the transition temperatures at low concentrations ($< 0.4M$). In general, the addition of all three humectants leads to the same thermotropic changes, despite slight disparities in the change in T_{pre} for the addition of AMEA, compared to betaine and sarcosine. The slight increase in T_M for all three humectants reflects their kosmotrope behaviour, as all kosmotropes tend to dehydrate the lipid/water interface leading to $c_L < c$ and hence to a positive value dT_w/dc , as discussed above.

When comparing the enthalpy trends to their corresponding transition temperatures, it is clear that the enthalpies do not follow the transition temperature trends. All three humectants lead to the same enthalpy trends in general, with the exception of the main transition enthalpy values for betaine, which do not show a significant concentration dependent trend. For both, the pre-transition and main transition, the enthalpy values decrease with increasing humectant concentration. The main transition is a first order transition and thus $\Delta H = T \Delta S$ where ΔS is the change in entropy. For both, the pre-transition and main transition, the decrease in enthalpy therefore suggests that there is an entropic contribution where the addition of humectant appears to lead to an increase in order for the system. It is important to note that Equation 13 assumes a first-order, infinitely narrow transition of a given enthalpy, therefore this equation is unable to explain the solute effect on the transition width and enthalpy. The observed decrease in cooperativity (or increase in peak FWHM) may well be a consequence of the fluid phase being unfavourable in the presence of humectant and thus the transition is less

cooperative. Additionally, the humectants may be acting as impurities, especially at high concentrations where it may be inevitable that some are located at the interfacial water layer, as a result this would lead to a decrease in cooperativity. However, further experiments need to be conducted to locate precisely the humectants within the bilayers to confirm this.

In previous studies, there are conflicting conclusions on whether betaine or sarcosine is the more effective osmolyte (64, 78, 107, 111). In this study, the effect of betaine and sarcosine is very similar and there is no clear indication of which humectant influences the phase behaviour of fully hydrated DPPC more. For T_{pre} betaine has a slightly larger effect on the temperature, where 2 M betaine leads to a 5.3 °C increase compared to a smaller increase of 4.5 °C for 2 M sarcosine. Therefore, it may give reason to conclude that betaine has a larger effect on T_{pre} . The increase in T_M is the same for both betaine and sarcosine. When comparing the enthalpy effects, 2 M sarcosine decreases both the pre-transition and main transition by 0.45 kcal/mol and 1.63 kcal/mol, respectively. Whereas 2 M betaine decreases the pre-transition temperature by 0.45 kcal/mol and no trend is observed for the main transition enthalpy values. Therefore, this may suggest that sarcosine has a larger effect on the enthalpy of transition for DPPC. The conflicting observations on the effect of betaine or sarcosine on both T_{pre} and T_M means that one cannot determine, which has a larger effect on the thermotropic properties of fully hydrated DPPC.

The ITC results show that the enthalpy of interaction between 0.4 M humectant and water is very small in magnitude, compared the enthalpy of the phase transitions of DPPC. Therefore, only a very small, negligible contribution to the phase transition enthalpy can be attributed to changes in the binding of humectant with water. The results also highlight the different binding enthalpies of each humectant with water; the addition of betaine to water leads to a combination of an endothermic and an exothermic interaction, the addition of sarcosine leads to an endothermic interaction and the addition of AMEA leads to an exothermic interaction. The enthalpy of binding depends on the endothermic energy required to break existing bonds and the exothermic energy released upon making new bonds (112). Therefore, the different binding enthalpies reflect the different bond strengths involved being broken and made as each humectant solution is diluted.

3.1.4.2 Structural Changes

The results from the SAXS data show that all three humectants are behaving as kosmotropes as the addition of humectant leads to less free water being available to the lipid bilayer thus being excluded from the interfacial region of the headgroup. All three humectants lead to an ordering of the bilayers, which is reflected in the slight but significant increase of d_{HH} . Equally this means that the Helfrich undulations are reduced with addition of humectants and hence the repulsive force between adjacent membranes diminishes, and consequently, the equilibrium distance between the adjacent bilayers, d_w , decreases significantly. Nevertheless, a possible additional increase of the attractive van der Waals forces between adjacent membranes cannot be excluded, since it would lead to the same observation of a decreased d_w . It should be noted that the sample preparation protocol was employed in an attempt to exclude osmotic effects in the system and there was lack of evidence of osmosis during the data reduction and analysis (i.e. no evidence of phase separation, by the splitting of the diffraction peaks, in the lipid system was observed). However, the results may be evidence to consider the possible presence of a small but residual osmotic pressure due to slight differing concentrations of humectant in the bulk and at the interfacial water region. This in principle, would could also lead to a decrease in d_w (113). Overall a decrease in the d spacing is observed with increasing concentration of humectant and this reproduces the behaviour of kosmotropes as published in (69, 114). An increase in the order of the bilayers also agrees with the interpretation of the thermal results, where an increase of the transition temperatures is observed for betaine and sarcosine, which is in agreement with (66). This notion is further supported by the observed narrower WAXS peak upon addition of humectant, again confirming that the bilayer in the gel phase becomes more ordered.

For the fluid phase, a slight increase in the Caillé parameter, η , was observed, which gives an indication to increased undulations of the bilayers, and often is caused by an increase in membrane fluidity (38). The Caillé parameter is a measure of the membrane fluctuations, taking into account the membrane rigidity and compressibility, see Equation 9. Other publications have also reported on an increased fluidity of the bilayers upon addition of kosmotropes, (108). However, such an increase in the fluidity of the bilayer is quite surprising, since it is expected to lead to an increase in the inter-bilayer repulsive forces. On the other hand, as mentioned before, (i) an increase of attractive van der Waals forces between adjacent layers caused by interlamellar

structured water and/or (ii) residual osmotic pressure effects would both lead to a decrease in d_w . Both d_w and η increases for increasing concentrations of AMEA, in comparison to betaine and sarcosine. But there is evidence to suggest that AMEA is able also to partition in the lipid headgroup interface, since molecular packing density changes have been clearly observed in in the gel-phase. This possible partitioning of AMEA also the lipid/water interface of the lamellar fluid phase could lead to a further increased fluidity of the bilayers, and hence, a significantly different trend in d_w and η when compared to sarcosine and betaine.

When comparing between the different humectants in the gel phase, Figure 44 shows that betaine decreases d_w the most at 2 M concentration with respect to sarcosine and AMEA. This may be interpreted that betaine to be the strongest kosmotrope of all three. Calculating the A_C for the gel phase and fluid phase provides insights to changes in packing density of the lipid chains, which have confirmed the ordering effect of all three humectants in the gel-phase. However, the observed $q_{20}:q_{11}$ peak ratio changes in the WAXS at high concentration of AMEA, indicates a change in the molecular electron contrast that might be caused by AMEA also partitioning in to the lipid headgroup interface. As this is not observed at the higher concentrations of betaine and sarcosine, it is evidence to support the preferential exclusion mechanism of betaine and sarcosine (78, 107). This mechanism of interaction would support the second proposed mechanism by Rudolph *et al.* (63) whereby the humectant affects the long range order of the water near the polar residues but does not interact directly with the lipid bilayer for sarcosine and betaine, but this does not strictly account for AMEA.

3.1.5 Conclusion

Three humectants named betaine, sarcosine and AMEA, and their influence on the structure and thermotropic behaviour of fully hydrated DPPC have been studied. The influence of each humectant on DPPC has been studied at a temperature range from 25 to 50 °C by X-ray scattering and DSC. In this temperature interval DPPC goes through two phase transitions: (i) at T_{pre} going from gel to ripple phase, and at (ii) T_M going from ripple to fluid phase. The addition of humectant has shown that T_{pre} is affected more than T_M reflecting its lower enthalpy for transition. The deduced enthalpy values from DSC results have shown that the enthalpy trends do not follow the corresponding transition temperature trends. The observed enthalpy trends might be explainable by

impurity effects, in particular at high solute concentrations, but further investigations will be necessary to clarify the exact lipid partition coefficients of all three humectants for both, the gel and fluid phases.

Changes to the nanostructure of DPPC has been studied by SAXS and WAXS. The results reveal that the addition of humectant leads to a decrease in d_w along with slight increase in d_{HH} . This behaviour suggests that the addition of humectant may lead to an increase in order of the membrane thereby reducing the inter-bilayer Helfrich repulsions. However, the possibility of increased van der Waals forces between the adjacent bilayers cannot be disregarded, since it would lead to the same reduction in d_w . The results from WAXS show that the addition of betaine and sarcosine does (i) increase the packing density of the chains slightly, but (ii) does not alter the electron density contrast. Thus, it can be interpreted that these humectants do not partition in to the lipid headgroup region and are acting as classical kosmotropes by the preferential exclusion mechanism from the lipid/water interface. In comparison, the addition of high concentrations of AMEA (> 0.4 M) the WAXS diffraction peaks display a changed intensity pattern, which suggests that there is a change in the molecular electron density as a result from AMEA being present in the lipid headgroup interface.

When considering the overall effects, by combining both the structural and thermal changes, it can be concluded that betaine and sarcosine behave as typical kosmotropes influencing DPPC phase behaviour the most, while AMEA is a weaker kosmotrope displaying less distinct preference between bulk water and the lipid/water interface.

3.2 The Structural and Thermotropic Properties of DPPC/DSPC Mixtures

3.2.1 Introduction

Due to the strong abundance of PCs in cells, the fluid phase of DPPC can be considered the biologically most relevant model system by which many structural properties of biological membranes can be understood. However, the lipid bilayer is not constructed by only one type of lipid but instead, a mixture of lipids in order to provide the optimum environment to house specific membrane-proteins (44) and in order to optimise various membrane functions (e.g. endo- and exocytosis) (49, 115). Biological cell membranes consist of complex lipid mixtures comprising not only phospholipid mixtures but also with glycolipids and sterols. Therefore, studying the thermotropic behaviour and nanostructure of phospholipid mixtures will provide further insights to the properties of biological membranes compared to studying pure lipid membranes. Furthermore, studying phospholipid mixtures has industrial relevance, for example, phospholipid based dermatological formulations using industrial lecithin samples which comprise a mixture of lipids and includes presence of impurities up to 10 %, see Table 8. Therefore, it is important to understand further the properties of such systems and compare their properties to that of equivalent, higher purity lipid mixtures which are more commonly used in fundamental research. Equipped with such information, the formulator is able to understand better the behaviour of industrial lipid samples and whether the learnings from model lipid systems can be applied to industrial lipid samples.

Table 8: Example composition of the commercial lipid sample Phospholipon 90H (P90H).

Fatty Acids	Impurities	Residual Solvents
Hydrogenated phosphatidylcholine (min. 90 %, of which approx. 85 % DSPC and 15% DPPC)	Hydrogenated Lysophosphatidylcholine (max. 4.0 %)	Ethanol (max. 0.5 %)
Unsaturated acids (max. 2%)	Oil/triglycerides (max. 2 %)	Acetone (max. 50 ppm)
	Moisture (max. 2 %)	Ethylmethylketone (max. 50 ppm)

In this study, a mixture of DPPC with DSPC, has been studied. The properties of both lipids on their own are very similar, due to their similar structure; the two lipids differ only in the hydrocarbon chain length where DSPC has two more methyl groups on each of the hydrocarbon chains. The thermotropic behaviour of both lipids on their own are summarised in Table 9. Furthermore, due to the longer hydrocarbon chain length, DSPC has a larger d spacing than DPPC of 6.75 nm compared to 6.38 nm, respectively, at 25 °C (17). The change in thermotropic and nanostructural properties for different DPPC/DSPC mixtures will be studied and also compared to a commercially available lecithin sample containing DPPC/DSPC lipids as listed in Table 8, named Phospholipon 90H, P90H. Here, any influence from the presence of impurities of industrial lipid samples may be highlighted in addition to their comparability to higher purity lipid systems.

Table 9: The phase transition temperatures of DPPC and DSPC. Adapted from (14).

Hydrocarbon chain length	$L_C \rightarrow L_{\beta'}$ T (°C)	$L_{\beta'} - P_{\beta'}$ T (°C)	$P_{\beta'} - L_{\alpha}$ T (°C)
16	18.8 ± 3.1	34.4 ± 2.5	41.3 ± 1.8
18	26.3 ± 5.2	49.1 ± 2.9	54.5 ± 1.5

3.2.2 Thermotropic Changes

The results from the DSC scans are summarised in Figure 55. Figure 55a also demonstrates the change in cooperativity for lipid mixtures compared their corresponding pure lipids where the main transition peak is clearly broadened for the lipid mixtures. This has been also observed with other PC mixtures (44) and the decreased cooperativity in the lipid mixtures indicates the presence of coexisting phases. For the 50:50 wt.% mixture, the DSC scans indicate significant instability and de-mixing of the lipids, as shown in Figure 55b, where both transition peaks show an overlap of two peaks. The overlapping of peaks suggests that there are two transitions occurring at very similar temperatures displaying similar enthalpies, thus there appears to be the melting of one lipid before the other and the presence of two co-existing phases especially at T_M , see Figure 56. Between the temperatures 38.0 and 39.2 °C the coexistence of the gel phase of DSPC and ripple phase of DPPC is given. Then between the temperatures 43.5 and 47.8 °C the coexistence of the ripple phase of DSPC and fluid phase of DPPC is observed.

Figure 56 shows that the DSC results agree well with literature values for the pure lipids (14) and shows that both T_{pre} and T_M increase with increasing concentration of DSPC. Results for the industrial P90H sample are also presented in Figure 56 showing good agreement with the higher purity sample of equivalent lipid composition. This suggests that the lipid thermotropic behaviour is not changed for the P90H sample with the presence of impurities. The shape of the phase diagram for DPPC/DSPC mixtures is similar to that of DMPC/DPPC mixtures (116) which exhibit close to ideal mixing, and despite decreased cooperativity, the presence of the 50:50 wt.% lipid mixture de-mixing has not been reported previously. Table 10 displays the phase transition temperatures for different DPPC/DSPC lipid mixture compositions.

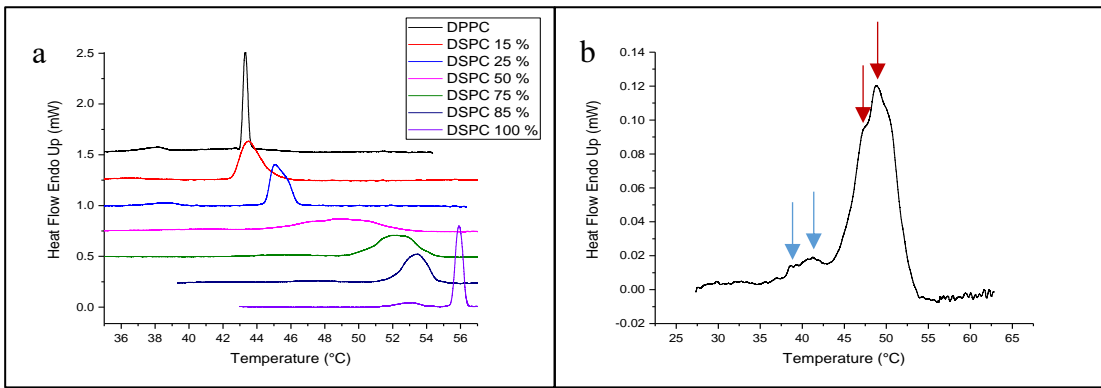


Figure 55: a) DSC heating thermograms for DPPC/DSPC mixtures at various compositions b) DSC heating thermogram for DPPC/DSPC mixture at 50:50 wt.% composition. The blue arrows indicate the splitting of the pre-transition temperatures of DPPC and DSPC, respectively, and the red arrows display the splitting of the main transition.

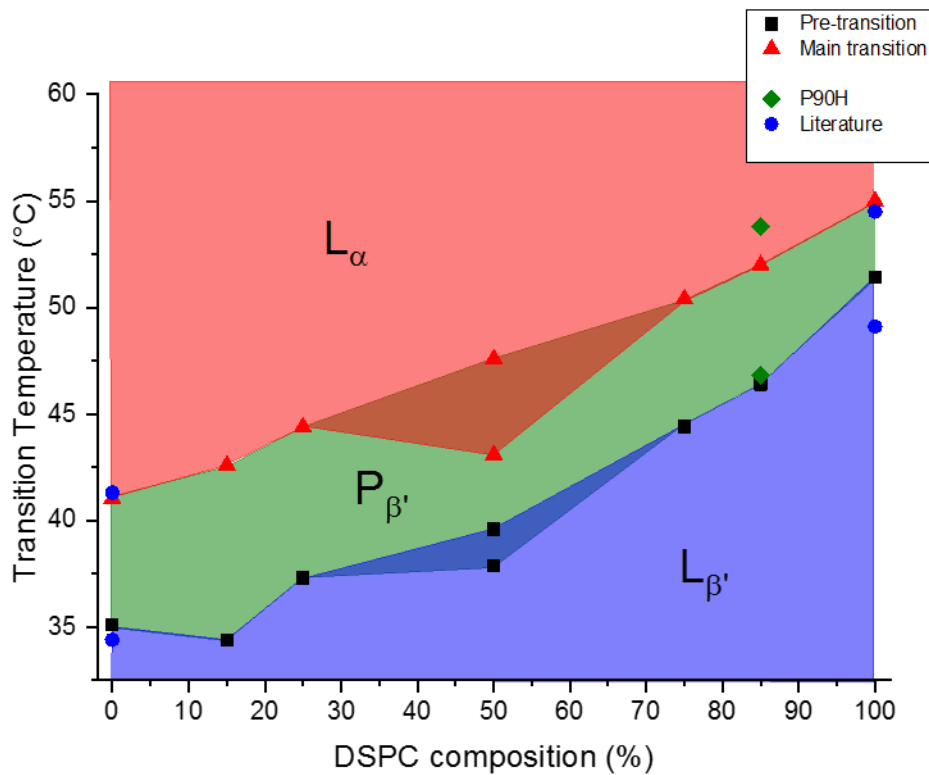


Figure 56: The phase diagram for DPPC/DSPC lipid mixture at different compositions. Literature values are taken from (14).

Table 10: The phase transition temperatures of different DPPC/DSPC mixtures and of commercial mixture P90H. Literature values taken from (14).

DSPC composition (%)	Pre-transition Temperature (°C)	Main transition Temperature (°C)	Literature		P90H	
			Pre-transition Temperature (°C)	Main transition Temperature (°C)	Pre-transition Temperature (°C)	Main transition Temperature (°C)
0	35.1	41.0	34.4	41.3	--	--
15	34.4	42.6	--	--	--	--
25	37.3	44.4	--	--	--	--
50	37.9	43.1	--	--	--	--
50	39.6	47.6	--	--	--	--
75	44.4	50.4	--	--	--	--
85	46.4	52.0	--	--	46.8	53.8
100	51.4	55.0	49.1	54.5	--	--

The change in peak width is plotted in Figure 57 for both the pre-transition and the main transition. An increase in the difference between the peak onset and offset, results in a “lens-shaped” plot as displayed in Figure 57a and b. This shape is similar to the behaviour of DMPC/DPPC mixtures studied by Garidel and Blume (44). Figure 57c and d show the change in full width half maximum, FWHM, of both transition peaks. This in turn, provides information on the cooperativity of the transition – the broader the peak, the lower the cooperativity of the transition i.e. the lipid chains are not melting as one unit as much. The FWHM plots show very clearly that the cooperativity is affected much more for the main transition compared to the pre-transition, as the FWHM does not change much in Figure 57c but there is a much more pronounced increase in FWHM for the mixtures at the main transition as shown in Figure 57d.

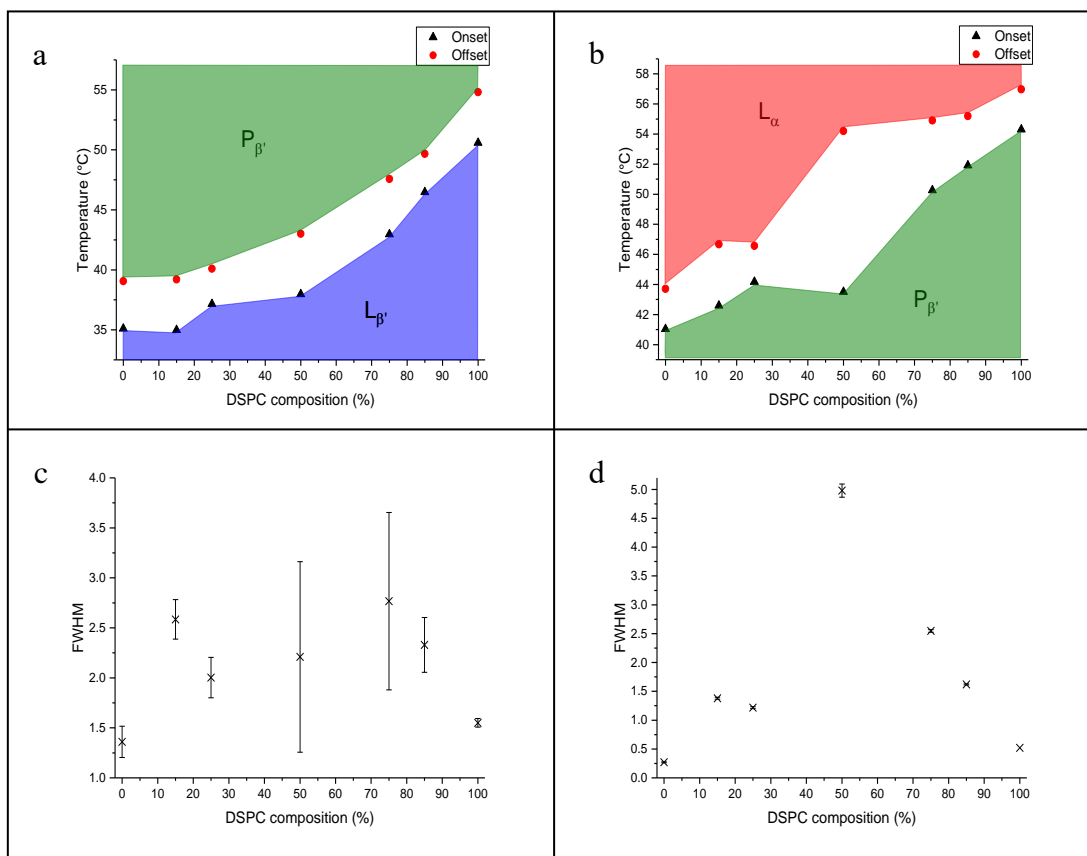


Figure 57: The change in peak full width half maximum for both phase transitions with change in DPPC/DSPC composition. a) the peak onset-offset difference for T_{pre} , b) the peak onset-offset difference for T_M , c) the change in FWHM for T_{pre} and d) the change in FWHM for T_M .

The change in enthalpy with change in composition for both the pre-transition and main transition is plotted in Figure 58. The plot shows that the experimental values for both pure lipid samples are in good agreement with literature (14). Furthermore, the enthalpy value for the pre- and main transition of P90H agree well with the higher purity sample. It is noted though, that the deviation is smaller concerning the pre-transition.

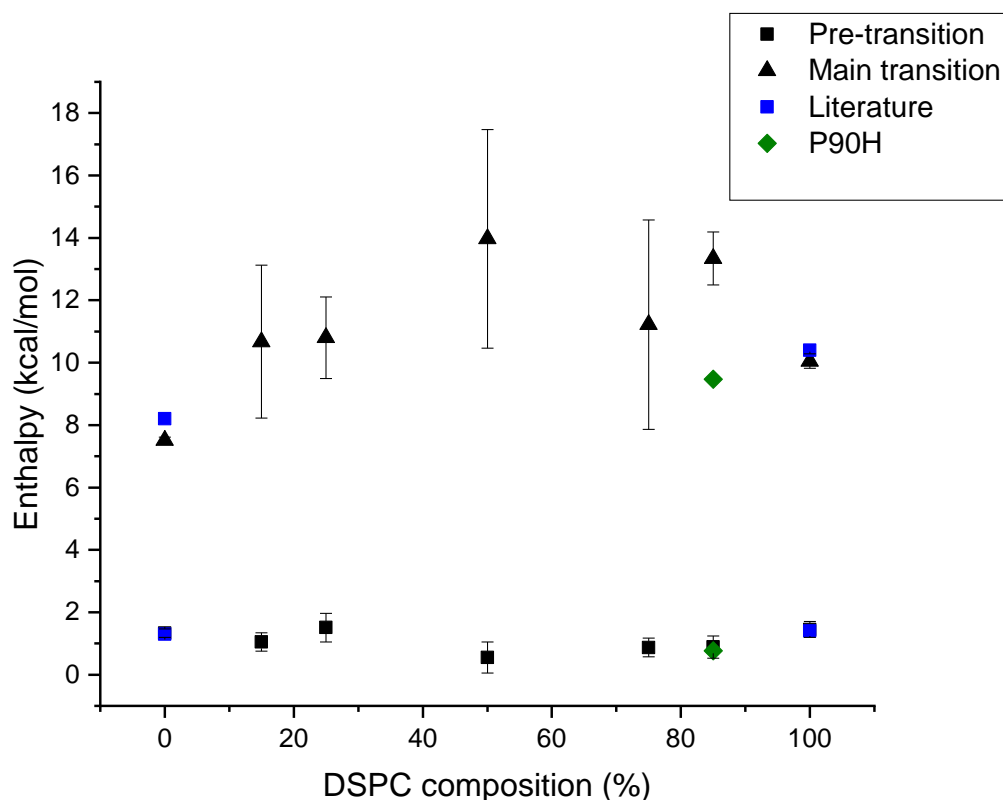


Figure 58: The change in enthalpy with change in DPPC/DSPC composition for both the pre-transition and the main transition. Literature values are taken from (14).

3.2.3 Structural Changes

The nanostructure of the lipid MLVs are compared for the higher purity mixture and the P90H sample. In Figure 59a the SAXS curves for both samples at 30 °C are very similar; both curves display 4 equally spaced *quasi*-Bragg peaks at very similar positions, reflecting the lamellar structure of the $L_{\beta'}$ phase. However, it can be seen that the peaks for the P90H sample are slightly broader than the higher purity sample, corresponding to a less ordered membrane stacking for the P90H sample. The SAXS curves for the P90H sample are shown in Figure 59b with increasing temperature. For the temperature range 20-60 °C studied, all three phases are observed: the gel, ripple and fluid phase. This behaviour is well represented by tracking the change in d spacing with increasing temperature, see Figure 60, reproducing the typical behaviour of PCs, see Figure 38 for comparison. The d spacing for P90H and higher purity sample have been measured and are 7.12 nm and 6.81 nm, respectively, at 30 °C. The d spacing for both samples are larger than the estimated d spacing, determined from literature values

(17) of DPPC as 6.38 nm and DSPC as 6.75 nm and correcting for the lipid composition of 85 % DSPC $((0.15 \times 6.38) + (0.85 \times 6.75))$, which is 6.69 nm. While the d spacing of the higher purity sample is only slightly larger than the estimated value, the d spacing for the P90H is significantly larger in comparison. Due to the larger stacking disorder shown in Figure 59a, it is tempting to assume that the main difference in the d spacing of P90H stems from a relatively higher hydration level of the MLVs. Nevertheless, the combined SAXS and DSC results of P90H shows that the presence of impurities does not affect the overall structure and thermal behaviour of the lipid very significantly.

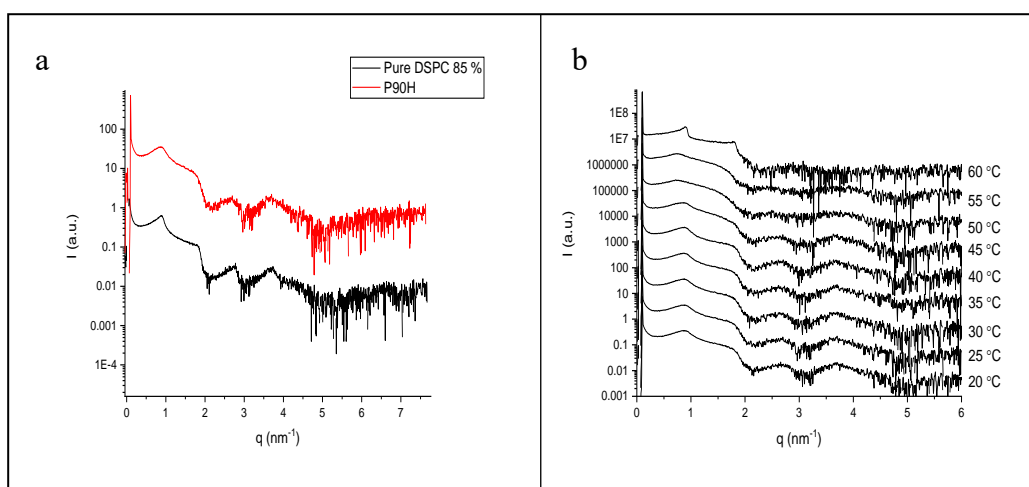


Figure 59: a) The SAXS curves of DSPC:DPPC, 85:15 wt.% mixtures respectively, and P90H at 30 °C. The black line is for higher purity lipid samples and the red line is for commercially available lipid sample named P90H. b) The SAXS curves of P90H at different temperatures. The SAXS curves have been stacked-plotted for clarity.

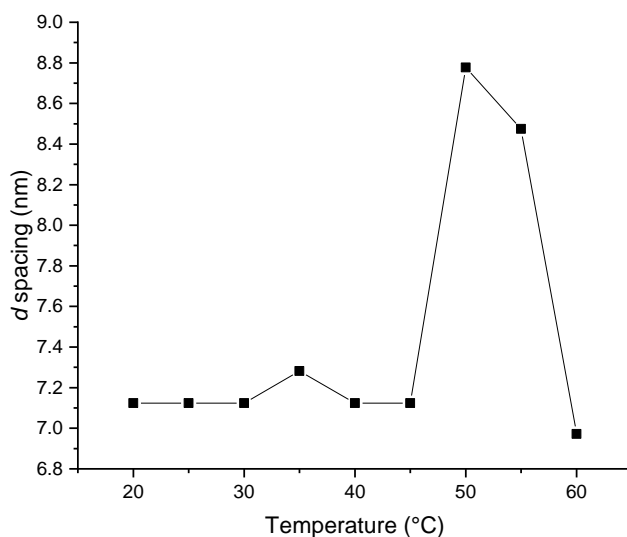


Figure 60: The change in d spacing with temperature for P90H.

The X-ray scattering results for the gel phase of the lipid bilayer, at 30 °C, shows that d_{HH} increases with increasing concentration of DSPC in the mixture, as shown in Figure 61a. This reflects the longer hydrocarbon chains of DSPC that is added increasingly to DPPC. Figure 61b displays only small changes in d_w where the addition of DSPC at small concentrations < 50 wt. % leads to a slight decrease, which suggests a relative stiffening of the bilayers (reduced Helfrich-undulation repulsion forces). However at concentrations \geq 50 wt.% DSPC, there is no further significant reduction in d_w , i.e. bilayer undulations do not decrease any further. The little change in d_w combined with a dominant increase in d_{HH} with increasing DSPC concentration, leads to an increase in d spacing with increasing DSPC concentration, see Figure 61c. A plot of the EDPs is shown in Figure 61d, illustrating the overall structural changes to the bilayer with different DPPC/DSPC compositions. It can also be seen nicely from the EDPs that the d_{HH} increases with increasing DSPC concentration.

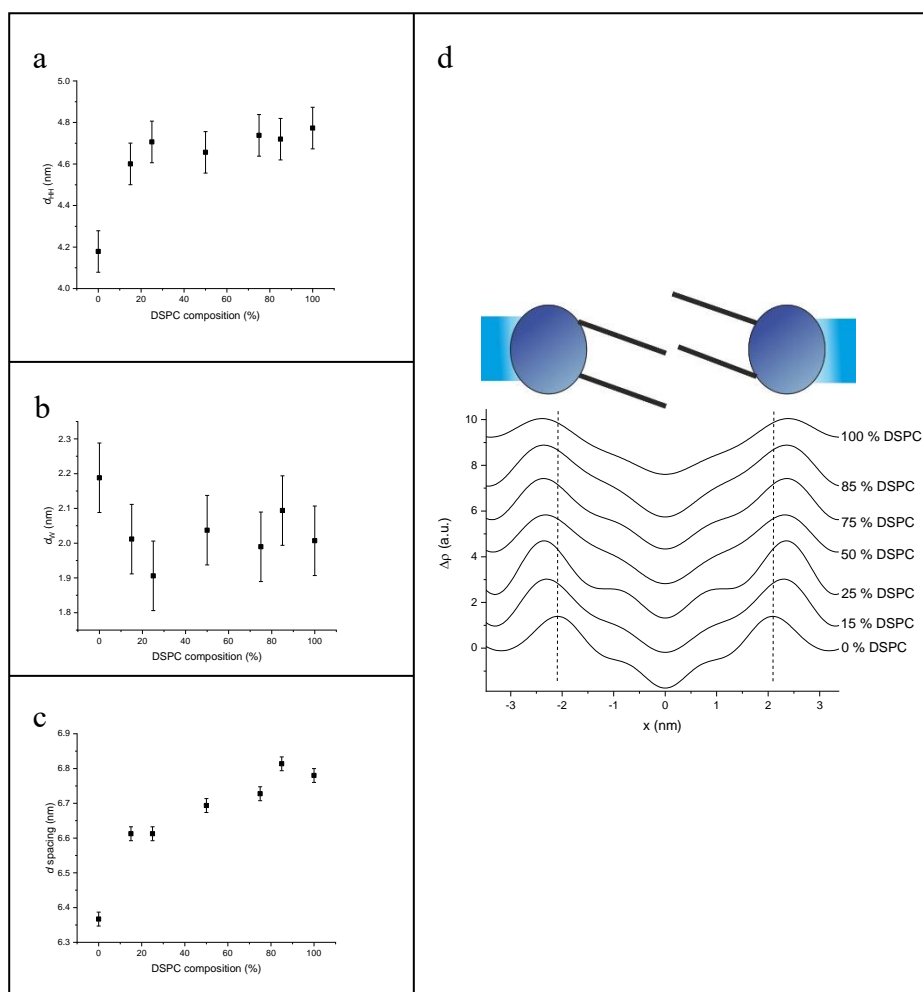


Figure 61: The change in structural parameters of the lipid bilayer with changing DSPC composition at 30 °C. The change in a) head-to-headgroup thickness b) water layer thickness c) d spacing. d) The electron density profiles for each composition.

The global fits of the fluid phase are presented in Figure 62, good fits for each temperature were achieved and are reflected by the red solid lines fitting nicely with the SAXS raw data. The fewer number of curves for the higher concentrations of DSPC reflects the increased T_M and hence fewer curves were recorded in the fluid phase. For the 50 wt.% DSPC, one may notice that despite obtaining acceptable fits, the *quasi*-Bragg peaks are less defined and instead more diffuse scattering observed which reflects a more disordered system and concomitant detachment of bilayers, when compared to the other concentrations, see Figure 62d.

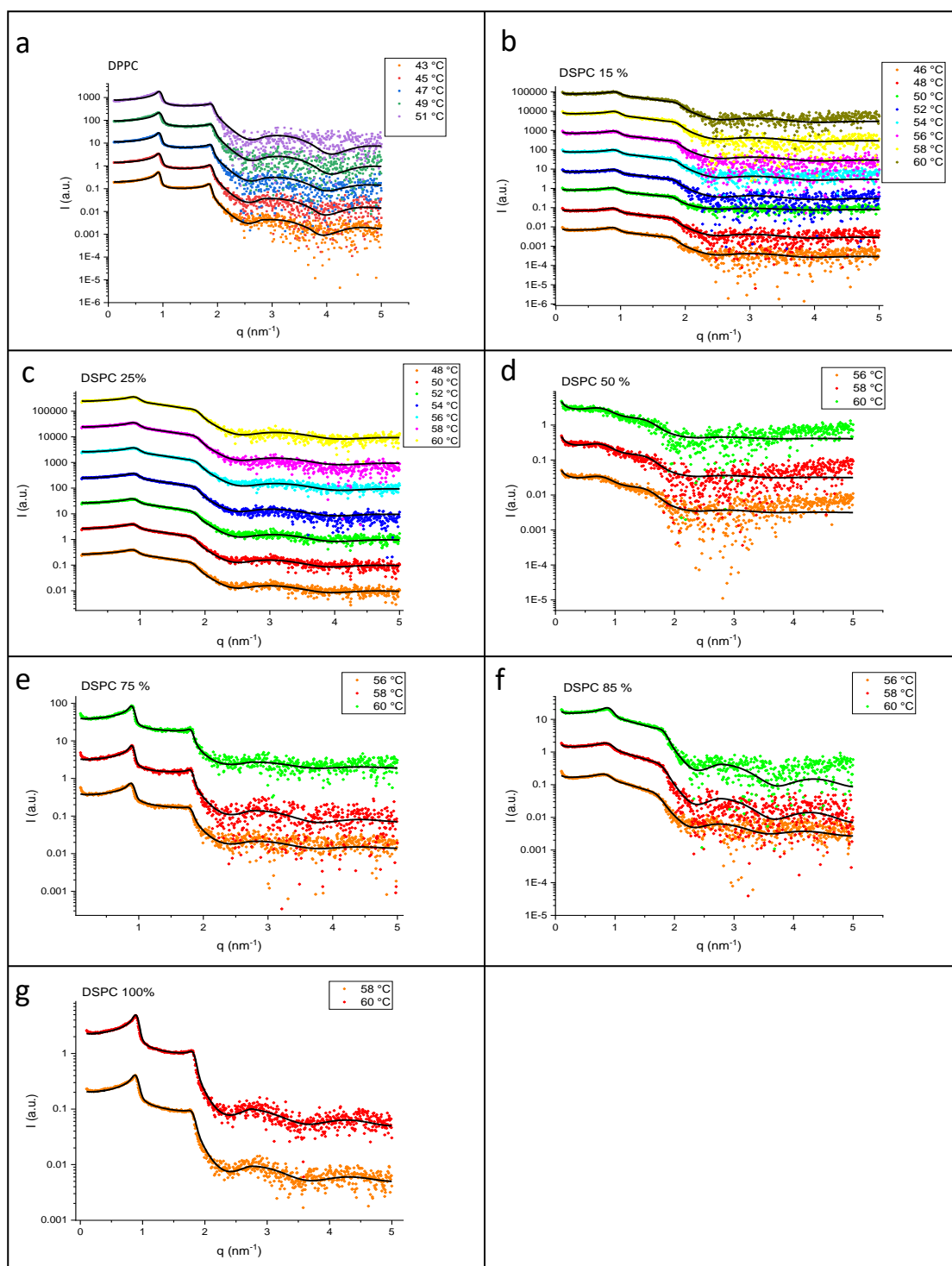


Figure 62: The SAXS curves of the fluid phase and their global fit results represented by the black lines of a) DPPC pure b) 15 % DSPC c) 25 % DSPC d) 50 % DSPC e) 75 % DSPC f) 85 % DSPC and g) 100% DSPC pure. The SAXS curves of different temperatures are stacked for clarity.

Results from the fluid phase fits show that the structural parameters change in the same manner as the gel phase. Figure 63 displays the results from fitting the fluid phase for all temperatures recorded. The change in T_M is highlighted in Figure 63, where the fluid

phase is observed at higher temperatures with increasing concentration of DSPC. A clear trend is observed for d_{HH} shown in Figure 63a, where it decreases with increasing temperature. This is expected from the general behaviour of PCs due to increased thermal mobility leading to an effective shrinkage of the hydrocarbon chain length from the all-*trans* to *trans-gauche* conformation. Moreover, a general trend is observed as d_{HH} increases with increasing concentration of DSPC. No such trend is observed for d_w as shown in Figure 63b, instead, a marked increase for 50 wt.% sample is noted. In the same way as the gel phase regime, it is most plausibly caused by an onset of stronger membrane undulations at this concentration. As a result of the changes in d_{HH} and d_w , the d spacing follows the observed trend of d_{HH} by increasing with increasing concentration of DSPC, with the exception of the 50 wt.% sample, see Figure 63c. The change in the mean fluctuations of the membrane position, σ , is plotted in Figure 63d with change in lipid composition, however no obvious trend in the fluctuations can be seen, but this parameter will be discussed again, when presenting the T_M plus 2 °C data. To eliminate the dependence of the change in T_M for the fluid phase, a plot for each structural parameter at temperature $T=T_M + 2^\circ\text{C}$ is presented in Figure 64. For d_{HH} the expected general trend is observed as it increases with increasing concentration of DSPC, see Figure 64a. For d_w on the other hand, there is very little change with change in lipid composition. However, it is notable that the 50:50 % sample leads to a strongly increased d_w , which suggests that the MLVs are much more swollen when compared to the other lipid mixtures. The d spacing, again follows the trend in d_{HH} as there is little effect on d_w with composition. In Figure 64d, the plot of σ with DSPC composition shows that the addition of increasing concentrations of DSPC increases σ , reflecting the dependence of σ on the increase in d spacing. Furthermore, plotting the average number of bilayers in registry with increasing concentration of DSPC, as in Figure 65, shows that the lipid mixture leads to a reduced number and thus less ordered bilayer systems reaching a minimum at 50:50 wt.% lipid composition, compared to either pure DPPC or DSPC.

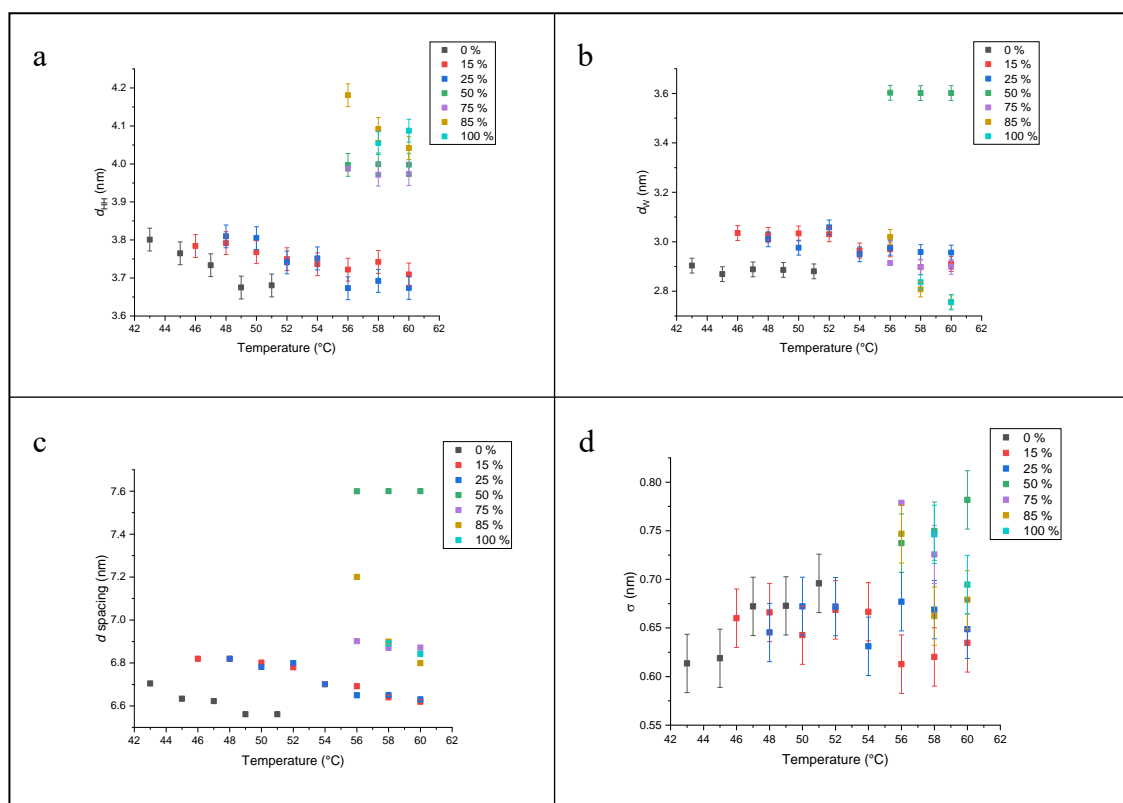


Figure 63: The change in structural parameters of the lipid bilayer with changing DSPC composition in the fluid phase. The change in a) head-to-headgroup thickness b) water layer thickness c) d spacing and d) mean fluctuations of the membrane position, σ .

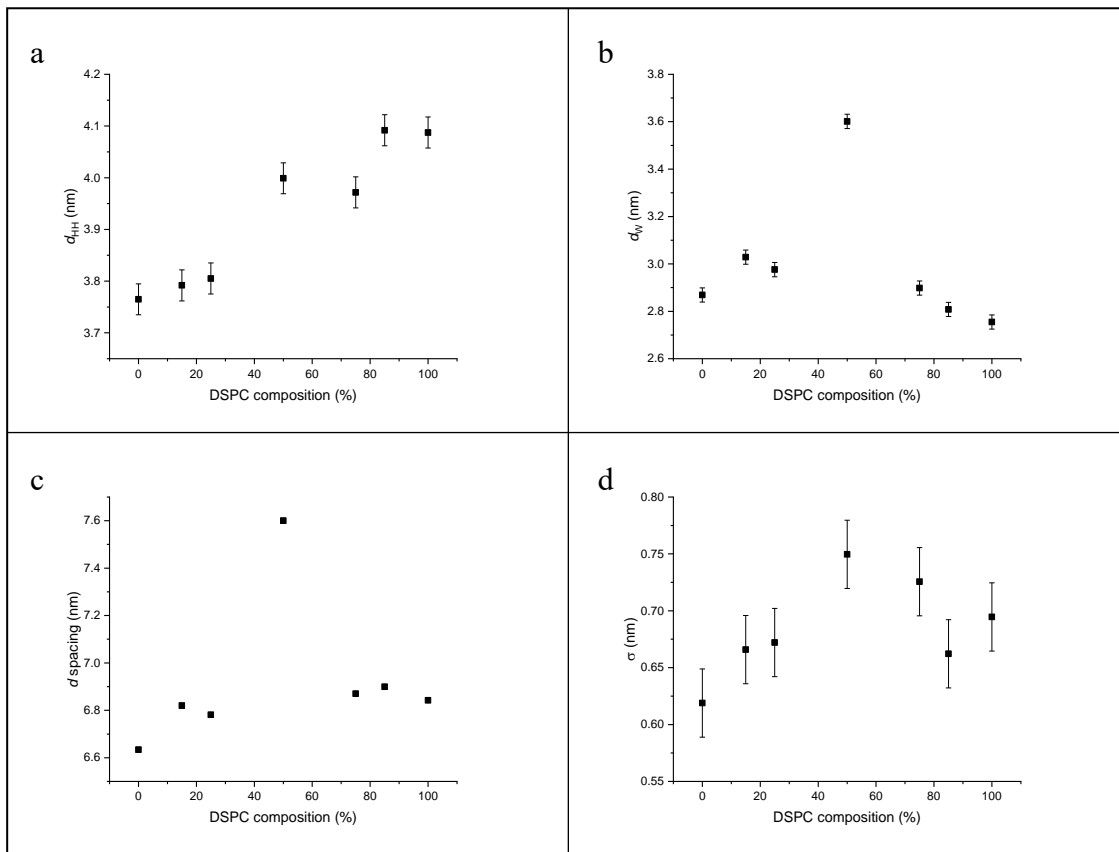


Figure 64: The change in structural parameters with change in lipid composition for the fluid phase at $T=T_M + 2$ °C. The change in a) head-to-headgroup thickness b) water layer thickness c) d spacing and d) mean fluctuations of the membrane position, σ .

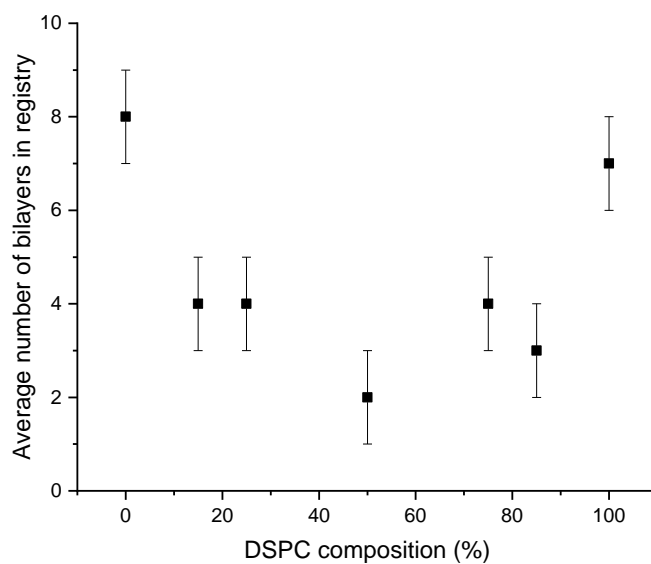


Figure 65: A plot of the change in average number of bilayers in registry in the fluid phase with increasing concentration of DSPC

3.2.4 Discussion

3.2.4.1 Thermotropic Changes

The observed changes to the transition temperatures were expected as the increasing concentration of DSPC, which has higher phase transition temperatures than DPPC, leads to an increase in both T_{pre} and T_M . The addition of DSPC increases the amount of intermolecular van der Waals forces in the system due to the presence of longer hydrocarbon chains which in turn, leads to increased transition temperatures. The DSC scans revealed that the 50:50 wt.% mixture was most unstable and appears to have de-mixed, reflected by the presence of two overlapping heat flow peaks at each transition. This de-mixing suggests inhomogeneities of the lipid mixture, thus giving rise to the possibility of lateral phase separation as observed by Shimshick and McConnell (45), however, the SAXS results have not revealed the presence of phase separation. To investigate this further, neutron scattering can be utilised where one lipid is deuterated and the extent of lateral lipid mixing can be visualised and/or atomic force microscopy measurements that would spot lateral de-mixing of phases even in the absence of stacking registry of the co-existing phases. A random, purely lateral phase separation would not give rise to distinct sets of diffraction peaks from X-ray scattering measurements (only one lattice would be apparent in this case), while in a phase separation with stacking-registry would allow X-ray scattering recordings to identify coexisting lattices, see Figure 66.

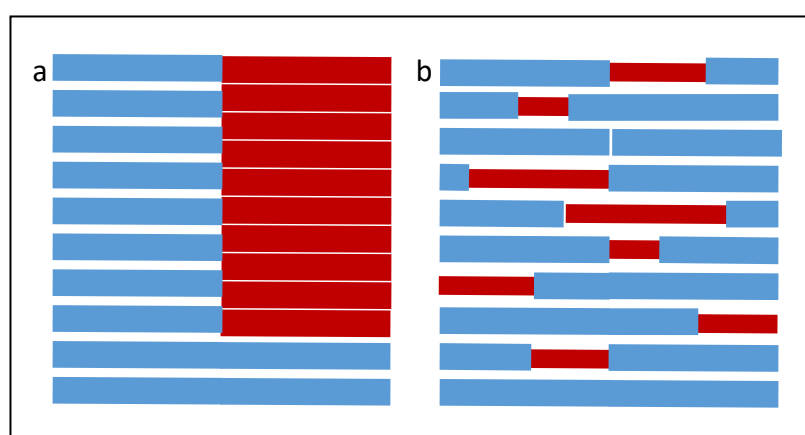


Figure 66: An illustration explaining two co-existing lamellar phases displaying (a) both phases in stacking-registry and (b) lateral phase separation without stacking-registry. SAXS measurements would show two distinct sets of Bragg peaks in the first case, while for the latter case the SAXS pattern would display only one set of diffraction peaks (i.e. 1 lattice is given).

When comparing an industrial lipid mixture sample, named P90H, of 85 % DSPC and 15 % DPPC with up to 10 % impurities, to its corresponding higher purity lipid mixture, DSC measurements have shown that the presence of impurities does not affect the phase behaviour of P90H significantly, where the phase transition temperatures are very similar. The enthalpy values for the pre-transition are very similar whereas the main transition enthalpy is decreased for the P90H sample. This is expected due to the presence of impurities which leads to a compromised cooperative transition with their presence consequently affecting the intermolecular interactions present in the overall system. Briefly, the inclusion of impurities leads to decreased intermolecular forces present and thus decreases the enthalpy for the main transition where the hydrocarbon chains melt.

The cooperativity of the lipid mixtures is decreased compared to their corresponding pure lipids as reflected by broader thermal phase transition peaks. This observed decrease in the cooperativity is due to the coexistence of gel and fluid domains which are melting at different temperatures at the transition (45, 52). Garidel and Blume (44) found that the miscibility of two lipids is lower in the gel phase than in the fluid phase, this is attributed to the tighter packing of the chains and the absence of in-plane lipid diffusion in the lamellar gel-phase. The degree of mixing is reflected in the shape of the phase diagram where the observed 'lens'-shaped reflects a two phased region between the gel and fluid phases, as observed in Figure 57. The phase diagram also shows close to ideal mixing, where the pair interactions between pure and mixed lipids are equal (116). The mixing behaviour is governed by a combination of lipid properties: the degree of hydrocarbon chain mis-match, difference in headgroup structure and charge and whether there is chain tilt present in the liquid crystalline phase, as well as the specific phase being studied (i.e. gel is more immiscible than fluid phase). Furthermore, it was observed that the cooperativity for the main transition is affected more so than for the pre-transition. This is a result of taking in to account the 50:50 wt.% mixture where the apparent main transition FWHM is increased substantially, due to a phase separation and overlap of two peaks from two separate phase transitions.

The lipid mixture compositions have influenced the enthalpies of the main transitions, however within measurement errors the pre-transition enthalpies are not affected. For the main transition, the introduction of a lipid mixture leads to an increase in the

enthalpy compared to pure DPPC. The increased enthalpy values for the lipid mixtures suggest that the lipid mixture leads to stronger intermolecular forces (49) due to possible increased van der Waals forces. This is the case as we introduce DSPC into pure DPPC, DSPC has longer hydrocarbon chains and therefore has more possible regions for van der Waals attractions. The increase in enthalpy may also suggest that, due to the increased intermolecular forces, there may be an increase in the molecular packing of the lipids. However, further experiments such as conducting WAXS measurements would need to be carried out to determine the area per lipid chain, A_c , to confirm this notion. When comparing the P90H sample, its enthalpy values are again similar to the higher purity sample, reflecting its similar nature.

3.2.4.2 Structural Changes

The SAXS results highlight the change in the nanostructure of the lipid bilayer as DSPC is incorporated at increasing concentrations to DPPC. In general, the same structural changes are observed for both the gel and the fluid phase. As the concentration of DSPC increases, d_{HH} increases while d_w is independent to any composition changes, and thus the overall effect results in an increase in the d spacing. The lack of trend for d_w is not surprising as all samples are prepared such that the lipid is in excess of water and thus the bilayers are fully hydrated. Note also, that the head groups are the same for DPPC and DSPC, and thus, the water/lipid interface remains structurally unaltered. Therefore, a constant value of d_w is reflecting full hydration and cannot be increased further, but also cannot decrease as dehydration was consciously avoided by providing excess water. However, relatively swollen MLVs are observed for the 50:50 wt.% mixture as its corresponding d_w is much larger than all the other lipid samples, as well as a substantial bilayer detachment is seen which is reflected in the global fitting where the fraction of unilamellar vesicles in this sample resulted the highest of all fits. The increase in d_{HH} reflects the longer hydrocarbon chain of DSPC compared to DPPC, and hence the higher concentration of DSPC leads to larger d_{HH} . For the fluid phase, the trend in d_{HH} is not as clear as in the gel phase as there is the additional complications given by the apparent anomalous swelling regime at the temperature range being studied, see Chapter 1.1.6.

Also, the 50 wt.% DSPC lipid bilayer appears to be the most unstable in the fluid phase with d_w being higher than expected, reflecting the sample with the largest chain length

mismatch and displaying the strongest repulsive undulation forces, see Figure 64d. This was also observed in the DSC results which showed the presence of two events at each transition reflecting the two overlapping transitions from each lipid. The marked immiscibility of the 50:50 wt.% mixture may be due to it being the composition with the highest hydrocarbon chain mismatch, where there is no dominant lipid. This instability is further reinforced at in the fluid phase where the bilayers appear to detach from each other due to increased thermal fluctuations, giving rise to diffuse scattering rather than *quasi*-Bragg peaks observed compared to the other lipid mixtures. This decreased order of the bilayers is observed for all of the mixtures, compared to the pure lipids. This is shown by the decreased average number of bilayers in registry for the mixtures (reduction in *quasi* long-range order). Furthermore, σ is calculated from the results of the global fits of the fluid phase, this provides an indication to the mean fluctuations of the membrane position. Within errors, σ , remains constant with the exception of the 50 wt.% sample. Here clearly increased membrane undulation are observed (as also displayed in the anonymously high d_w value) and it is tempting to assume that the lateral de-mixing of DPPC and DSPC may lead to a mechanically less rigid membranes.

Furthermore, studying the higher impurity P90H sample by SAXS has revealed that the presence of up to 10 % impurities does not affect the overall structure of the lipid. P90H still exhibits the lamellar structure and displays the same phase behaviour as its corresponding higher purity lipid mixture. The only observed effect of the impurities is a slight compromise on the order of the system, as broader *quasi* -Bragg peaks are observed for the gel phase. Additionally, the d spacing is larger than the calculated d spacing and the d spacing of the higher purity sample, suggesting the possibility of slightly swollen MLVs due to the impurities. It may well be that the impurities lead to an increased fluidity and in turn lead to stronger Helfrich undulation forces that would explain the relatively higher membrane to membrane distance.

3.2.5 Conclusion

Mixtures of DPPC and DSPC compositions have been studied by DSC and SAXS to reveal their phase behaviour and changes in structure. Additionally, an industrial sample of a lipid mixture named P90H has been studied and compared to its corresponding

higher purity lipid mixture to understand the effect of the impurities present on the lipid behaviour.

The DSC results reveal an increase in both the T_{pre} and T_M with the addition of increasing concentration of DSPC to DPPC. The cooperativity of the transitions, especially for T_M , is reduced as the mixtures are introduced, which is reflected by the broader transition peaks (increased FWHM). Importantly, at 50:50 wt.% composition the sample immiscibility reaches maximum with the FWHM of T_M being the largest and both transitions displaying an overlapping of two transition peaks. This overlapping of the heat flow peaks suggests that the transition is not only the least cooperative, but also that the lipid system does not act as one cooperative unit, but two. This puts into question the homogeneity of the MLVs and suggests there is the possibility of lateral phase separation of the two lipids. The instability of the 50:50 wt.% composition was also observed in the fluid phase of SAXS results; as the temperature is increased, there is increased thermal disorder, which has led to detachment of bilayers reflecting the diffuse scattering present instead of *quasi*-Bragg peaks and the lowest number of bilayers in registry (2).

Results from the SAXS measurements also revealed nanostructural changes to the bilayers where, for both the gel and fluid phases, there is a sigmoidal increase in d_{HH} with increasing concentration of DSPC, reflecting its longer hydrocarbon chain compared to DPPC. With little trend observed for d_w , the resulting d spacing, the sum of d_{HH} and d_w , increases with increasing concentration of DSPC. Importantly however, the fluid phase with a 50:50 wt.% mixture displays a larger d_w than expected, this suggests a swollen system present. By performing global fits of the fluid phase, further structural changes to the bilayers are revealed. When comparing the lipid mixtures to their corresponding pure lipids, it was observed that the number of bilayers in registry to each other is decreased for the lipid mixtures. Furthermore, the membrane undulations are increased for the mixtures, again displaying the strongest effect for the 50:50 wt.% mixture.

Finally, by studying the P90H sample and comparing it with the corresponding 85 wt.% DSPC high-purity sample, it can be concluded that the presence of up to 10 % impurities has little effect on the overall lipid behaviour. DSC results show that the phase transition temperatures and their corresponding enthalpies are similar. The SAXS results show that the nanostructure is also very similar displaying the lamellar structure

and typical behaviour of PCs for the d spacing with increasing temperature. The only difference observed for P90H is a larger d spacing and broader *quasi*-Bragg peaks in the gel phase compared to the higher purity sample reflecting slightly swollen and less ordered MLVs.

3.3 The Nanostructure of Commercial Lecithin-Containing Novel Multi-Component Formulations

3.3.1 Introduction

The previous two results sections have studied the behaviour of phospholipids in aqueous environment. This section will now study the behaviour of phospholipids in multi-component systems, i.e. more than three components in the system. The oil in water emulsion comprise the P90H phospholipid vesicles with long chained alcohols, long chained fatty acids, isostearyl isostearate, ISIS, as well as shea butter and a commercially available polymer named Sepimax Zen™. Typically, such phospholipid-based formulations can be used to tackle dry skin conditions.

It is well known that the stratum corneum has a high barrier to penetration for the skin which has caused challenges to deliver drugs into the body via the skin (117). The evaporation of water is 10x slower through the human skin than the evaporation of water through the cucumber skin (118). Dry skin arises when the skin barrier is compromised and unable to maintain water retention and therefore there is a shortage of water in the stratum corneum. The barrier function stems from the lipid matrix consisting mainly of ceramides, cholesterol and free fatty acids, surrounding the flat cells found in the stratum corneum called corneocytes (119), see Figure 67. The lipid-based membranes are organised parallel to the surface of the skin, wherein the lipid chains are packed onto an orthorhombic or hexagonal lattice. See Figure 67 to understand the difference in the lipid arrangement between orthogonal and hexagonal packing. It is found that the more permeable hexagonal packing is commonly found on the outer layers of the skin compared to the orthorhombic packing found deeper (120), and the hexagonal packing can be induced by increasing the temperature (119). It is believed that the orthorhombic packing of the skin lipids combined with the lamellar structure is responsible for its barrier properties (120). Therefore, the gel phase of PCs which exhibit orthorhombic packing is well suited for skin cream applications for enhancing the barrier function of the skin, and hence are suitable components for dermatological formulations to reduce dry skin conditions. Skin creams can interact with the skin in various ways depending on their function; the use of phospholipids as carriers for drug delivery in topical applications has shown promising results (7, 8),

surfactants can also be used to increase permeation of the skin for drug delivery (121). However, the purpose of the skin cream formulation studied herein, is for the phospholipid in the skin cream to interact with the outermost layer of the stratum corneum. Such skin creams are delivered to the skin to increase the skin barrier permeation and as reinforcement to damaged parts of the dry skin (122).

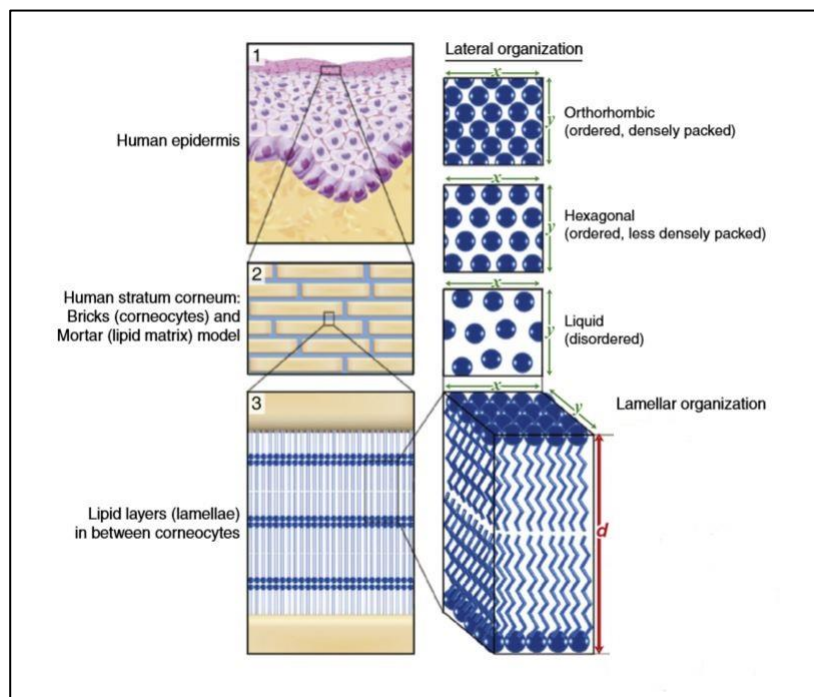


Figure 67: The structure of the upper layer of skin – 1) the stratum corneum, 2) using the bricks and mortar analogy and 3) showing the structure of the lipids surrounding the corneocytes. The right-hand side also shows the difference in lateral organisation of the lipids between orthorhombic, hexagonal and liquid packing. Adapted from (123).

ISIS is commonly used in dermatological formulations for its emollient properties (124). Fourier transform infra-red spectroscopy, FT-IR, studies by Caussin *et al.* (119) have shown that the addition of ISIS favours the orthorhombic packing of lipid systems containing ceramides, cholesterol and free fatty acids, the more tightly packed lipids therefore leads to decreased permeability of the skin. Pennick *et al.* (120) found that whilst the addition of ISIS to formulations leads to increased stability of the orthorhombic packing of the lipids, it also improves the skin barrier's water permeation resulting in increased hydration, rather than increasing the occlusivity of the skin barrier. This increased water permeation may be due to the structure of ISIS, see Figure 68, where the molecule penetrates the membrane and the presence of the side branches

on the hydrocarbon chains may prevent tight lipid packing and thus, increase the permeability (124). The addition of long chained fatty acids also improve dry skin conditions, by reducing the skin permeability barrier through inducing the more tighter orthorhombic packing state (91, 125).

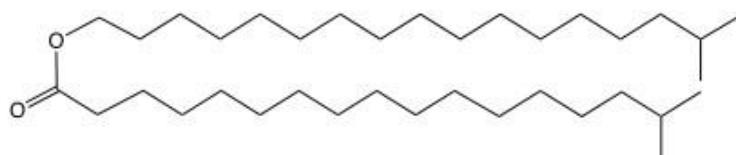


Figure 68: The structure of isostearyl isostearate.

Moreover, Hartkamp *et al.* (126) studied the effects of long chained alcohols on the gel phase of DSPC lipid membranes. It was found that the difference in length of the hydrocarbon chains between the alcohol and the lipid is crucial to determining the overall structure. The alcohols are interdigitated within the lipid membranes and the alcohol headgroups would be located deeper into the membrane than the lipid headgroups. A consequence is that alcohols similar in chain length as the lipid would protrude into the centre of the bilayer. Therefore, if shorter chained alcohols are added to the membrane, there is less protrusion into the centre of the membrane. It was concluded that to gain a denser chain packing, alcohols with hydrocarbons chains shorter than the lipid are favoured.

Shea butter is a triglyceride consisting of various fatty acids (127) mainly of stearic and oleic acid. It is a popular component in skin care products (128) with benefits including anti-inflammatory and anti-oxidant effects due to its high content of unsaponifiable molecules (e.g. phenols and sterols), and thus a natural source of vitamin E (129).

So far in the published literature, studies on the effect of long chained alcohols, free fatty acids and ISIS on lipid structures have been conducted, however of each component individually. In this study, the stability of the lipid lamellar structure to all of the aforementioned components present together will be investigated. Furthermore, the influence of shea butter and Sepimax ZenTM polymer on the structure will be investigated. Thus, the overall objective of this study is to determine the structure of a typical oil in water skin cream as it would be found before application (wet samples)

and after application to the skin as a dried film (dried samples). The outcomes of this study will therefore enable the formulator to understand how the overall structure of an end-product phospholipid formulation is, as well as understand whether this structure is maintained when the cream dries upon film formation on the surface of the skin.

3.3.2 Nanostructural Changes

The structure of the samples, compositions as detailed in Section 2.2.5, are investigated by SAXS. It is already known, from Section 3.2, that the main lipid component named P90H forms MLVs when in excess water. Therefore, the now multi-component systems will provide insight to the stability of this lamellar phase from P90H.

3.3.2.1 “Wet” samples

SAXS measurements were performed on a variety of formulations containing the same components but differing in their concentrations. The reader is referred to Table 4 in Section 2.2.5 for the full details. Briefly, each formulation code refers to the concentration of (i) lipid structural component, (ii) Sepimax ZenTM and (iii) shea butter, in that order. 0 refers to the zero or low concentration of the component and 1 refers to high concentration. For instance, the formulation code 100 refers to the formulation with high concentration of lipid structure component and low concentration of Sepimax ZenTM polymer and shea butter.

Figure 69 shows the different formulations lead to different SAXS patterns at 25 °C. The conditions of these samples simulate the conditions of the formulations as they would be, if they are stored at room temperature either at the store shelves or at the consumer’s home, therefore offering insight to the structure of such formulations found in skin cream bottles. Overall, all SAXS curves show the presence of one or more lamellar phase existing in stacking-registry in each sample. Throughout all samples studied, three different and mostly lamellar phases are identified corresponding to different d spacings, with each set of peaks labelled by colour coded arrows corresponding to the 1st, 2nd ...etc. order reflections of the different phases. The orange arrows correspond to a lamellar phase with d spacing of 17.8 nm for samples 110 and 111 and 21.4 nm for sample 100 (see Table 4 in Section 2.2.5 for code details). Note, that here reflections up to the 3rd order are recorded. The blue arrows correspond to a

lamellar phase with d spacing of 5.88. In this case only the 1st order reflection is observed. Finally, the black arrows indicate a lamellar phase with a d spacing = 4.44 nm. Here the 1st and 3rd order reflections are seen. The samples with formulation code 000 and 110 contain only the lipid structural component and polymer, Sepimax ZenTM, but no shea butter is present. 000 displays the presence of one phase only, whereas the 110 formulation shows the co-existence of two phases. Therefore, this suggests that at high concentrations of lipid and polymer, two phases form with distinct lattices, one being lipid component rich and the other polymer component rich. However at low concentrations (000), the scattering pattern of the polymer-rich phase dominates.

In order to further identify the phases, it can be seen that formulation 001, with high concentration of shea butter, displays only one lamellar phase corresponding to d spacing of 4.44 nm. As these peaks are not present in the samples with no shea butter, it can be deduced that the peaks labelled with the blue arrows and corresponding to the d spacing of 4.44 nm are due to the shea butter triglycerides phase. Interestingly, as mentioned above, only the 1st and 3rd order reflection are recorded, which gives a very clear indication for the formation of the α -polymorph with a hexagonal packing of the hydrocarbon chains (130). Other common triglyceride polymorphs exist (i.e., β' and β polymorphs (130)), however they do not suppress the 2nd order reflection, but display an intense 2nd order reflection. The other two phases correspond to the lipid structural component and a polymer-rich phase. The 010 sample has a high concentration of polymer and only shows the 1st order reflection corresponding to a d spacing 5.88 nm. Since for the polymer-rich phase only one diffraction peak is observed, one cannot conclude, which kind of lattice is given. It might be of lamellar type, but future expanding and deepening studies will be necessary to confirm the true nature of the polymer-rich aggregates. In contrast, the samples high in concentration of the lipid component display up to 4 diffraction orders corresponding to a lamellar phase with a repeat distance d of 17.8 or 21.4 nm.

The deduced d spacing of 17.8 nm for the lipid structural component reveals the effect of the long-chained alcohols, free fatty acid and ISIS on P90H. In the previous results section, the d spacing of P90H was 7.12 nm in the gel phase, therefore the other components present have interacted and increased the d spacing of P90H by 10.68 nm. Overall, the presence of other components in the formulation has shown that the lamellar phase of P90H is still stable despite the d spacing being much larger. 3 to 4

reflection orders are recorded in the lipid-rich phases which signifies that the lamellar stacks are still, quite well ordered.

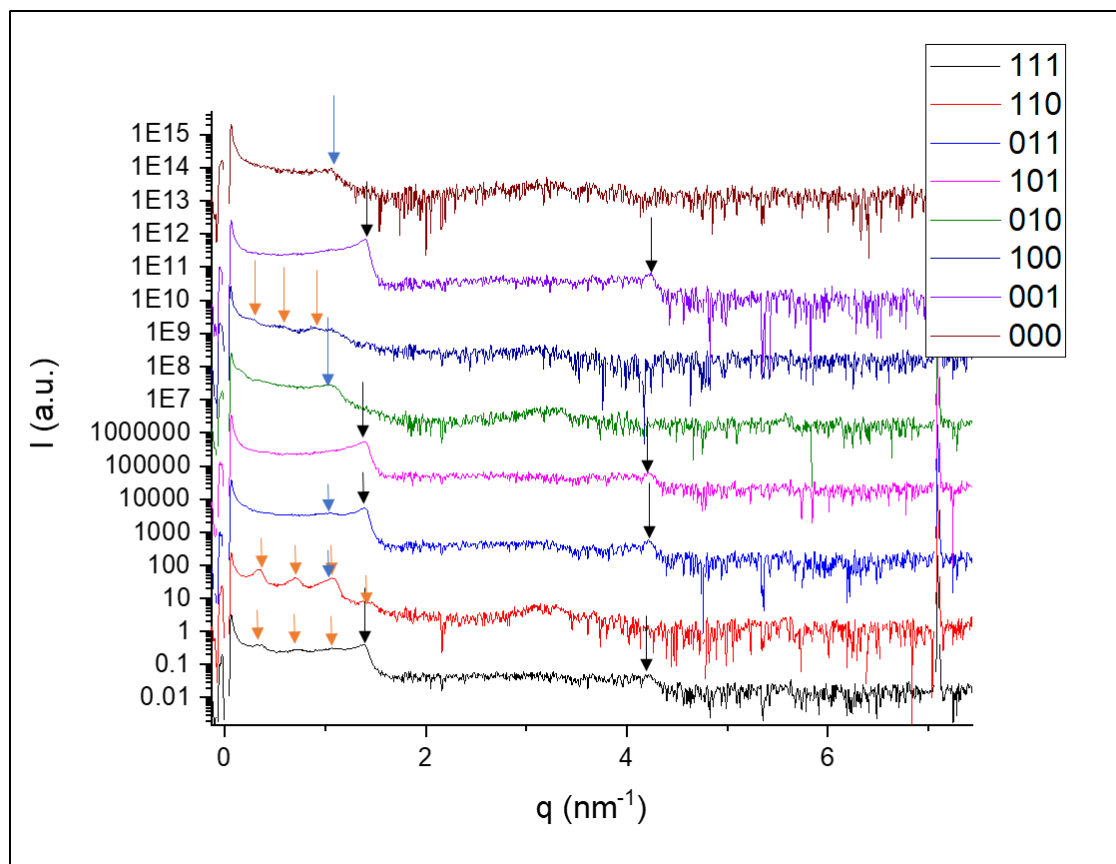


Figure 69: The SAXS curves of the different sample compositions at 25 °C with their formulation code shown in the legend. The reader is referred to Table 4 in Section 2.2.5 for details of each formulation code. The red arrows correspond to d spacing = 17.0 nm, the blue arrows, d spacing = 5.92 nm and the black arrows, d spacing = 4.47 nm. The curves have been stacked for clarity.

The stability of the phases described above with temperature have been studied and presented in Figure 70 for each formulation. It is clear that all samples are unstable at 70 °C as all SAXS curves at this temperature show little or no peaks and hence lack of ordered structure. For the 000 formulation, the dominant polymer lamellar phase at 25 °C appears to melt at 45 °C as the peak at $q = 1.37 \text{ nm}^{-1}$ disappears, see Figure 70a. The 100 formulation contains a high concentration of the lipid component but still at 25 °C two co-existing phases are seen, Figure 69 and Figure 70b. The swollen lipid phase with a d spacing 21.4 nm display rather small crystallite sizes as reflected by the broad FWHM of the Bragg peaks at $q = 0.25, 0.55$ and 0.88 nm^{-1} , it is also noted that the d spacing is bigger, when compared to the other lipid-rich samples (110 and 111: panels g

and h respectively in Figure 70). A closer look reveals, that in the vicinity of the third order peak, another diffraction peak partially overlaps at $q = 1.07 \text{ nm}^{-1}$, thus identified this second phase with the polymer-rich matrix. Interestingly, the diffraction peaks stemming from the lipid-rich phase appear more pronounced at temperatures between 40 to 60 °C, suggesting an increase in order in the lamellar order and an increased long-range order. The peaks shift to lower q values of 0.29, 0.56 and 0.85 nm^{-1} indicating an increased d spacing of 22.29 nm. Judging from both above observations and based on the melting point of P90H at 54 °C (cp. Section 3.2), it is conclusive to suggest that the gel to fluid phase transition is the main cause for an enhanced order in the lipid-rich phase. The peak at 1.07 nm^{-1} does not show any change in d spacing with temperature and thus no phase-change behaviour until 70 °C, where the increase thermal energy appears to break all structures present in the sample. The polymer rich 010 sample displayed in Figure 70c shows a very similar behaviour to the 000 sample (Figure 70a), although the appearance of an unidentified phase at temperatures between 45 and 60 °C is noted (most probable an intermediate appearance of a lipid-rich fluid lamellar phase). The shea butter rich sample 001 in Figure 70d shows the presence only of the lamellar phase of the shea butter at 25 °C with the first and third order peaks at $q = 1.40$ and 4.23 nm^{-1} respectively, corresponding to a d spacing of 4.44 nm. As stated above, displaying the L_{α} -polymorph of triglycerides. The shea butter then appears to melt at about 45 °C with the disappearance of the diffraction pattern.

Turning to the formulations with more than one high concentration component. The formulations rich in shea butter leads to a dominant shea butter structure; as the polymer and shea butter rich 011 sample shown in Figure 70e) and the lipid and shea butter rich 101 samples in Figure 70 show the sole presence of the shea butter lamellar structure with d spacing of 4.44 nm, which melts at 50 °C. For the 011 sample, at low temperatures of 35 °C and below, there is a hint of the polymer structure with the presence of a weak peak at around 0.98 nm^{-1} . The lipid and polymer rich sample 110 (panel a) shows the coexistence of two structures. The first three peaks at $q = 0.35, 0.71$ and 1.1 nm^{-1} correspond to the lipid lamellar structure with a d spacing of 17.5 nm. As the temperature increases, the lipid d spacing increases to 18.6 nm at 50 °C, reflecting a possible phase transition (gel to fluid phase; compare also with observations made for the 100 sample in Figure 70a). The peak at 1.07 nm^{-1} corresponds to the polymer phase with d spacing of 5.88 nm. An interesting observation, when comparing this 110 sample to 100 sample, is that the increased concentration of polymer appears to stabilize and

enhance the ordering of the lipid lamellar phase, resulting in more pronounced peaks compared to the peaks present in the 100 SAXS curve at 25 °C.

Finally, the high content of all three components 111 sample shows the co-existence of all three phases. At 25 °C the lipid lamellar structure is present shown by the peaks at 0.35, 0.71 and 1.1 nm⁻¹, the shea butter phase is also present with the peaks at 1.4 and 4.23 nm⁻¹ which then disappear above 45 °C as the shea butter melts. The lipid *d* spacing increases at higher temperature just as described above for sample 110.

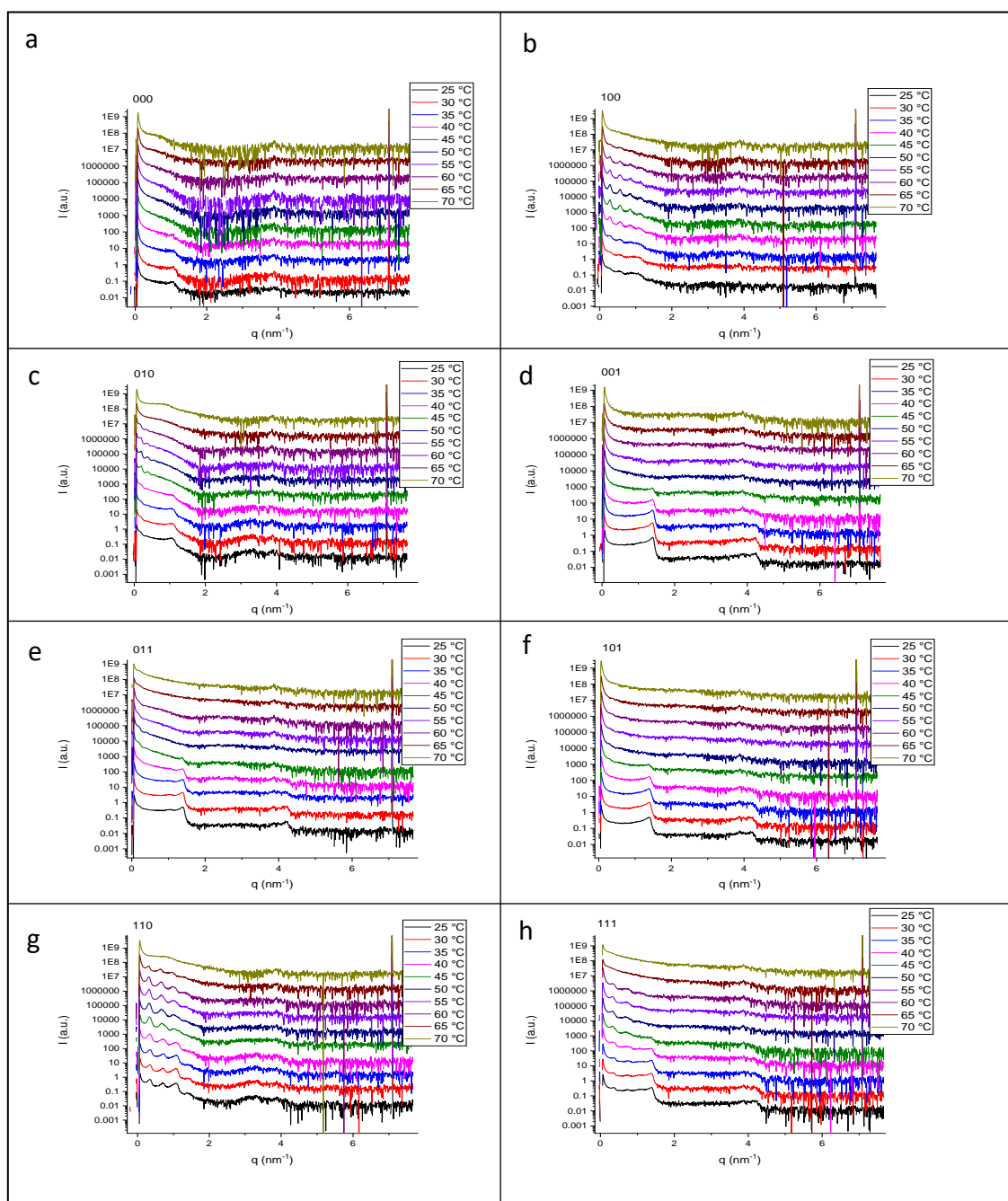


Figure 70: The thermal behaviour of each formulation code a) 000 b) 100 c) 010 d) 001 e) 001 f) 101 g) 110 h) 111 between 25 – 70 °C. The SAXS curves of each temperature have been stack-plotted for clarity.

3.3.2.2 “Dried” samples

The samples were subjected to a drying protocol and their structures analysed at 32 °C to simulate the conditions of the dried lipid film formed on the surface of the skin after being applied (91). It can be seen from Figure 71 that overall, the structures for the dried samples at 32 °C are similar to the structures of the wet samples at 25 °C, as the three structures from the three main components are observed. The lamellar structure of the

shea butter is easiest to identify in samples 001, 101, 011 and 111 from its distinctive first and third order peaks at $q = 1.40$ and 4.18 nm^{-1} . The lipid peaks are somewhat less pronounced than in the wet samples as shown in the 110 formulation, by the first two order peaks of the SAXS.

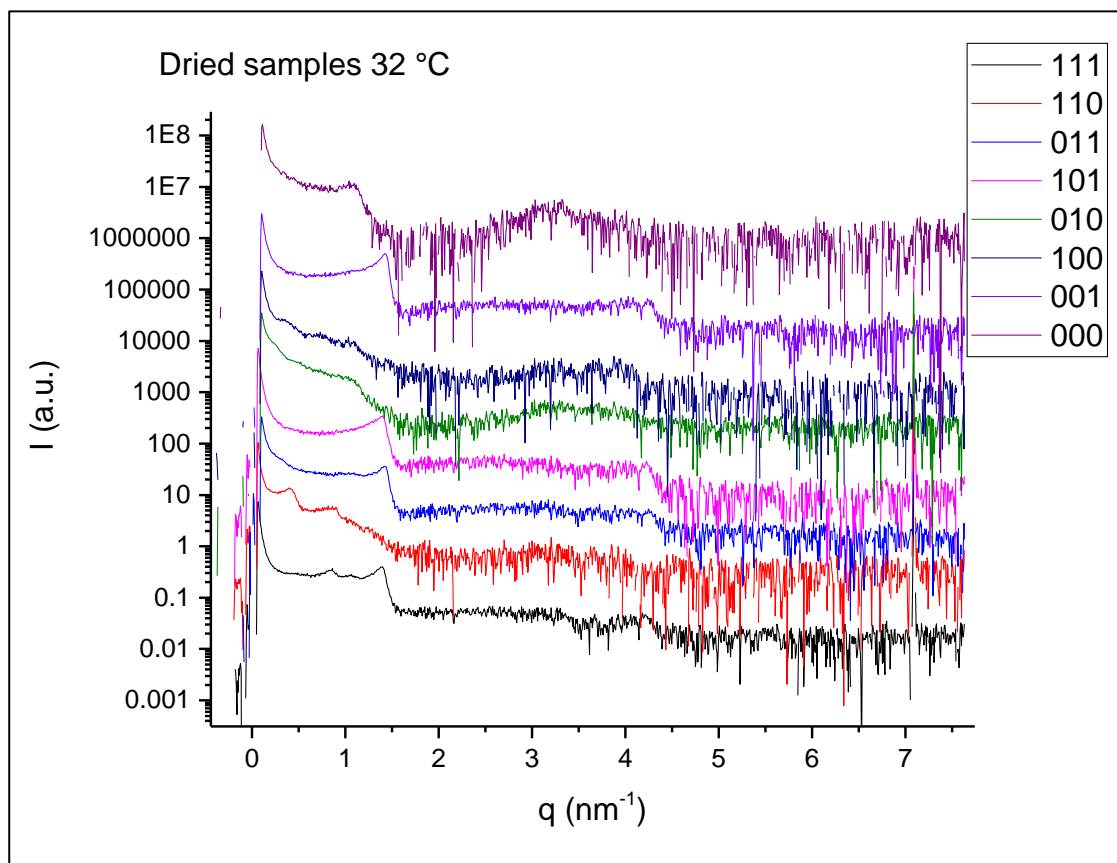


Figure 71: The SAXS curves of the “dried” formulations at 32 °C. The curves have been stacked for clarity.

A direct comparison between the structures of the wet and dried samples are shown in Figure 72. It is clear that the structures remain very similar for the formulations in conditions as would be found in the bottle (wet) and as a lipid film forming on the surface of the skin after application (dried). All formulations form the same phase(s) after being dried as resulting in very similar SAXS curves. The only formulation that shows slight difference is the 110 sample, where the dried sample seems to compromise the lipid lamellar structure, as noted above. The samples showing a coexistence of more than one phase (100, 011, 110 and 111 formulations) have, for clarity again, been arrow labelled. The direct comparison between the wet and dried samples show that the shea butter lamellar phase is stable to dehydration and the d spacing remains at 4.44 nm,

reflecting the typical triglyceride behaviour independent of hydration due to the absence of the interstitial water layer between the layers (130). Whereas for the lipid lamellar structure, the d spacing is decreased for the dried samples. The extent of reduction depends on the sample formulation, sample 100 decreases from 23.6 to 18.3 nm, samples 110 and 111 decreases from 17.8 nm to 15.5 nm and 11.8 nm, respectively. The third phase with d spacing 5.88 appears to be independent of dehydration with no change for the dried samples. Furthermore, the arrows displayed in Figure 72 shows the presence of some peaks corresponding to possible unidentified structures, for samples 100, 110 and 111, as labelled by the arrows.

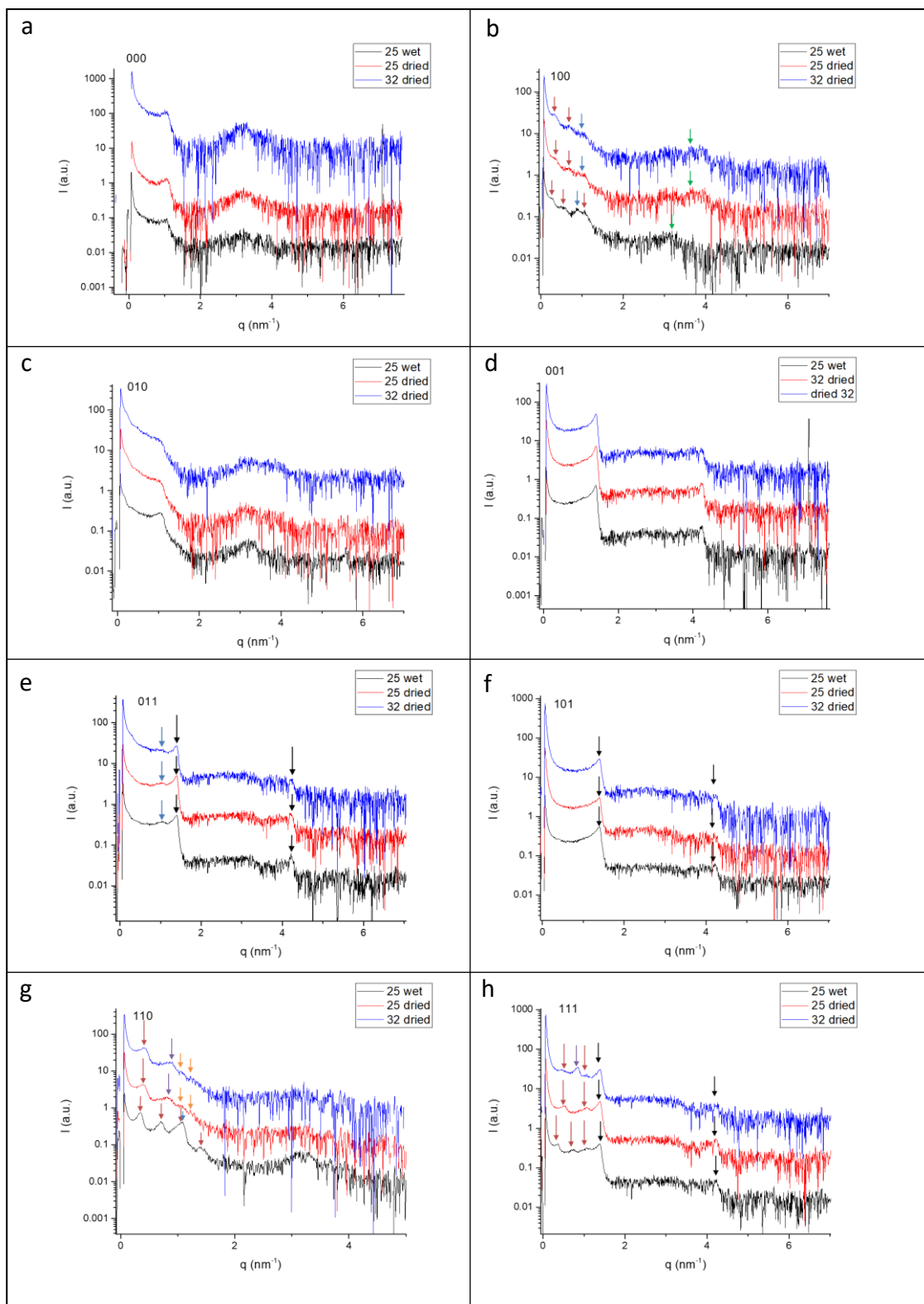


Figure 72: A comparison of the SAXS curves for each formulation after their “wet” and “dried” protocol. The SAXS curves are stacked for clarity.

Influence of temperature on the dried samples have been studied and the SAXS curves presented in Figure 73. The 000 dried sample (Figure 73a) behaves similarly to the wet

sample as the peak at 1.07 nm^{-1} disappears at temperatures above $40 \text{ }^\circ\text{C}$ reflecting a possible melting of the polymer phase. No significant temperature difference is observed for the 100 dried sample (Figure 73b). For the 101 dried sample (Figure 73f), as the polymer phase with repeat distance 5.88 nm disappears at $45 \text{ }^\circ\text{C}$, a lamellar phase with d spacing of 25.3 nm emerges, possibly due to the formation of an ordered lamellar lipid-rich phase. For both samples 001 and 101 (Figure 73d and f), the dominant shea butter phase at low temperatures disappears at temperatures above $45 \text{ }^\circ\text{C}$ due to the melting of the butter, then at $50 \text{ }^\circ\text{C}$ a peak for an unidentified phase with d spacing of 7.82 nm appears. Similar behaviour is also observed for the 011 dried sample (Figure 73e), where the dominant shea butter peak, with a slight appearance of a broad peak at around 1.07 nm^{-1} , disappears above $45 \text{ }^\circ\text{C}$, then a peak emerges corresponding to a d spacing of 24.8 nm , which could be the lipid-rich aggregate dominating. The 110 dried sample (Figure 73g) does not show any significant change with temperature, whereas the 111 dried sample (Figure 73h) shows a combination of structural changes with temperature. The shea butter peaks disappear as seen before at temperatures above $45 \text{ }^\circ\text{C}$ and a peak with d spacing of 7.82 appears, as well as the lipid lamellar phase undergoing a possible transition at around $40 \text{ }^\circ\text{C}$ as the d spacing increases from 11.8 nm to 13.3 nm .

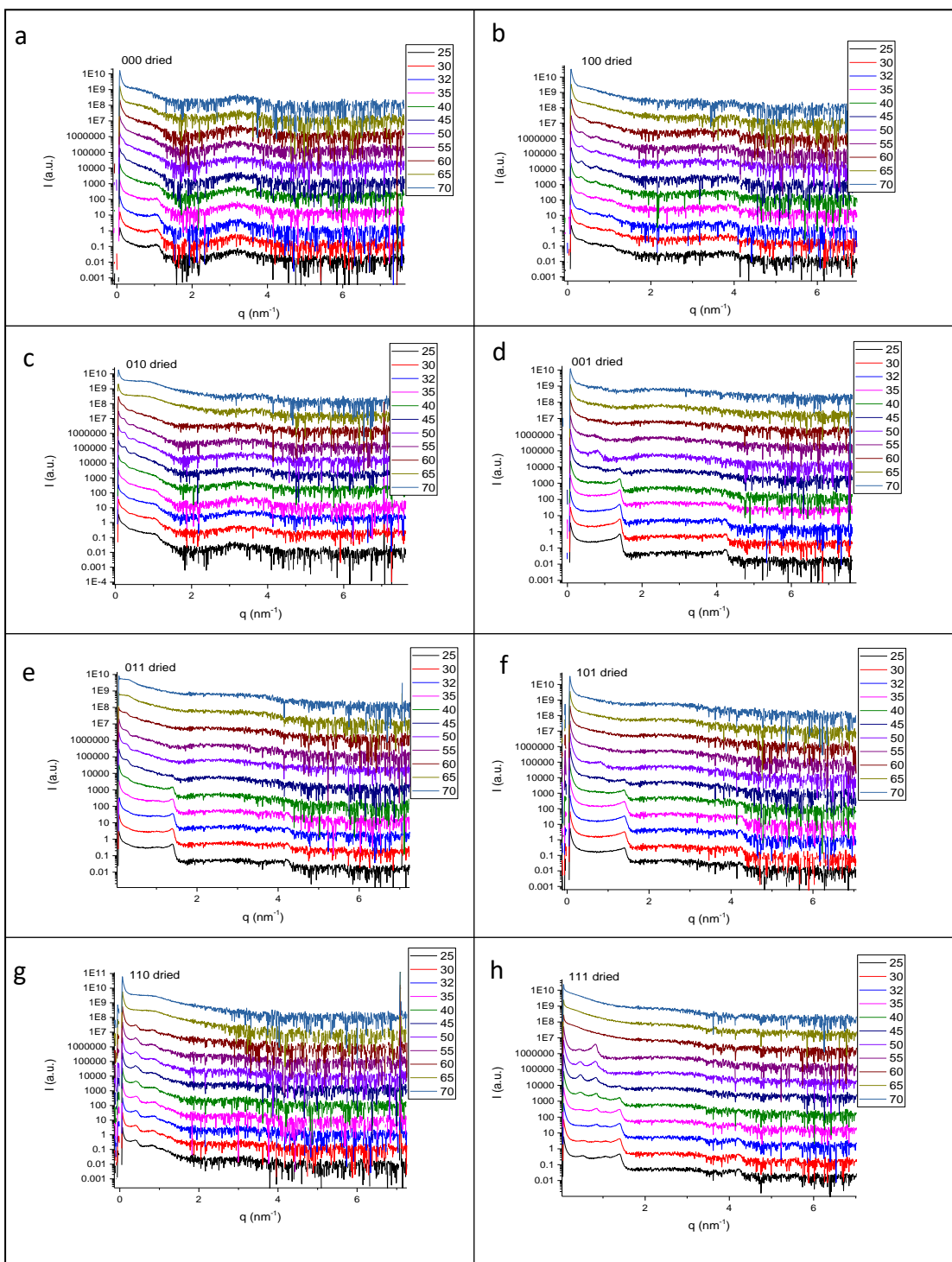


Figure 73: The thermal behaviour of each dried formulation a) 000 b) 100 c) 010 d) 001 e) 001 f) 101 g) 110 h) 111 between 25 – 70 °C as shown in the legends. The SAXS curves of each temperature have been stack-plotted for clarity.

3.3.3 Discussion

In both the wet and dried samples studied, three main phases have been observed, all displaying distinct lattices with the absence of perfect mixing of the three main components. The lipid lamellar structure appears to be highly swollen due to the presence of the long-chained alcohols, free fatty acid and ISIS with a d spacing of 17.5 nm, as the d spacing of pure P90H is 7.12 nm, a possible explanation of this is provided at the end of this discussion section. Furthermore, there appears to be a reduction in the order of the lipid lamellar phase, as the peaks are less pronounced (increased FWHM), and mainly, only three diffraction orders are observed in the SAXS curves, compared to four orders observed for the P90H sample, see Figure 59. There is also a dominant lamellar phase from the shea butter with d spacing of 4.44 nm and another phase possibly from polymer-rich aggregates with d spacing 5.88 nm.

For the “wet” samples, the lipid lamellar structure is present and stable when at high concentrations, such as 100, 110 and 111 formulations. The difference in SAXS curves between 111 and 101 samples show how the shea butter lamellar structure dominates, when the concentration of the polymer is low, however by increasing the polymer concentration, the lipid lamellar structure becomes enhanced. This observation suggests that the polymer appears to be surface active by increasing the stability of the lamellar structure when present, rather than creating a new phase itself (a new lipid/polymer mixture or continuous polymer matrix), as shown in the 010 sample when the concentration of the lipid is low. Moreover, the presence of the high content of polymer appears to induce a smaller d spacing as the 100 sample with low concentration of polymer gives a lipid lamellar d spacing of 23.6 nm, compared to 17.8 nm for the 110 and 111 samples with high polymer content.

Moreover, the lamellar phase of the shea butter giving a d spacing of 4.44 nm does not change with hydration or temperature, thus is a very stable structure until the triglycerides melt. Shea butter contains a mixture of different fatty acid chains, with the main components being stearic and oleic acid. Triglycerides can form lamellar phases with two- or three-chained layers (130), see Figure 74. The d spacing of 1,3-distearoyl-2-oleoyl-*sn*-glycerol, SOS, in the two-chained $L_{\alpha 1}$ phase is 4.91 nm compared to the d spacing of 7.18, 6.89 and 6.45 nm for L_{γ} , $L_{\beta'}$ and L_{β} respectively (130). Therefore, given the composition, recorded d spacing of the shea butter as 4.44 nm in the novel multi-component formulations and due to observed suppression of the 2nd order diffraction

peak (note as mentioned before, that β' and β polymorphs display an intense 2nd order reflection (ref 12, 13)), it is very likely that the shea butter is in the $L_{\alpha 1}$ phase. The slightly smaller d spacing observed in the formulations may be due to a possible presence of more oleic chains (which are shorter than stearoyl chains) in the shea butter than in the SOS. Finally, the $L_{\alpha 1}$ phase is known to form at 23.5 °C (131); interestingly, the shea butter rich $L_{\alpha 1}$ phase seems to be stable, while in nearly pure triglyceride samples the $L_{\alpha 1}$ phase (hexagonal chain packing) is only metastable and transforms commonly by time into β' polymorphs (orthogonal chain packing) followed by the formation of β polymorphs (triclinic chain packing). Note, that the chain packing is getting denser from the hexagonal to orthogonal to triclinic form. Hence it is likely that in these novel multi-component formulations a denser chain packing than the hexagonal chain packing is suppressed by the presence of impurities such as high contents of sterols and phenols present in shea butter.

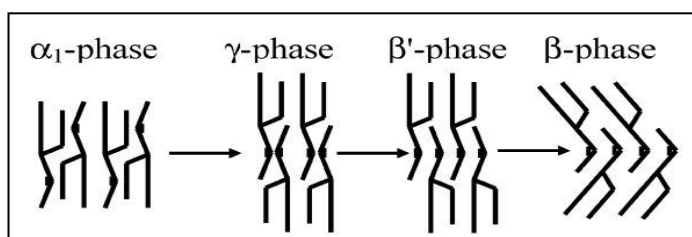


Figure 74: The different sub-phases of the lamellar structures formed for triglycerides. Two-chained layers exhibited by the α_1 -phase and three-chained layers exhibited by the other phases. Figure taken from (12).

Studies into the structure of the dried formulations to simulate the conditions of the lipid as a dry film after application of the cream onto the skin, show that the nanostructure of the formulation remains relatively unchanged. Please see Section 2.2.5 for the drying protocol. The lipid lamellar structure still remains and only the d spacing is decreased compared to the corresponding wet sample, reflecting a partial dehydration of the lipid from the drying process (132). The thermal effects on the dried samples are also similar to that of the wet samples. All samples are unstable at high temperatures of 70 °C, reflecting the maximum temperature for any structural stability of the formulations. When increasing the temperature from 25 °C, the 111 sample shows a possible phase transition of the lipid lamellar structure going from $L_{\beta'}$ to L_{α} reflecting a slight increase in the d spacing at a temperature around the phase transition of P90H of 54 °C. Nearly

all diffraction patterns identified lipid-, polymer- or shea butter-rich aggregates, and only a few diffraction peaks appearing with increasing temperature could not yet be unidentified, which is a reflection of the complexity of the formulations with more than one co-existing phase in most samples.

Having identified three main structural components, it is possible to speculate the overall microstructure. The formulations studied are oil in water emulsions, where the shea butter oil is dispersed within the continuous water matrix. Given the stability of phospholipids in water due to their self-assembled structures, as described in the previous two Sections, it is reasonable to assume that the MLVs formed by P90H would be dispersed in the continuous water matrix. Therefore, the two lamellar structures each, from the lipid P90H and the shea butter are distinct lattices with their own stacking registry from their own particles which are phase separated by the oil and water phases in the emulsion. The question remains, for the role of the polymer and its location in such a formulation. It is observed that the presence of the polymer at relatively high concentration appears to stabilise the lipid structure, as described above, and is also described as a “stabilizer” by its supplier (133). In other experiments not published within, oil in water emulsions have been successfully stabilised with only oil, water and polymer present. Therefore, the stability of the sample again suggests the potential surface activity of the polymer to stabilise such systems. These results suggest that the polymer may be located at the oil-water interface, stabilising the co-existence of the two phases. Sepimax Zen™ is a polyelectrolyte microgel (133), it contains hydrophobic and hydrophilic side groups to control the stability of the system – electrostatic repulsions can be reduced by being partially compensated by hydrophobic interactions. Given the nature of the polymer as a microgel, it is foreseen that the continuous water network also includes the polymer gel. As the polymer is a polyelectrolyte, it is highly likely that the charge from the polymer is impacting on the lipid and resulting repulsive interactions between membranes and a more swollen bilayer (larger d spacing) compared to the lipid in its pure form.

3.3.4 Conclusion

SAXS measurements have been conducted on a series of novel multi-component formulations containing three main components: the lipid structural component, shea butter and a polymer. Two different types of samples for each formulation have been

studied, the “wet” samples correspond to measurements made of the formulation with no modification and simulating the conditions of the formulations as they would be in the bottle; the “dried” samples have been subjected to a drying protocol to simulate the dried lipid film formed after the user has applied the cream on to the skin.

Overall, the formulations show the presence of three main phases and are very similar for the wet and dried samples. The lipid lamellar structure is present and stable despite a reduction in the order of the structure due to a reduced number and less pronounced *quasi*-Bragg peaks, when compared to pure P90H lipid samples. The d spacing of 17.5 nm is also largely increased with the presence of long-chained alcohols, free fatty acids and ISIS. Nonetheless, the lipid lamellar phase displays typical PC behaviour with hydration and temperature. As the samples are dehydrated by the drying protocol, the samples with the lipid phase present show a reduction in the d spacing compared to their corresponding wet samples. Its main transition with a simultaneous increase in the d spacing and stacking order, has been observed at about 50 °C, close to the phase transition temperature of P90H of 54 °C. Another lamellar phase with d spacing of 4.44 nm has been identified as the $L_{\alpha 1}$ phase of the shea butter. This lamellar phase is stable to hydration and disappears at temperatures above 45 °C as the shea butter melts. Finally, a third phase stems from the polymer-rich aggregates, and is present with a d spacing of 5.88 nm, which is relatively stable to both, temperature and extent of hydration

Chapter 4 General Conclusion

In this investigation, different types of phospholipid systems for dermatological formulations have been studied. The types of phospholipids of interest are PCs due to their complimentary properties to skin lipids and improvements to dry skin conditions after application. The literature attributes the skin barrier properties to the orthogonal packing of the skin lipids in the lamellar structure (120). Dry skin arises when the barrier properties are compromised and as the gel phase of long-chained PCs exhibit not only the lamellar phase but also the orthorhombic packing, they have suitable properties to enhance the skin barrier and prevent or reduce dry skin conditions. Therefore, the stability of the properties of PC to other components found in typical dermatological formulations has been studied. The content of this thesis and the outcomes has been split into three sections: (i) studying the effects of humectants on the nanostructure and thermal behaviour on PCs, (ii) studying the nanostructure and thermal behaviour of PC mixtures and how commercially available PC mixtures differ to higher purity PC mixtures, and (iii) the stability of PCs in oil-in-water formulations.

The structure and thermal behaviour of PCs are well described in literature. The self-assembled structure of PCs in water were first described by Luzzati and Husson (134). When immersed in water PCs will form ordered structures such as liposomes, which are onion-like spherical objects containing layers of bilayers stacked on top of each other; the lipid molecules arranged in such a manner that the hydrophobic chains are shielded away from the water. Such structures are known as liquid crystalline Smectic phases or the lamellar phase. DPPC, a fully saturated PC with 16 carbon chain length forms such lamellar structures when immersed in excess water. Within the lamellar phase, it forms different sub-phases. At room temperature, DPPC forms the lamellar gel phase where the hydrocarbon chains are tilted at around 32° perpendicular to the lateral plane. The hydrocarbon chains are in the extended all-*trans* conformation and pack on to an orthogonal lattice. At 35°C a phase transition occurs from the lamellar gel phase to the ripple phase. Here, the bilayers are no longer flat sheets but instead a wave-like asymmetric saw-tooth height modulation of the bilayers is present and the chains are packed on to a hexagonal lattice. Another phase transition occurs at 41°C from the

ripple phase to the fluid phase. The bilayers return to being flat but now the hydrocarbon chains are in a *trans-gauche* conformation and the lipid chains are free to laterally diffuse.

Humectants are found in dermatological formulations as sources of moisture, delivering pleasant sensory effects to the user. The effect of three different humectants named betaine, sarcosine and AMEA on DPPC were studied. The addition of humectants to DPPC alters its phase properties as described above. Firstly, the phase transition temperatures are changed. In general, both, the pre-transition and main transition temperatures are increased with increasing concentration of humectant added. For both betaine and sarcosine, T_{pre} was increased at a larger magnitude compared to T_M . This was not observed for AMEA, in fact no change in T_{pre} was observed overall. The increase in phase transition temperatures reflects the kosmotropic nature of humectants; the gel phase is favoured over the fluid phase as kosmotropes prefer to be in the bulk rather than at the interface (53). Therefore, minimising the interfacial water layer, d_w , is favoured in the presence of humectants. As a consequence, the gel phase, including the ripple phase, is observed at a larger range of temperatures with the addition of humectant. The absence in the change in T_{pre} for AMEA may suggest that it is the least effective humectant compared to betaine and sarcosine.

Turning to the nanostructure, it has been observed that the addition of humectant to DPPC leads to a decrease in d_w despite a slight increase in d_{HH} and thus an overall decrease in d spacing is observed with increasing concentration of humectant. These results combined with the WAXS results, showing a decrease in the FWHM of the gel phase peak upon addition of humectant, suggests that the addition of humectant leads to an increase in the order of the bilayers. Additionally, the decrease in d_w indicates a change in the forces acting between the bilayers has occurred, either a decrease in the inter-bilayer Helfrich repulsive forces, or an increase in van der Waals forces, or a combination has resulted. WAXS measurements enable the A_C to be deduced and show that the addition of humectants does not affect the A_C and thus does not affect the packing of the lipid chains. There is evidence however, in the WAXS results that the addition of AMEA leads to a different electron density contrast as the ratio of the peaks q_{20} and q_{11} has changed at high concentrations (≥ 1 M). As this is not observed for betaine and sarcosine, it suggests that AMEA may be a weaker kosmotrope in comparison as it may partition into the lipid headgroup interface to influence the electron density.

Commercial lipid samples are commonly used in dermatological formulations as the main structural component. Commercial lipid samples such as P90H are not only lipid mixtures but also contain up to 10 % of impurities. DPPC/DSPC pure lipid mixtures were studied and their properties compared to P90H which contains 15 % DPPC and 85 % DSPC. The thermal behaviour of pure DPPC and DSPC are very similar due to their similar structures; DSPC have 18C hydrocarbon chain length compared to 16C hydrocarbon chain length for DPPC. The longer chain length for DSPC leads to higher phase transition temperatures due to their increased van der Waals forces between the chains, compared to DPPC. Therefore, the addition of increasing concentrations of DSPC to DPPC leads to an increase in both T_{pre} and T_M . Comparing the lipid mixtures to their pure lipid, the cooperativity is compromised for the lipid mixtures, reflected by increase FWHM of the phase transition peaks in the DSC scans. The FWHM increases to a maximum for the 50:50 wt.% sample with highest amount of chain mis-match where evidence for sample de-mixing was observed. De-mixing was displayed by the DSC scans as an overlap of two peaks at both phase transitions, showing not only the co-existence of the two lipids in different phases, but also the transitions no longer occur as one event for both lipids. Furthermore, the enthalpy values for the main transitions are increased for the lipid mixtures compared to the pure lipid transitions, this could be a consequence of increased van der Waals forces as DSPC is added to DPPC, thus more energy is required to overcome the increased forces for the transition to occur. What is surprising though, is the enthalpy values for the mixtures are also larger than for pure DSPC which should contain the higher amount of intermolecular forces in the sample. Therefore, the question remains how the presence of DPPC, which decreases the intermolecular forces with shorter chain length and hence less van der Waals forces, would lead to an increase in enthalpy. Comparing the thermal behaviour of P90H with its equivalent, higher purity sample of 85 % DSPC shows that the presence of impurities in P90H does not affect the thermal behaviour with similar phase transition temperatures and enthalpy values.

The addition of DSPC to DPPC leads to an increase in d_{HH} and little change in d_w resulting in an overall increase in d spacing. The increase in d_{HH} reflects the longer hydrocarbon chains for DSPC compared to DPPC. There is little change in d_w as all samples are fully hydrated in excess water. Global fits of the SAXS measurements for the fluid phase also support the observed instability of the 50:50 wt.% sample showing very little order and a swollen structure, reflected by the unusually larger d_w compared

to the other lipid mixtures in the fluid phase and a nonlinear increase in d_{HH} due to a large increase at 50:50 wt.% mixture. Furthermore, the fluid phase of 50:50 wt.% shows possible detachment of the bilayers due to more diffuse scattering observed compared to *quasi*-Bragg peaks observed for the other samples and consequently, the average number of bilayers in registry is at a minimum value of 2 for the sample. Comparing the nanostructure of P90H with the structure of high purity 85 % DSPC sample, the SAXS curves for P90H show broader *quasi*-Bragg peaks which suggests the sample is less ordered compared to the higher purity sample. However, still four *quasi*-Bragg peaks are observed which are equally spaced from each other reflecting a lamellar structure. Therefore, the overall structure of P90H is the same compared to its equivalent higher purity sample. When comparing the d spacing in the gel phase, the presence of impurities in the P90H sample appears to increase the d spacing resulting in a value of 7.12 nm compared to a d spacing of 6.81 nm for the higher purity sample. This increased d spacing may be a result of a possible increase in fluidity of the membrane with the presence of impurities for the P90H, which would lead to an increase in the inter-membrane Helfrich repulsions and a larger d spacing.

More complex multi-component formulations have been studied by SAXS. The oil-in-water formulations containing the main lipid component, P90H, with long chained alcohols, free fatty acids and ISIS, alongside shea butter and a polymer, shows the stability of different lamellar phases co-existing. Three main phases have been observed. The presence of shea butter leads to a dominant lamellar phase and as the first and third order peaks are dominant, this is specifically the L_α phase of the triglycerides with a d spacing of 4.44 nm. The peaks then disappear at temperatures above 45 °C indicating a melting transition of the triglycerides. A lamellar phase from the lipid component is observed, however the d spacing is hugely increased compared to pure P90H, from 7.12 nm to 17.8 or 21.4 nm. This increased d spacing is a result of the presence of long chained alcohols, free fatty acids and ISIS, as the addition of long chained alcohols to lipid membranes have shown to increase the d spacing by Hartkamp *et al.* (126). The presence of these compounds has also resulted in a loss of order as not only are there only three *quasi*-Bragg peaks observed in the gel phase (compared to four for pure P90H), but also the peaks are broader. There also appeared to be a transition reflected by a slight increase in the d spacing of the lipid lamellar phase at around 50 °C, close to the main transition of P90H. The presence of the polymer in high concentration appears to stabilise the lipid lamellar phase by decreasing the d spacing

from 21.4 nm to 17.8 nm as well as producing more pronounced *quasi*-Bragg peaks. Finally, a third phase with a d spacing of 5.88 nm is observed for high concentration of polymer presence, thus suggesting a polymer-rich phase. As only the first order peak is observed for this phase, it is difficult to ascertain the lattice structure of this phase.

The same multi-component samples were subjected to a drying protocol in vain of mimicking the dried film formed on the surface of the skin after application. Overall, very similar structures to their corresponding “wet” samples were observed. The drying protocol did not affect the lamellar phase of the shea butter, with the same d spacing of 4.44 nm observed and melting at the same temperature. The lack of change reflects the lack of d_w in the lamellar structure compared to the structure of lipids and so the structure is independent to extent of hydration. No changes were observed for the polymer-rich phase at 5.88 nm. The lipid lamellar structure is affected slightly from the drying protocol with a reduced d spacing reflecting a dehydration of the bilayers. The extent of decrease in the d spacing depends on the formulation composition.

The aim of this investigation was to understand the structure and stability of phospholipid membranes found in dermatological formulations. Overall, the lipid lamellar structure is present in all systems studied. The addition of other components typically found in dermatological formulations, as well as the presence of impurities, influences the nanostructure and thermotropic behaviour of the lamellar structure of phospholipids. The properties of the phospholipids have been studied by DSC to track changes in the thermal behaviour and X-ray scattering to visualise changes to the nanostructure. DSC characterises the temperatures and enthalpies of phase transitions. The results have shown that the main transition temperature is relatively stable, compared to the pre-transition temperature; where the addition of humectants lead to a small increase in the main transition temperature and even at more complex, multi-component formulations, the main transition is still apparent at temperatures around the main transition for the lipid only sample. Therefore, it can be concluded that the main phase transition is stable to the addition of other components. X-ray scattering results have shown that the overall lamellar structure is conserved. The presence of impurities compromises the order by producing broader *quasi*-Bragg peaks and a larger d spacing. The higher the complexity of the formulation, the more the order is compromised and the larger the d spacing, as observed by the multi-component systems.

Chapter 5 Outlook

5.1 FT-IR Spectroscopy

FT-IR spectroscopy is another non-invasive experimental technique which can be used to study the properties of lipid bilayers. FT-IR spectroscopy works by passing infra-red radiation through the sample where some of the radiation will be absorbed but some will also pass through and be detected. This provides information on the chemical structure by not only producing a unique molecular “fingerprint” of the sample but also highlight specific chemical bond information. Specifically, FT-IR spectroscopy is well suited to studying the interactions present at the lipid-water interface as the extent of hydrogen bonding at the polar headgroup can be monitored effectively. FT-IR spectroscopy will not only study the phase behaviour of lipids but also facilitates the observation of chemical changes, such as the amount of hydrogen bonding in the system or the extent of dehydration. Therefore, this technique will confirm the location and presence or absence of hydrogen bonds between the humectants and the lipid headgroups.

FT-IR spectroscopy has already been used for studying both the effect of dehydration and the interaction of amino acids on lipid bilayers. The most common vibrational modes studied for phospholipids are for the phosphate and carbonyl groups. The result of hydrogen bonding to the oxygen atom to these two groups leads to a weakening of the vibrational forces constants of this bond and thus leads to a decrease in the vibrational frequency (135). Fringeli and Günthard (136) discovered that the phosphate PO_2^- vibrational band is extremely sensitive to hydration. Arrondo *et al.* (137) studied the FT-IR spectra of DPPC both fully hydrated and partially hydrated and came to several conclusions: (i) there are three main vibration bands observed at 1060, 1086 and 1222 cm^{-1} , corresponding to the R-O-P-O-R' vibration and the symmetric and asymmetric PO_2^- stretching vibrations respectively; (ii) the FT-IR spectra for these three vibration bands are the same for both the gel and the fluid phases; (iii) the position of these vibrations bands shift towards higher wavenumber upon dehydration of the lipid, see Figure 75.

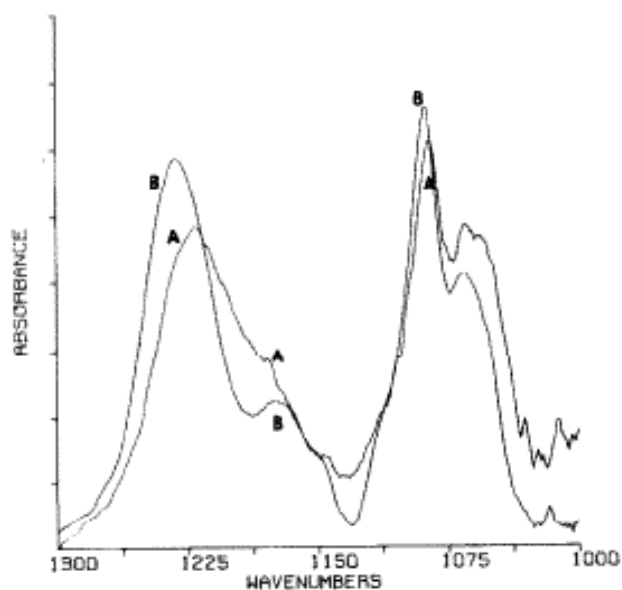


Figure 75: The FT-IR spectra of DPPC at 47 °C for a) fully hydrated MLVs and b) partially hydrated MLVs. Taken from (137).

Crowe *et al.* (138) studied the effect of carbohydrates on lipid bilayers and found the presence of interaction by direct hydrogen bonding of the -OH groups from the carbohydrates to the phosphate headgroups. FT-IR spectroscopy highlighted the hydration effect of carbohydrates as a result of the hydrogen bonding which could bring the FT-IR spectrum of a dehydrated DPPC comparative to fully hydrated, when studying the PO_2^- asymmetric vibrational band. Figure 76 shows how the addition of trehalose leads to a shift in the band towards a lower wavenumber, corresponding to a hydrating effect as discussed above, and the addition of heating the sample to 60 °C and thus, above T_M , results in a further shift of the band towards lower wavenumber comparable to that of a fully hydrated DPPC.

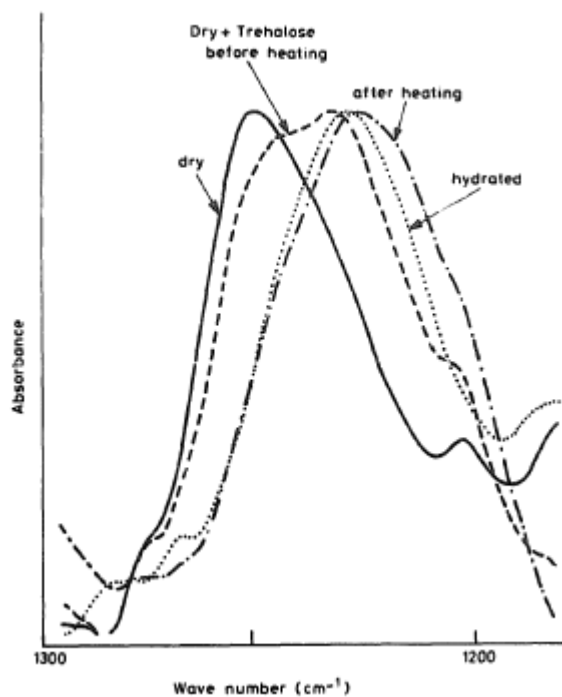


Figure 76: FT-IR spectra of DPPC either dehydrated in the presence or absence of trehalose, or in the presence of trehalose and after heating to 60 °C or fully hydrated. Taken from (138).

Furthermore, Porasso *et al.* (139) studied the interactions of other small molecules, specifically amino acids, with DPPC bilayers by using the FT-IR spectroscopy. The authors studied the interaction of glycine, whose structure is similar to betaine and sarcosine, and found that the molecule does not affect the hydrophobic region of DPPC bilayer and instead interacts with the phosphate head group also by hydrogen bonding and leading to a shift in the PO_2^- vibration bands.

Changes to the vibrational bands of particular bonds facilitates the interpretation to changes in the lipid structure and interactions. Therefore, future experiments to study the interactions of humectants with DPPC bilayers would include performing FT-IR spectroscopy to highlight not only any changes to the hydrophobic or hydrophilic regions of the lipid bilayer, but also any intermolecular interactions by hydrogen bonding changes to the system for which specific groups.

5.2 Neutron Scattering

Neutron scattering provides structural information in the same manner as X-ray scattering. A key difference between X-ray and neutron scattering is that neutron scattering detects a large difference in the scattering-length densities between hydrogen and deuterium. Therefore, one can easily study a specific part of the system by deuterating particular molecules. Neutron scattering can be used to study lipid mixtures, as published by Knoll *et al.* (140), deuterating one lipid results in a large difference in the scattering-length density and thus a large contrast between two segregated phases. This will illustrate clearly the miscibility of the lipids and whether the mixtures are homogenous or heterogeneous, and whether there is lateral phase separation of the two lipids. Knoll *et al.* demonstrated how the use of contrast variation technique, it is clear if a lipid mixture is homogeneous or not, as DMPC/DPPC lipid mixtures showed homogenous mixing and were successfully solvent matched with 45 % D₂O and 55 % H₂O solvent. Whereas solvent contrast matching is not possible for heterogeneous mixtures such as DMPC/DSPC which have phase separated.

Thus, this technique would definitely shine more light onto the studied DPPC/DSPC mixtures, and moreover, can be applied to the DPPC with humectants samples. By deuterating the humectants, this will provide new insights on the specific location of the humectants within the bilayer. Thus, offering information on whether the humectants interact with the lipid directly through hydrogen bonding or indirectly by structuring the intermediate water layers in the MLVs.

5.3 Molecular Dynamics Simulations

Computer simulations are becoming increasingly popular as a complimentary technique to experimental methods. Successful molecular dynamics simulations have been performed on the fluid phase of DPPC using the Amber Lipid Forcefield as described in (141). 64 lipids on each leaflet were simulated in excess water at 91 °C, see Figure 77. Calculating the area per lipid during the simulation provides an indication of the stability of the lipids and thus the area per lipid should converge after a period of simulation time (141). It can be seen from Figure 78 that quite immediately, the area per lipid for DPPC converges to a stable average value of 70.01 Å², slightly larger than the

compared to experimental literature value of 64.00 \AA (96). Furthermore, EDPs of the time average measurement of the electron density through the bilayer, thus detailed structural information can be gathered complimentary to X-ray scattering data. Figure 79 shows the EDP from the 150 ns simulation and the calculated d_{HH} of 35.8 \AA (96) is slightly lower than the experimental literature value of 38.3 \AA , but is to be expected due to the higher temperature and thus more *trans-gauche* conformations present.

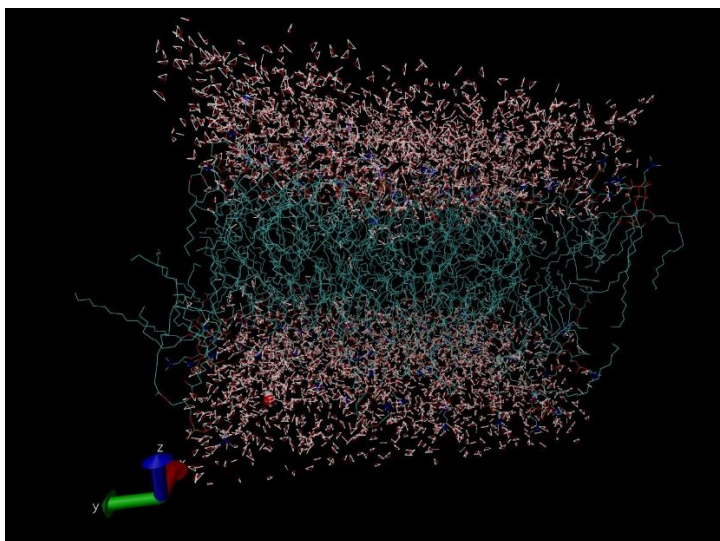


Figure 77: A snapshot of a molecular dynamics simulation of 164 DPPC lipids in excess water at $91 \text{ }^\circ\text{C}$.

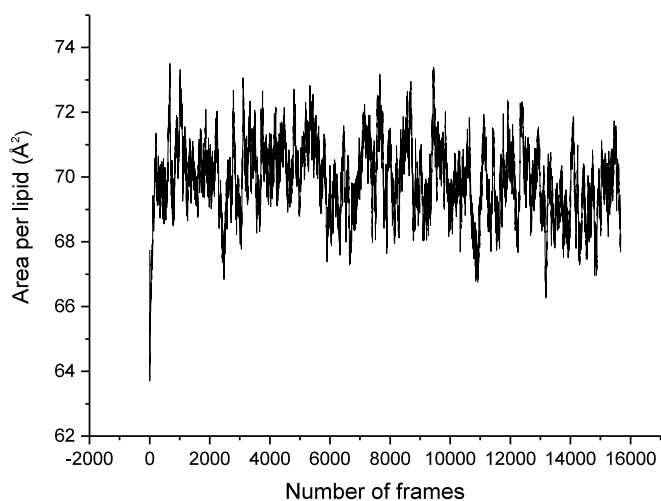


Figure 78: The calculated area per lipid of DPPC at $91 \text{ }^\circ\text{C}$ over the simulation period of 150 ns.

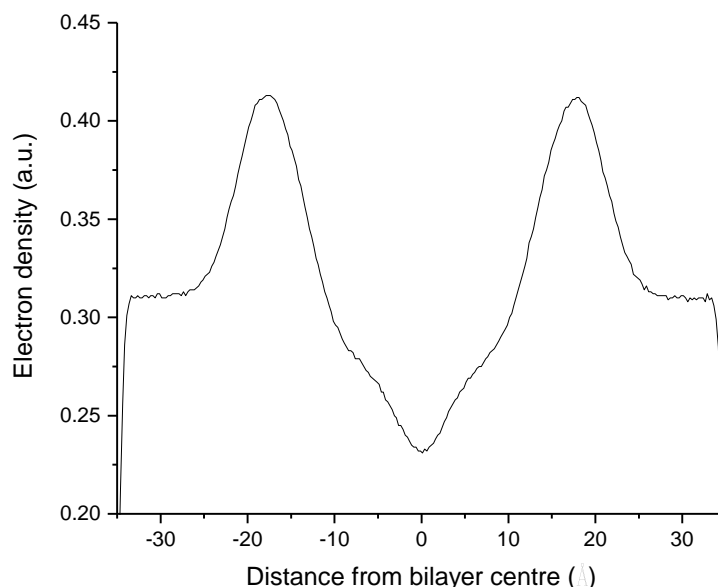


Figure 79: The electron density profile of DPPC at 91 °C over 150 ns simulation.

Atomic simulations have been improved vastly over the recent years due to improved computer power where initially, the gel phase has been particularly difficult to simulate due to the large timesteps required for the slow dynamics of the lipid. Now even phase transitions have been simulated successfully by Leekumjorn and Sum (142) for DPPC and in high detail. Thus, atomistic computer simulations are now a hugely powerful technique to provide detailed insights to the structure of lipid bilayers.

Moreover, simulations offer further atomic insights to the microscopic interactions between lipids and other molecules. Chiu *et al.* (143) studied the influence of cholesterol on lipid bilayers using atomistic simulations. The authors not only showed that the simulations reproduced the same ordering effects of cholesterol on the lipid bilayers as observed in experimental measurements, but also showed the structural changes to the lipids due to interactions with cholesterol when comparing between saturated and unsaturated lipids. The results of the simulations showed that the lipids can pack more effectively around cholesterol compared to unsaturated lipids and therefore, cholesterol induces a tighter packing of the saturated lipids compared to unsaturated lipids.

MacCallum *et al.* looked at the interactions of amino acids with DOPC which revealed the precise location of each amino acid and its orientation within the lipid bilayer. The

authors found that the location of the amino acid depends on its hydrophilicity – the hydrophobic amino acids preferably locate within the hydrocarbon chains of the lipid bilayer whereas the hydrophilic amino acids are found at the headgroup interface. Strikingly, the authors observed the presence of stable water defects formed to hydrate the polar amino acids as they penetrate the bilayer into the hydrocarbon chain region, see Figure 80.

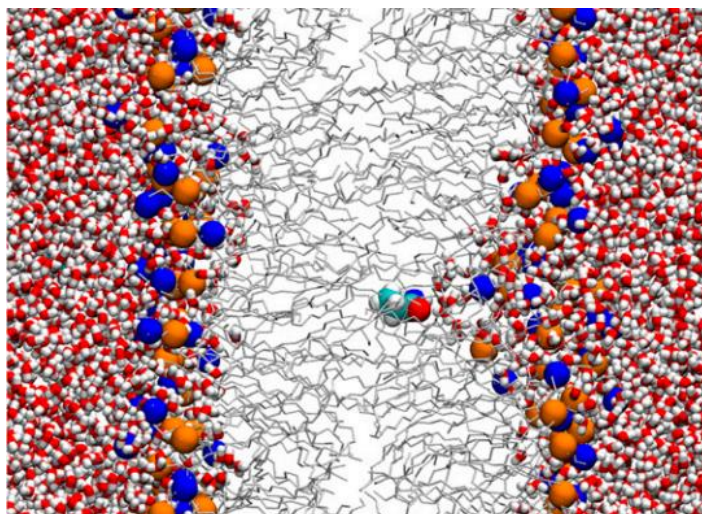


Figure 80: The formation of a water defect as a result of asparagine penetrating a DOPC bilayer captured by simulations performed by MacCallum *et al.* (144).

Both literature and preliminary experiments have shown that molecular dynamics simulations serve both as a compliment to experimental techniques and as further insights to specific structural changes and interactions between lipids and other molecules. Therefore, it is worthwhile to use simulations in the future to visualise not only the precise location of humectants found within lipid bilayers, but also the specific regions of the lipid bilayer with which they interact.

5.4 Calculation of the Van der Waals Forces

In Chapter 3.1, the addition of humectants to DPPC leads to a decrease in the d spacing due to a reduction of d_w . The question remains on whether this is a result of increased inter-bilayer van der Waals forces and/or reduced Helfrich repulsive forces. Feng *et al.* (69) successfully calculated any change in van der Waals forces when studying the

effect of urea and urea derivatives of lipid bilayers. The authors calculated the van der Waals force per unit area between two planar surfaces, P_v , by using the following equation:

$$P_v = \frac{-H}{6\pi D^3} \quad (14)$$

Where H is the Hamaker constant and D is the d spacing. The authors found that the Hamaker constant decreases upon addition of urea and therefore the van der Waals forces between the bilayers decreases, resulting in an increase in the d spacing with increasing concentrations of urea. In principle, this method can be applied to the humectants to probe any increase in the van der Waals forces. By using this method, one would be able to deduce whether the decrease of d_w is also due to increased van der Waals forces or if there is no change, then one can assume that there a reduction in the Helfrich repulsions to be the dominant factor. As DPPC has no net charge, it is safe to assume that any changes to electrostatic forces are negligible (145).

5.5 Mass Spectrometry

It is generally accepted that phospholipid bilayers are chemically inert, however recently Dods *et al.* (146) have demonstrated that phospholipids are able to chemically react with peptides spontaneously, known as lipidation. This chemical reaction is possible as the peptide is able to undergo acylation by accepting an acyl group. The lipid appears to selectively target amino groups at the N-terminal end of the peptide (147) as shown by mass spectrometry measurements. As both, betaine and sarcosine are derivatives of the amino acid glycine, it is therefore of interest to understand if these molecules are also able to chemically react with phospholipids by undergoing lipidation.

Mass spectrometry is a widely used analytical technique used to identify compounds and their chemical structures by ionising a chemical compound and sorting the ion fragments in order of their mass-to-charge-ratio. Pridmore *et al.* (147) used mass spectrometry to identify the successful acyl transfer from POPC to a peptide named melittin, see Figure 81. The mass spectrum shows peaks in the 3080 – 3150 m/z region correspond to fragments of melittin bound to the palmitoyl groups from POPC. The studies show very clearly the products from the acylation of the peptide. Therefore,

mass spectrometry would be a very useful technique to discover any chemical reactions that occur from the addition of humectants to DPPC. This could also be used for the novel multi-component systems to understand any chemical interactions present in the systems.

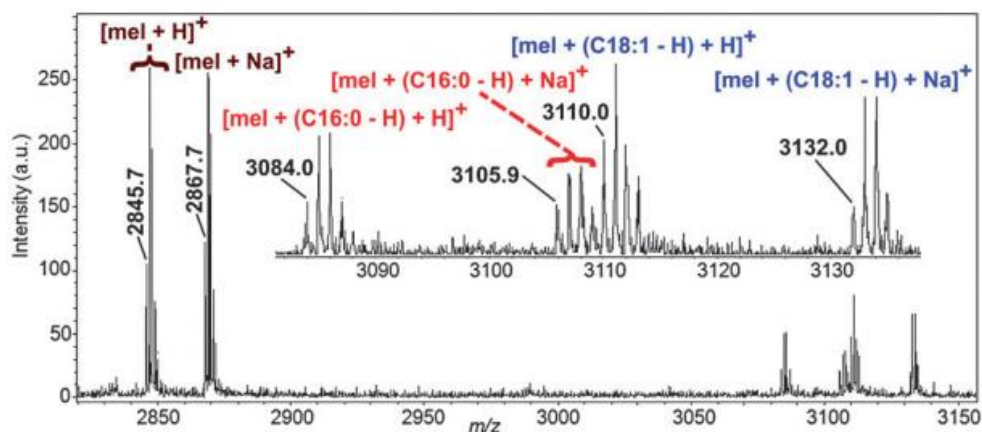


Figure 81: The mass spectrum of melittin with POPC liposomes. Taken from (147).

5.6 Further X-ray Scattering Measurements

WAXS measurements of DPPC MLVs reveal how the lipid pack together laterally and A_C , can be deduced. WAXS measurements of the lipid mixtures and the novel multi-component formulations would provide insights to how the presence of impurities in commercial lipid mixture samples influence the packing of the lipids, compared to pure DPPC, as studied in Chapter 3.1. Further, more complex formulations with the presence of long-chained alcohols, free fatty acids and ISIS and the lipid packing in these systems can be revealed.

5.7 Further DSC Measurements

DSC studies the thermal behaviour of a sample and reveals any thermal events occurring at the temperatures studied. DSC measurements of the novel multi-component systems would reveal the precise temperature for the melting of the shea butter, which SAXS measurements suggest a temperature above 45 °C. Additionally, the possible

main phase transition from the lipid component at around 50 °C was observed from the SAXS data, this can be confirmed by DSC and the enthalpy of transition as well as its cooperativity measured and compared to that of pure lipid mixtures.

References

1. Brooks, N.J. et al. Soft interfacial materials: from fundamentals to formulation. *Philosophical Transactions of the Royal Society A: Mathematical, Physical and Engineering Sciences*. 2016, **374**(2072).
2. Bangham, A.D. Physical Structure and Behavior of Lipids and Lipid Enzymes. In: Paoletti, R. and Kritchevsky, D. eds. *Advances in Lipid Research*. Elsevier, 1963, pp.65-104.
3. Betz, G. et al. In vivo comparison of various liposome formulations for cosmetic application. *International Journal of Pharmaceutics*. 2005, **296**(1), pp.44-54.
4. Bombardelli, E. Phytosome: new cosmetic delivery system. *Bollettino chimico farmaceutico*. 1991, **130**(11), pp.431-438.
5. Costa, R. and Santos, L. Delivery systems for cosmetics - From manufacturing to the skin of natural antioxidants. *Powder Technology*. 2017, **322**, pp.402-416.
6. Li, J. et al. A review on phospholipids and their main applications in drug delivery systems. *Asian Journal of Pharmaceutical Sciences*. 2015, **10**(2), pp.81-98.
7. Betz, G. et al. Heparin penetration into and permeation through human skin from aqueous and liposomal formulations in vitro. *International Journal of Pharmaceutics*. 2001, **228**(1-2), pp.147-159.
8. Boinpally, R.R. et al. Lecithin vesicles for topical delivery of diclofenac. *European Journal of Pharmaceutics and Biopharmaceutics*. 2003, **56**(3), pp.389-392.
9. Cevc, G. *Phospholipids Handbook*. Taylor & Francis, 1993.
10. Cevc, G. and Marsh, D. *Phospholipid bilayers: physical principles and models*. Wiley, 1987.
11. Verwey, E.J.W. et al. *Theory of the Stability of Lyophobic Colloids: The Interaction of Sol Particles Having an Electric Double Layer*. Elsevier Publishing Company, 1948.
12. Hwang, H. *DLVO theory*. [Online]. 2011. [Accessed 10/08/2018]. Available from: http://soft-matter.seas.harvard.edu/index.php/DLVO_theory
13. Huang, C.-h. and Li, S. Calorimetric and molecular mechanics studies of the thermotropic phase behavior of membrane phospholipids. *Biochimica et Biophysica Acta (BBA) - Reviews on Biomembranes*. 1999, **1422**(3), pp.273-307.
14. Koynova, R. and Caffrey, M. Phases and phase transitions of the phosphatidylcholines. *Biochimica et Biophysica Acta (BBA) - Reviews on Biomembranes*. 1998, **1376**(1), pp.91-145.
15. Nagle, J.F. and Wilkinson, D.A. Dilatometric studies of the subtransition in dipalmitoylphosphatidylcholine. *Biochemistry*. 1982, **21**(16), pp.3817-3821.
16. Tristram-Nagle, S. et al. Measurement of chain tilt angle in fully hydrated bilayers of gel phase lecithins. *Biophys J*. 1993, **64**(4), pp.1097-1109.
17. Sun, W.J. et al. Structure of gel phase saturated lecithin bilayers: temperature and chain length dependence. *Biophys J*. 1996, **71**(2), pp.885-891.
18. Tardieu, A. et al. Structure and polymorphism of the hydrocarbon chains of lipids: A study of lecithin-water phases. *Journal of Molecular Biology*. 1973, **75**(4), pp.711-733.

19. Tristram-Nagle, S. et al. Structure of Gel Phase DMPC Determined by X-Ray Diffraction. *Biophys J.* 2002, **83**(6), pp.3324-3335.
20. Rappolt, M. et al. Structure and elasticity of phospholipid bilayers in the L_α phase: A comparison of phosphatidylcholine and phosphatidylethanolamine membranes. *Recent Research and Development in Biophysics.* 2004, **3**, pp.363-393.
21. Sun, W.J. et al. Anomalous phase behavior of long chain saturated lecithin bilayers. *Biochimica et Biophysica Acta (BBA) - Biomembranes.* 1996, **1279**(1), pp.17-24.
22. Wiener, M.C. et al. Structure of the fully hydrated gel phase of dipalmitoylphosphatidylcholine. *Biophys J.* **55**(2), pp.315-325.
23. Rappolt, M. and Rapp, G. Structure of the stable and metastable ripple phase of dipalmitoylphosphatidylcholine. *European Biophysics Journal.* 1996, **24**(6), pp.381-386.
24. Ruocco, M.J. and Shipley, G.G. Characterization of the sub-transition of hydrated dipalmitoylphosphatidylcholine bilayers. Kinetic, hydration and structural study. *Biochimica et Biophysica Acta (BBA) - Biomembranes.* 1982, **691**(2), pp.309-320.
25. Sun, W.J. et al. Structure of the ripple phase in lecithin bilayers. *Proceedings of the National Academy of Sciences of the United States of America.* 1996, **93**(14), pp.7008-7012.
26. Rappolt, M. et al. New evidence for gel-liquid crystalline phase coexistence in the ripple phase of phosphatidylcholines. *European Biophysics Journal.* 2000, **29**(2), pp.125-133.
27. Sengupta, K. et al. Novel structural features of the ripple phase of phospholipids. *EPL (Europhysics Letters).* 2000, **49**(6), p.722.
28. Akabori, K. and Nagle, J.F. Structure of the DMPC lipid bilayer ripple phase. *Soft Matter.* 2015, **11**(5), pp.918-926.
29. De Vries, A.H. et al. Molecular structure of the lecithin ripple phase. *Proceedings of the National Academy of Sciences of the United States of America.* 2005, **102**(15), pp.5392-5396.
30. Sengupta, K. et al. Structure of the ripple phase of phospholipid multibilayers. *Physical Review E - Statistical, Nonlinear, and Soft Matter Physics.* 2003, **68**(3), pp.317101-3171012.
31. Doniach, S. A thermodynamic model for the monoclinic (ripple) phase of hydrated phospholipid bilayers. *The Journal of Chemical Physics.* 1979, **70**(10), pp.4587-4596.
32. Lubensky, T.C. and MacKintosh, F.C. Theory of "Ripple" Phases of Lipid Bilayers. *Physical Review Letters.* 1993, **71**(10), pp.1565-1568.
33. Heimburg, T. A Model for the Lipid Pretransition: Coupling of Ripple Formation with the Chain-Melting Transition. *Biophys J.* 2000, **78**(3), pp.1154-1165.
34. Chapman, D. Living systems. Liquid crystalline properties of phospholipids and biological membranes. *Symposia of the Faraday Society.* 1971, **5**(0), pp.163-174.
35. Lewis, R.N.A.H. et al. A differential scanning calorimetric study of the thermotropic phase behavior of model membranes composed of phosphatidylcholines containing linear saturated fatty acyl chains. *Biochemistry.* 1987, **26**(19), pp.6118-6126.
36. Nagle, J.F. et al. X-ray structure determination of fully hydrated L alpha phase dipalmitoylphosphatidylcholine bilayers. *Biophys J.* 1996, **70**(3), pp.1419-1431.

37. De Wolff, P.M. R. Hosemann und S. N. Bagchi: Direct Analysis of Diffraction by Matter. North-Holland Publishing Company, Amsterdam 1962. 734 Seiten. Preis: 72.— s. *Berichte der Bunsengesellschaft für physikalische Chemie*. 1963, **67**(1), pp.134-135.
38. Caille, A. Remarks on the scattering of x-rays by A-type smectics. *Comptes Rendus Hebdomadaires des Seances de l'Academie des Sciences, Serie B*. 1972, **274**, pp.891-893.
39. Fernandez-Puente, L. et al. Temperature and Chain Length Effects on Bending Elasticity of Phosphatidylcholine Bilayers. *EPL (Europhysics Letters)*. 1994, **28**(3), pp.181-186.
40. Lemmich, J. et al. Pseudocritical Behavior and Unbinding of Phospholipid Bilayers. *Physical Review Letters*. 1995, **75**(21), pp.3958-3961.
41. Pabst, G. et al. Structure and fluctuations of phosphatidylcholines in the vicinity of the main phase transition. *Physical Review E*. 2004, **70**(2).
42. Richter, F. et al. Sterols sense swelling in lipid bilayers. *Physical Review E*. 1999, **59**(3), pp.3483-3491.
43. Mason, P.C. et al. Anomalous swelling in phospholipid bilayers is not coupled to the formation of a ripple phase. *Physical Review E*. 2001, **63**(3), p.030902.
44. Garidel, P. and Blume, A. Miscibility of phospholipids with identical headgroups and acyl chain lengths differing by two methylene units: Effects of headgroup structure and headgroup charge. *Biochimica et Biophysica Acta (BBA) - Biomembranes*. 1998, **1371**(1), pp.83-95.
45. Shimshick, E.J. and McConnell, H.M. Lateral phase separation in phospholipid membranes. *Biochemistry*. 1973, **12**(12), pp.2351-2360.
46. Schmidt, M.L. et al. Phase equilibria in DOPC/DPPC: Conversion from gel to subgel in two component mixtures. *The Journal of Chemical Physics*. 2009, **131**(17), p.175103.
47. Soloviov, D.V. et al. Ripple phase behavior in mixtures of DPPC/POPC lipids: SAXS and SANS studies. *Journal of Physics: Conference Series*. 2012, **351**(1).
48. Lohner, K. et al. Thermal phase behaviour and structure of hydrated mixtures between dipalmitoyl- and dihexadecylphosphatidylcholine. *Chemistry and Physics of Lipids*. 1987, **44**(1), pp.61-70.
49. Mondal Roy, S. and Sarkar, M. Effect of Lipid Molecule Headgroup Mismatch on Non Steroidal Anti-Inflammatory Drugs Induced Membrane Fusion. *Langmuir*. 2011, **27**(24), pp.15054-15064.
50. Silvius, J.R. Solid- and liquid-phase equilibria in phosphatidylcholine / phosphatidylethanolamine mixtures. A calorimetric study. *Biochimica et Biophysica Acta (BBA) - Biomembranes*. 1986, **857**(2), pp.217-228.
51. Majumdar, A. and Sarkar, M. Small Mismatches in Fatty Acyl Tail Lengths Can Effect Non Steroidal Anti-Inflammatory Drug Induced Membrane Fusion. *The Journal of Physical Chemistry B*. 2016, **120**(21), pp.4791-4802.
52. Chapman, D. et al. Biomembrane Phase Transitions: STUDIES OF LIPID-WATER SYSTEMS USING DIFFERENTIAL SCANNING CALORIMETRY. *Journal of Biological Chemistry*. 1974, **249**(8), pp.2512-2521.
53. Koynova, R. et al. Modulation of lipid phase behavior by kosmotropic and chaotropic solutes. Experiment and thermodynamic theory. *European Biophysics Journal*. 1997, **25**(4), pp.261-274.
54. Crowe, J.H. et al. Preservation of structural and functional activity in lyophilized sarcoplasmic reticulum. *Archives of Biochemistry and Biophysics*. 1983, **220**(2), pp.477-484.

55. Crowe, J.H. et al. Interactions of Phospholipid Monolayers with Carbohydrates. *Biochimica et Biophysica Acta*. 1984, **769**, pp.151-159.
56. Nagase, H. et al. Effect of water on lamellar structure of DPPC/sugar systems. *Biochimica et Biophysica Acta (BBA) - Biomembranes*. 1997, **1328**(2), pp.197-206.
57. Crowe, L.M. et al. Interaction of carbohydrates with dry dipalmitoylphosphatidylcholine. *Archives of Biochemistry and Biophysics*. 1985, **236**(1), pp.289-296.
58. Demé, B. et al. Swelling of a Lecithin Lamellar Phase Induced by Small Carbohydrate Solutes. *Biophys J*. 2002, **82**(1), pp.215-225.
59. Roy, A. et al. A Comparative Study of the Influence of Sugars Sucrose, Trehalose, and Maltose on the Hydration and Diffusion of DMPC Lipid Bilayer at Complete Hydration: Investigation of Structural and Spectroscopic Aspect of Lipid–Sugar Interaction. *Langmuir*. 2016, **32**(20), pp.5124-5134.
60. Tian, J. et al. Taste of Sugar at the Membrane: Thermodynamics and Kinetics of the Interaction of a Disaccharide with Lipid Bilayers. *Biophys J*. 2013, **104**(3), pp.622-632.
61. Andersen, H.D. et al. Reconciliation of opposing views on membrane–sugar interactions. *Proceedings of the National Academy of Sciences*. 2011, **108**(5), pp.1874-1878.
62. Rudolph, A.S. and Goins, B. The effect of hydration stress solutes on the phase behavior of hydrated dipalmitoylphosphatidylcholine. *Biochimica et Biophysica Acta (BBA) - Biomembranes*. 1991, **1066**(1), pp.90-94.
63. Rudolph, A.S. et al. Effects of Three Stabilising Agents-Proline, Betaine, and Trehalose-on Membrane Phospholipids. *Archives of Biochemistry and Biophysics*. 1986, **245**(1), pp.134-143.
64. Anchoroguy, T.J. et al. MODES OF INTERACTION OF CRYOPROTECTANTS WITH MEMBRANE PHOSPHOLIPIDS DURING FREEZING. *Cryobiology*. 1987, **24**(4), pp.324-331.
65. Arakawa, T. and Timasheff, S.N. The stabilization of proteins by osmolytes. *Biophys J*. 1985, **47**(3), pp.411-414.
66. Popova, A.V. and Busheva, M.R. Cryoprotective effect of glycine betaine and glycerol is not based on a single mechanism. *Cryoletters*. 2001, **22**(5), pp.293-298.
67. Meersman, F. et al. Counteraction of Urea by Trimethylamine N^+ -Oxide Is Due to Direct Interaction. *Biophys J*. 2009, **97**(9), pp.2559-2566.
68. Zou, Q. et al. The Molecular Mechanism of Stabilization of Proteins by TMAO and Its Ability to Counteract the Effects of Urea. *Journal of the American Chemical Society*. 2002, **124**(7), pp.1192-1202.
69. Feng, Y. et al. Effect of urea, dimethylurea, and tetramethylurea on the phase behavior of dioleoylphosphatidylethanolamine. *Chemistry and Physics of Lipids*. 2002, **114**(2), pp.149-157.
70. Chandler, D. Interfaces and the driving force of hydrophobic assembly. *Nature*. 2005, **437**, p.640.
71. Tanford, C. The hydrophobic effect and the organization of living matter. *Science*. 1978, **200**(4345), pp.1012-1018.
72. Valerio, J. et al. Effect of urea and tmao on lipid bilayers. 2017, **64**(2), p.24.
73. Makhatadze, G.I. and Privalov, P.L. Protein interactions with urea and guanidinium chloride: A calorimetric study. *Journal of Molecular Biology*. 1992, **226**(2), pp.491-505.

74. Feng, Y. et al. Experimental and theoretical investigations on the direct interactions between urea and phospholipids in aqueous solutions. *Biomedical Spectroscopy and Imaging*. 2013, **2**(3), pp.141-153.
75. Sanderson, P.W. et al. The Hofmeister effect in relation to membrane lipid phase stability. *Biochimica et Biophysica Acta (BBA) - Biomembranes*. 1991, **1067**(1), pp.43-50.
76. Smiatek, J. et al. Properties of compatible solutes in aqueous solution. *Biophysical Chemistry*. 2012, **160**(1), pp.62-68.
77. Gesslein, B.W. Humectants in personal care formulation: a practical guide. *Cosmetic Science and Technology Series*. 1999, pp.95-110.
78. Thoppil, A.A. et al. Mode of action of betaine on some amino acids and globular proteins: Thermodynamic considerations. *The Journal of Chemical Thermodynamics*. 2017, **111**, pp.115-128.
79. Kempf, B. and Bremer, E. Uptake and synthesis of compatible solutes as microbial stress responses to high-osmolality environments. *Archives of Microbiology*. 1998, **170**(5), pp.319-330.
80. Kumar, N. and Kishore, N. Structure and effect of sarcosine on water and urea by using molecular dynamics simulations: Implications in protein stabilization. *Biophysical Chemistry*. 2013, **171**, pp.9-15.
81. Takis, P.G. et al. CHAPTER 4 The Chemistry of Betaine. In: *Betaine: Chemistry, Analysis, Function and Effects*. The Royal Society of Chemistry, 2015, pp.47-61.
82. Patel, V.B. and Mehta, K. CHAPTER 1 Betaine in Context. In: *Betaine: Chemistry, Analysis, Function and Effects*. The Royal Society of Chemistry, 2015, pp.3-8.
83. Hayashi, Y. et al. Comparative study of urea and betaine solutions by dielectric spectroscopy: Liquid structures of a protein denaturant and stabilizer. *Journal of Physical Chemistry B*. 2007, **111**(40), pp.11858-11863.
84. Venkatesu, P. et al. Thermodynamic Characterization of the Osmolyte Effect on Protein Stability and the Effect of GdnHCl on the Protein Denatured State. *The Journal of Physical Chemistry B*. 2007, **111**(30), pp.9045-9056.
85. Jolivet, Y. et al. Osmoregulation in halophytic higher plants: The protective effect of glycine betaine against the heat destabilization of membranes. *Plant Science Letters*. 1982, **25**(2), pp.193-201.
86. Lever, M. and Slow, S. The clinical significance of betaine, an osmolyte with a key role in methyl group metabolism. *Clinical Biochemistry*. 2010, **43**(9), pp.732-744.
87. Sharma, P. et al. Study of hydration of sarcosine, formation of its zwitterion and their different oligomers in aqueous media: A Raman spectroscopic and theoretical study. *Spectrochimica Acta Part a-Molecular and Biomolecular Spectroscopy*. 2013, **116**, pp.74-83.
88. Chaudhari, A. et al. Hydrogen bonding interaction in sarcosine-water complex using ab initio and DFT method. *International Journal of Quantum Chemistry*. 2005, **101**(1), pp.97-103.
89. Venkatesan, S. and Lee, S.-L. Computational investigation on microsolvation of the osmolyte glycine betaine [GB (H₂O)₁₋₇]. *Journal of Molecular Modeling*. 2012, **18**(12), pp.5017-5028.
90. Koynova, R. and Caffrey, M. An index of lipid phase diagrams. *Chemistry and Physics of Lipids*. 2002, **115**(1-2), pp.107-219.

91. Bulsara, P.A. et al. The rational design of biomimetic skin barrier lipid formulations using biophysical methods. *International Journal of Cosmetic Science*. 2017, **39**(2), pp.206-216.
92. Zemb, T. and Lindner, P. *Neutrons, X-rays and Light: Scattering Methods Applied to Soft Condensed Matter*. Elsevier, 2002.
93. Glatter, O. and Kratky, O. *Small Angle X-ray Scattering*. Academic Press, 1982.
94. Bragg, W.H. and Bragg, W.L. The reflection of X-rays by crystals. *Proceedings of the Royal Society of London. Series A*. 1913, **88**(605), pp.428-438.
95. Brian Richard, P. Everything SAXS: small-angle scattering pattern collection and correction. *Journal of Physics: Condensed Matter*. 2013, **25**(38), p.383201.
96. Nagle, J.F. and Tristram-Nagle, S. Structure of lipid bilayers. *Biochimica et Biophysica Acta (BBA) - Reviews on Biomembranes*. 2000, **1469**(3), pp.159-195.
97. Pabst, G. et al. Structural information from multilamellar liposomes at full hydration: Full q -range fitting with high quality x-ray data. *Physical Review E*. 2000, **62**(3), pp.4000-4009.
98. Li, N.Y.D. et al. My first electron density map: A beginner's guide to small angle X-ray diffraction. *Elektrotehniski Vestnik/Electrotechnical Review*. 2017, **84**(3), pp.69-75.
99. *X-ray diffraction*. [Database]. Reading: Addison-Wesley Pub. Co, 1969.
100. Pabst, G. et al. Structural analysis of weakly ordered membrane stacks. *Journal of Applied Crystallography*. 2003, **36**(6), pp.1378-1388.
101. Rappolt, M. Bilayer thickness estimations with “poor” diffraction data. *Journal of Applied Physics*. 2010, **107**(8), p.084701.
102. Petrache, H.I. et al. Interbilayer interactions from high-resolution x-ray scattering. *Physical Review E*. 1998, **57**(6), pp.7014-7024.
103. Sun, W.J. et al. Order and disorder in fully hydrated unoriented bilayers of gel-phase dipalmitoylphosphatidylcholine. *Physical Review E*. 1994, **49**(5), pp.4665-4676.
104. Spaar, A. and Salditt, T. Short Range Order of Hydrocarbon Chains in Fluid Phospholipid Bilayers Studied by X-Ray Diffraction from Highly Oriented Membranes. *Biophys J*. 2003, **85**(3), pp.1576-1584.
105. Lewis, E.A. and Murphy, K.P. Isothermal Titration Calorimetry. In: Ulrich Nienhaus, G. ed. *Protein-Ligand Interactions: Methods and Applications*. Totowa, NJ: Humana Press, 2005, pp.1-15.
106. Freire, E. et al. Isothermal titration calorimetry. *Analytical chemistry*. 1990, **62**(18), pp.950A-959A.
107. Bruździak, P. et al. Influence of Osmolytes on Protein and Water Structure: A Step To Understanding the Mechanism of Protein Stabilization. *The Journal of Physical Chemistry B*. 2013, **117**(39), pp.11502-11508.
108. Smiatek, J. et al. Low concentrated hydroxyectoine solutions in presence of DPPC lipid bilayers: A computer simulation study. *Biophysical Chemistry*. 2013, **180**, pp.102-109.
109. Powers, L. and Clark, N.A. Preparation of large monodomain phospholipid bilayer smectic liquid crystals. 1975, **72**(3), pp.840-843.
110. Pabst, G. et al. Structure and Interactions in the Anomalous Swelling Regime of Phospholipid Bilayers. *Langmuir*. 2003, **19**, pp.1716-1722.
111. Gopal, S. and Ahluwalia, J.C. Effect of osmoregulatory solutes on the stability of proteins. *Journal of the Chemical Society, Faraday Transactions*. 1993, **89**(15), pp.2769-2774.
112. Housecroft, C.E. and Constable, E.C. *Chemistry: An Introduction to Organic, Inorganic and Physical Chemistry*. Pearson Prentice Hall, 2006.

113. Rappolt, M. et al. Salt-induced phase separation in the liquid crystalline phase of phosphatidylcholines. *Colloids and Surfaces A: Physicochemical and Engineering Aspects*. 2001, **183-185**, pp.171-181.
114. Parsegian, V.A. Forces between Lecithin Bimolecular Leaflets Are Due to a Disordered Surface Layer. *Science*. 1967, **156**(3777), pp.939-942.
115. Fang, N. et al. Effect of acyl chain mismatch on the contact mechanics of two-component phospholipid vesicle during main phase transition. *Biophysical Chemistry*. 2003, **104**(1), pp.141-153.
116. Lee, A.G. Lipid phase transitions and phase diagrams II. Mixtures involving lipids. *Biochimica et Biophysica Acta (BBA) - Reviews on Biomembranes*. 1977, **472**(3), pp.285-344.
117. Rawlings, A.V. and Harding, C.R. Moisturization and skin barrier function. *Dermatologic Therapy*. 2004, **17**(s1), pp.43-48.
118. Engblom, J. How do lipid aggregates permeate skin. In: *15th Euro Fed Lipid Congress Uppsala*. 2017.
119. Caussin, J. et al. FTIR studies show lipophilic moisturizers to interact with stratum corneum lipids, rendering the more densely packed. *Biochimica et Biophysica Acta (BBA) - Biomembranes*. 2008, **1778**(6), pp.1517-1524.
120. Pennick, G. et al. Superior effect of isostearyl isostearate on improvement in stratum corneum water permeability barrier function as examined by the plastic occlusion stress test. *International Journal of Cosmetic Science*. 2010, **32**(4), pp.304-312.
121. Ita, K.B. et al. Dermal delivery of selected hydrophilic drugs from elastic liposomes: effect of phospholipid formulation and surfactants. *Journal of Pharmacy and Pharmacology*. 2007, **59**(9), pp.1215-1222.
122. GSK. *GSK Probiol N03043 Pre-read Technical Review* 2015.
123. van Smeden, J. et al. The important role of stratum corneum lipids for the cutaneous barrier function. *Biochimica et Biophysica Acta (BBA) - Molecular and Cell Biology of Lipids*. 2014, **1841**(3), pp.295-313.
124. Hartkamp, R. et al. Investigating the Structure of Multicomponent Gel-Phase Lipid Bilayers. *Biophys J*. 2016, **111**(4), pp.813-823.
125. Bouwstra, J.A. et al. pH, cholesterol sulfate, and fatty acids affect the stratum corneum lipid organization. In: *Journal of Investigative Dermatology Symposium Proceedings*: Elsevier, 1998, pp.69-74.
126. Hartkamp, R. et al. Structural Properties of Phospholipid-based Bilayers with Long-Chain Alcohol Molecules in the Gel Phase. *The Journal of Physical Chemistry B*. 2016, **120**(50), pp.12863-12871.
127. LODEN, M. and ANDERSSON, A.-C. Effect of topically applied lipids on surfactant-irritated skin. *British Journal of Dermatology*. 1996, **134**(2), pp.215-220.
128. Lin, T.-K. et al. Anti-Inflammatory and Skin Barrier Repair Effects of Topical Application of Some Plant Oils. *International Journal of Molecular Sciences*. 2018, **19**(1), p.70.
129. Maranz, S. and Wiesman, Z. Influence of Climate on the Tocopherol Content of Shea Butter. *Journal of Agricultural and Food Chemistry*. 2004, **52**(10), pp.2934-2937.
130. Mykhaylyk, O.O. and Hamley, I.W. The Packing of Triacylglycerols from SAXS Measurements: Application to the Structure of 1,3-Distearoyl-2-oleoyl-sn-glycerol Crystal Phases. *The Journal of Physical Chemistry B*. 2004, **108**(23), pp.8069-8083.

131. Sato, K. et al. Polymorphism of POP and SOS. I. occurrence and polymorphic transformation. *Journal of the American Oil Chemists' Society*. 1989, **66**(5), pp.664-674.
132. Torbet, J. and Wilkins, M.H.F. X-ray diffraction studies of lecithin bilayers. *Journal of Theoretical Biology*. 1976, **62**(2), pp.447-458.
133. Seppic. *Seppimax Zen* [Online]. 2018. [Accessed 10/09/2018]. Available from: <https://www.seppic.com/sepimax-zen>
134. Luzzati, V. and Husson, F. THE STRUCTURE OF THE LIQUID-CRYSTALLINE PHASES OF LIPID-WATER SYSTEMS. *The Journal of Cell Biology*. 1962, **12**(2), pp.207-219.
135. Hübner, W. and Blume, A. Interactions at the lipid–water interface. *Chemistry and Physics of Lipids*. 1998, **96**(1), pp.99-123.
136. Fringeli, U.P. and Günthard, H.H. Infrared Membrane Spectroscopy. In: Grell, E. ed. *Membrane Spectroscopy*. Berlin, Heidelberg: Springer Berlin Heidelberg, 1981, pp.270-332.
137. Arrondo, J.L.R. et al. Infrared spectroscopy of phosphatidylcholines in aqueous suspension a study of the phosphate group vibrations. *Biochimica et Biophysica Acta (BBA) - Lipids and Lipid Metabolism*. 1984, **794**(1), pp.165-168.
138. Crowe, J.H. et al. Interactions of sugars with membranes. *Biochimica et Biophysica Acta (BBA) - Reviews on Biomembranes*. 1988, **947**(2), pp.367-384.
139. Porasso, R.D. et al. Interaction of glycine, lysine, proline and histidine with dipalmitoylphosphatidylcholine lipid bilayers: A theoretical and experimental study. *RSC Advances*. 2015, **5**(54), pp.43537-43546.
140. Knoll, W. et al. Small-angle neutron scattering of aqueous dispersions of lipids and lipid mixtures. A contrast variation study. *Journal of Applied Crystallography*. 1981, **14**(3), pp.191-202.
141. Dickson, C.J. et al. Lipid14: The Amber Lipid Force Field. *Journal of Chemical Theory and Computation*. 2014, **10**(2), pp.865-879.
142. Leekumjorn, S. and Sum, A.K. Molecular studies of the gel to liquid-crystalline phase transition for fully hydrated DPPC and DPPE bilayers. *Biochimica et Biophysica Acta (BBA) - Biomembranes*. 2007, **1768**(2), pp.354-365.
143. Chiu, S.W. et al. Combined Monte Carlo and Molecular Dynamics Simulation of Hydrated Lipid-Cholesterol Lipid Bilayers at Low Cholesterol Concentration. *Biophys J*. 2001, **80**(3), pp.1104-1114.
144. MacCallum, J.L. et al. Distribution of amino acids in a lipid bilayer from computer simulations. *Biophys J*. 2008, **94**(9), pp.3393-3404.
145. Vierl, U. et al. Solute effects on the colloidal and phase behavior of lipid bilayer membranes: ethanol-dipalmitoylphosphatidylcholine mixtures. *Biophys J*. 1994, **67**(3), pp.1067-1079.
146. Dods, R.H. et al. Acyl Transfer from Membrane Lipids to Peptides Is a Generic Process. *Journal of Molecular Biology*. 2013, **425**(22), pp.4379-4387.
147. Pridmore, C.J. et al. Acyl transfer from phosphocholine lipids to melittin. *Chemical Communications*. 2011, **47**(5), pp.1422-1424.